

AD _____

Award Number: W81XWH-08-1-0783

TITLE: Generation of Soluble Receptor Activator of NF-KappaB Ligand is Critical for Osteolytic Bone Metastasis

PRINCIPAL INVESTIGATOR: Mr. Kalyan Nannuru

CONTRACTING ORGANIZATION: University of Nebraska Medical Center
Omaha, NE 68196

REPORT DATE: October 2010

TYPE OF REPORT: Annual Summary

PREPARED FOR: U.S. Army Medical Research and Materiel Command
Fort Detrick, Maryland 21702-5012

DISTRIBUTION STATEMENT: Approved for public release; distribution unlimited

The views, opinions and/or findings contained in this report are those of the author(s) and should not be construed as an official Department of the Army position, policy or decision unless so designated by other documentation.

REPORT DOCUMENTATION PAGE

Form Approved
OMB No. 0704-0188

Public reporting burden for this collection of information is estimated to average 1 hour per response, including the time for reviewing instructions, searching existing data sources, gathering and maintaining the data needed, and completing and reviewing this collection of information. Send comments regarding this burden estimate or any other aspect of this collection of information, including suggestions for reducing this burden to Department of Defense, Washington Headquarters Services, Directorate for Information Operations and Reports (0704-0188), 1215 Jefferson Davis Highway, Suite 1204, Arlington, VA 22202-4302. Respondents should be aware that notwithstanding any other provision of law, no person shall be subject to any penalty for failing to comply with a collection of information if it does not display a currently valid OMB control number. **PLEASE DO NOT RETURN YOUR FORM TO THE ABOVE ADDRESS.**

1. REPORT DATE (DD-MM-YYYY) 01-10-2010		2. REPORT TYPE Annual Summary		3. DATES COVERED (From - To) 1 Oct 2009 - 30 Sep 2010	
4. TITLE AND SUBTITLE Generation of Soluble Receptor Activator of NF-KappaB Ligand is Critical for Osteolytic Bone Metastasis				5a. CONTRACT NUMBER	
				5b. GRANT NUMBER W81XWH-08-1-0783	
				5c. PROGRAM ELEMENT NUMBER	
6. AUTHOR(S) Mr. Kalyan Nannuru E-Mail: knannuru@unmc.edu				5d. PROJECT NUMBER	
				5e. TASK NUMBER	
				5f. WORK UNIT NUMBER	
7. PERFORMING ORGANIZATION NAME(S) AND ADDRESS(ES) University of Nebraska Medical Center Omaha, NE 68196				8. PERFORMING ORGANIZATION REPORT NUMBER	
9. SPONSORING / MONITORING AGENCY NAME(S) AND ADDRESS(ES) U.S. Army Medical Research and Materiel Command Fort Detrick, Maryland 21702-5012				10. SPONSOR/MONITOR'S ACRONYM(S)	
				11. SPONSOR/MONITOR'S REPORT NUMBER(S)	
12. DISTRIBUTION / AVAILABILITY STATEMENT Approved for Public Release; Distribution Unlimited					
13. SUPPLEMENTARY NOTES					
14. ABSTRACT Abstract on next page.					
15. SUBJECT TERMS Tumor-stromal interaction, RANKL sRANKL osteolysis breast cancer					
16. SECURITY CLASSIFICATION OF:			17. LIMITATION OF ABSTRACT	18. NUMBER OF PAGES	19a. NAME OF RESPONSIBLE PERSON
a. REPORT	b. ABSTRACT	c. THIS PAGE			19b. TELEPHONE NUMBER (include area code)
U	U	U	UU	55	USAMRMC

14. ABSTRACT

Bone is the most common site of metastasis in human breast cancer. The tropism of breast cancer cells for bone and their tendency to induce the osteolytic phenotype is a result of interactions between breast cancer cells and bone stromal cells and is of paramount importance for bone metastasis. The capacity of breast cancer cells to collaborate with bone stromal cells is likely to be mediated by specific molecules. The underlying molecular mechanisms of tumor-stromal interaction in bone metastasis remain poorly understood. In our study, we examined whether interaction between breast cancer cells and stromal cells in the bone microenvironment play a critical role in the tumor-induced osteolysis and whether inhibition of such interactions using targeted therapeutics will inhibit osteolysis during bone metastasis. We used microarray analysis for gene expression profiling at the tumor bone interface versus the tumor alone area from syngenic mice injected with three different mammary tumor cell lines that differ in their metastatic potential. Up-regulation of mRNA and protein expression of receptor activator of nuclear factor κ B ligand (RANKL) and matrix metalloproteinase (MMP)-13 at the tumor bone interface in all three groups was observed. Furthermore, upregulation of these genes was associated with tumor-induced osteolysis. To determine the functional role of RANKL and MMP-13 in tumor induced osteolysis, mice bearing Cl66 tumors were treated with RANKL antisense, MMP-13 antisense or control scrambled oligonucleotides. Analysis of tumor and tumor bone samples revealed knockdown of RANKL and MMP-13 expression at the tumor bone interface and a significant reduction in bone destruction. Further analysis to evaluate the mechanistic role of RANKL and MMP-13 in tumor-induced osteolysis, revealed that generation of soluble RANKL and increased RANKL-osteoprotegerin (OPG) ratios at TB interface promote osteoclast activation and bone destruction. MMP13 regulates osteolysis by activating MMP9 and TGF β signaling at the TB interface. Collectively our studies demonstrated that identifying the molecules involved in osteolytic bone metastasis and developing therapeutic strategies to target these molecules may help to inhibit mammary tumor induced osteolysis.

Table of Contents

	<u>Page</u>
Introduction.....	4
Body..... (Results/Discussion)	6
Key Research Accomplishments.....	14
Reportable Outcomes.....	16
Conclusion.....	17
List of Personnel.....	17
References.....	18
Appendices.....	23

Introduction:

Breast cancer is the most common cancer among women in the United States. Annually, breast cancer is responsible for over 40,000 deaths, making it the second leading cause of cancer death (Jemal *et al.*, 2009). A large portion of breast cancer-related mortality is due to metastatic disease rather than the primary tumor itself. Breast cancer cells demonstrate strong predilection for metastasis to bone resulting in lesions that are predominantly osteolytic. These lesions significantly reduce the quality of life of the patient by causing intractable bone pain, anemia, hypercalcemia, increasing the risk of pathologic fracture and dramatically increase the risk of mortality (Boyce *et al.*, 1999; Coleman, 1997).

Malignant breast cancer cells entry to bone microenvironment initiates a vicious cycle of bidirectional communication between tumor and stromal cells that promotes osteolytic metastases (Kakonen and Mundy, 2003; Roodman, 2004a). One of the critical signaling molecules involved in this cycle is receptor activator of NF- κ B ligand (RANKL). RANKL is a membrane-bound protein expressed on the cell surface of osteoblasts and bone marrow stromal cells (Lacey *et al.*, 2000; Dougall and Chaisson, 2006; Morrissey *et al.*, 2007; Roodman, 2004a). Binding of RANKL to its receptor, RANK, expressed on the surface of osteoclast precursors leads to their differentiation into mature osteoclasts (Lacey *et al.*, 2000; Dougall and Chaisson, 2006; Dallas *et al.*, 2002). Another molecule intimately tied to the RANKL-RANK signaling axis is osteoprotegerin (OPG) which is a soluble, decoy receptor of RANKL that prevents RANKL from engaging RANK and initiating signaling (Dougall and Chaisson, 2006; Lacey *et al.*, 1998). Malignant cells secrete soluble factors such as parathyroid hormone related peptide (PTHrP) that up-regulates RANKL expression (Kitazawa and Kitazawa, 2002) and enhanced RANKL signaling appears to be the driving force behind tumor-induced osteolytic lesions (Kitazawa and Kitazawa, 2002; Tanaka *et al.*, 2005; Roodman and Dougall, 2008; Zhang *et al.*, 2001; Zhang *et al.*, 2003; Zhang *et al.*, 2003; Morony *et al.*, 2001). However, very little is known about the role of tumor-bone interaction in regulation of RANKL expression.

While RANKL-RANK signaling is critical to the osteolytic metastasis, it is also the rate limiting step of the cycle since signaling requires cell to cell contact to bring both membrane-bound proteins into contact. One mechanism by which this requirement can be bypassed is the generation of a soluble form of RANKL (sRANKL) that allows wide spread osteoclast activation. Recently, Cathepsin G was identified as a protein that is upregulated at the TB-interface of mammary tumor-induced osteolytic lesions and was shown to be capable of generating sRANKL (Wilson *et al.*, 2008; Wilson and Singh, 2008). Other proteases known to be capable of generating sRANKL include matrix metalloproteinase (MMP)3, MMP7, a disintegrin and metalloproteinase (ADAM)-17, and ADAM-19 (Lynch *et al.*, 2005; Chesneau *et al.*, 2003; Schlondorff *et al.*, 2001). Inhibition of Cathepsin G significantly reduced mammary tumor-induced osteolysis suggesting the importance of sRANKL (Wilson *et al.*, 2008). However, while the centrality of RANKL-RANK signaling has been clearly established the relative contributions of RANKL and sRANKL during TB-interactions remain unclear.

In the present study, we sought to determine the functional significance of RANKL during tumor-stromal interaction in mammary tumor-induced osteolytic lesions. Our data demonstrate upregulation of RANKL expression and generation of sRANKL at the TB-interface in tumor-induced osteolysis. Furthermore, targeting RANKL expression using antisense-RANKL oligonucleotide decreased RANKL levels and RANKL:OPG ratio at the TB- interface and significantly reduced tumor-induced osteolysis.

Metastasis of breast cancer cells to distant organs is an ominous sign in disease progression. Breast cancer cells show a strong predilection for bone (Coleman, 1997). Arrival of tumor cells in the bone microenvironment initiates a “vicious cycle” of bi-directional interactions between tumor cells and stromal cells (Yoneda and Hiraga, 2005). Tumor cells produce various factors such as parathyroid hormone-related peptide (PTHrP) (Powell *et al.*, 1991;Guise *et al.*, 1996), interleukin (IL)-8, and IL-1 to stimulate osteoblasts to induce expression of receptor activator of NF- κ B ligand (RANKL) to induce bone resorption (Roodman, 2004b). Increased bone resorption causes the release of sequestered factors that favor the growth of malignant tumor cells including bone derived growth factor (BDGF), fibroblast growth factor (FGF) and transforming growth factor- β (TGF β) (Mundy, 2002). The underlying molecular mechanisms of tumor-bone interaction are poorly understood. In this report, we hypothesize that tumor-stromal interaction in the bone microenvironment alters gene expression creating a unique expression signature that promotes osteolytic bone metastasis and that inhibition of such interactions can be targeted for development of novel therapeutics.

Extracellular Matrix (ECM) degradation is an essential step in the growth, invasion and metastasis of malignant tumors. The molecules responsible for ECM degradation in both physiological and pathological conditions are matrix metalloproteinases (MMPs). MMPs are a family of human zinc endopeptidases that can degrade virtually all ECM components (Birkedal-Hansen, 1987). The MMPs have two conserved domains common to all MMPs which contain a zinc-binding domain and a cysteine-switch. The cysteine-switch is found in the propeptide domain while the zinc-binding motif is found in the catalytic domain. The interaction between the cysteine-switch and zinc maintains the latency of the pro-MMPs (Van Wart and Birkedal-Hansen, 1990). Currently, at least 26 known MMP genes in humans are identified (Kondratiev *et al.*, 2008). On the basis of the ECM components cleaved, the MMPs can be divided into collagenases, gelatinases, and stromelysins/matrilysins. Based on secretion status, MMPs are also classified as secreted MMPs or membrane-associated (MTMMPs) (Kondratiev *et al.*, 2008).

MMPs can mediate tumor invasion through basement membrane degradation (Nelson *et al.*, 2000). Apart from their ECM degradation functionality latest research in MMPs reveals their specific roles in cleaving several extracellular and membrane associated proteins and regulating cellular signaling pathways. MMP7 promotes osteolytic bone metastasis in prostate cancer through generation of sRANKL from membrane bound RANKL (Lynch *et al.*, 2005). MMP2 and MMP-9 have been associated with tumor angiogenesis (John and Tuszynski, 2001) (Stetler-Stevenson, 2001). Expression of these proteases is also associated with poor clinical outcome in various malignancies such as bladder, breast, lung cancer and head and neck squamous

cell carcinomas (Dunne *et al.*, 2003;Djonov *et al.*, 2002;Pinto *et al.*, 2003;Ruokolainen *et al.*, 2004). MMP13 was first identified from the overexpressing breast carcinomas (Freije *et al.*, 1994). IL-1 α , IL-1 β and TGF β are potential candidates for inducing expression of MMP13 in breast carcinomas (Mauviel, 1993;Uria *et al.*, 1998;Selvamurugan *et al.*, 2002). In case of Squamous Cell Carcinoma (SCC) MMP-13 is predominantly expressed by the tumor cells at the invading front and to some extent by stromal fibroblasts surrounding tumor cells (Johansson *et al.*, 1997;Cazorla *et al.*, 1998). Expression of MMP-13 in the head and neck SCCs correlates with the invasion and metastasis capacity of the tumor, indicating that MMP-13 expression could be an indicator for the invasive capacity of SCCs (Johansson *et al.*, 1997;Cazorla *et al.*, 1998). In laryngeal and vulvar carcinomas the expression of MMP-13 colocalizes with the expression of MT1-MMP and MMP-2 suggesting that these three MMPs form a proteolytic cascade that leads to potent extracellular collagenolytic activity (Johansson *et al.*, 1999;Cazorla *et al.*, 1998). In non-small cell lung carcinoma tumor cells expressing MMP13 have a potential to shed from the primary tumor and aggregate in the bone marrow and associated with poorer survival rates (Hsu *et al.*, 2006). But the specific role of upregulated MMP13 in malignant breast cancer in metastatic site is yet to be investigated. Our study is focused on their role in the tumor-stromal interaction, with particular attention to the tumor-bone microenvironment.

In our microarray analysis of tumor bone samples with tumor alone area, we identified matrix metalloproteinase (MMP)-13, as one of the highly upregulated gene at the tumor bone (TB)-interface. Moreover, we demonstrated that knockdown of MMP-13 expression at the TB-interface leads to a significant reduction in bone destruction, and the number of activated osteoclasts at the TB-interface. MMP13-ASO treatment decreased the RANKL:OPG ratio, active MMP-9 and TGF β levels at the TB-interface. Together, our data demonstrated that upregulation of MMP-13 at the TB-interface is important for regulation of tumor-induced osteolysis. Since MMP-13 is not expressed in most adult human tissues under normal conditions, targeting MMP-13 expression may serve as an important and safe strategy in the development of novel therapeutics for metastatic disease.

Results/Discussion:

During the research period under this award, my research work in understanding the molecular events that mediate tumor-induced osteolytic bone metastasis has made important observations that aid in better understanding of functional significance of RANKL expression and mechanisms of soluble RANKL generation in tumor-bone microenvironment during osteolytic bone metastasis and important role of MMP13 expression in tumor-bone interface and its role in promoting osteolytic bone metastasis. These findings will help in understanding the pathophysiology of bone metastasis in breast cancer and development of novel therapeutic strategies to alleviate the suffering of the patients.

Gene expression profile at the tumor bone interface: We utilized microarray analysis to examine the gene expression pattern at the TB-interface compared to the tumor alone area in tumors derived from all three cell lines. We observed a set of 414 genes commonly upregulated among the three cell lines and 27 genes commonly down-regulated among the three cell lines at the TB interface compared to the tumor alone area. The highly upregulated genes were *IBSP*, *RANKL*, *MMP-13*, Insulin growth factor binding protein (*IGFBP*)5, *Lumican*, Lysyl oxidase (*Lox*), Kinesin family 5B (*Kif5b*) and Wnt inhibitory factor 1(*Wif1*) (**Figure 1**). *RANKL* is found to be one of the highly upregulated genes at TB interface. We did not observe any significant difference in *RANK* expression at the TB-interface compared to the tumor alone area. We validated the microarray data using qRT-PCR (**Figure 1**). We observed upregulation of *RANKL* mRNA at the TB-interface compared to the tumor alone area in all three groups. We further validated upregulation of *RANKL* at the tumor-bone interface by using immunohistochemical analysis to demonstrate upregulation of *RANKL* at the protein level. In agreement with the mRNA expression data, we observed higher expression of *RANKL* protein at the TB-interface. Osteoblasts, stromal cells and tumor cells at the TB-interface stained strongly positive for *RANKL* (2009 Annual Report & Appendix 1).

***RANKL*, *sRANKL* and *OPG* expression at the TB-interface:** Our findings demonstrate an increased *RANKL*:*OPG* ratio at the TB-interface compared to the tumor alone area for all tumors. Our data demonstrate upregulation of *RANKL* and likely upregulation of free, active *sRANKL* during tumor-induced osteolysis. (2009 Annual Report & Appendix 2)

Soluble RANKL generation by proteolytic cleavage of RANKL by Cathepsin G: In our previous work in prostate cancer model we reported that *MMP7* plays a role in prostate tumor-induced osteolysis through the cleavage of cell-surface *RANKL* into a soluble form of *RANKL* that is capable of enhancing osteoclast differentiation and subsequent osteolysis (Lynch *et al.*, 2005). Incubation of full length *RANKL* with *Cathepsin G* generated a soluble version of *RANKL* (~24 kDa). To confirm *cathepsin G*-mediated cleavage of *RANKL*, we used *TPCK*, a *cathepsin G* inhibitor, before incubation with full-length *RANKL* protein. *TPCK* is an inhibitor of the chymotrypsin-like group of proteases and is a potent inhibitor of *cathepsin G* (Overall and Blobel, 2007; Selak *et al.*, 1988). We confirmed the soluble *RANKL* generation by Western blot analysis with an anti-*RANKL* antibody that recognizes an epitope near the COOH terminus confirmed that the cleaved protein was *RANKL* and that the soluble product generated was derived from full-length *RANKL* cleaved near the NH₂ terminus within the extracellular domain (2009 Annual Report and Appendix 3).

Upregulation of MMP13 at the tumor-bone interface

Recognizing the important role of proteases in tumor progression, we evaluated the expression of *MMP13* at the Tumor-bone interface. Our microarray analysis revealed the upregulation of *MMP13* at the tumor-bone interface in all three tumor models. We further evaluated the functional role of *MMP-13* in mammary tumor-induced osteolysis. We examined *MMP-13* protein expression at the TB-interface by immunohistochemistry. *MMP-13* specific antibody staining revealed a significant upregulation of *MMP-13* in *Cl66* tumors at the TB-interface but not at the tumor alone area (**Figure 2 A**). Antibody controls did not show any non specific staining. This protein level analysis further

confirmed the earlier observation of increased MMP-13 transcript levels by cDNA microarray and qRT-PCR analyses.

Kinetics of MMP-13 expression and tumor-induced osteolysis

In the next set of experiments, we examined the kinetics of MMP-13 expression and its association with tumor-induced osteolysis and the number of activated osteoclasts. Mice bearing Cl66 tumors were killed 2, 3 or 4-weeks after tumor implantation and tumors were examined for bone destruction, osteoclast number and MMP-13 expression at the TB-interface and tumor alone areas. We quantified the severity of lesions by measuring bone destruction index (BDI), which is a ratio of the length of the bone that is destroyed by the tumor to the total length of the bone at the TB-interface. Results shown in **Figure 2B** demonstrate an increase in bone destruction and osteoclast number over time. We observed higher levels of MMP-13 mRNA expression at the TB-interface as compared to tumor alone areas (**Figure 2C**).

Inhibiting MMP-13 expression abrogates mammary tumor-induced osteolysis and number of activated osteoclasts at the TB-interface

Next, we examined whether knocking down MMP-13 expression in Cl66 tumor bearing mice using ASOs inhibited mammary tumor-induced osteolysis (**Figure 3A**). We observed smaller tumors in MMP13-ASO treated group as compared to Control-ASO treated group; however the decrease in tumor size was not significant. H&E staining of tumor sections demonstrated severe bone destruction in control-ASO treated tumors (**Figure 3Bi**) whereas MMP13-ASO treated tumors showed no osteolysis (**Figure 3Bii**). We observed a significant decrease in osteolysis in the MMP13-ASO treated group compared to the control-ASO treated group (**Figure 3Biii**). Similarly, we observed a significant decrease in the number of activated osteoclasts lining the TB-interface in the MMP13-ASO treated group (**Figure 3C**).

We then examined the expression of MMP-13 in tumors from MMP13-ASO and control-ASO treated mice using qRT-PCR. The expression of MMP-13 at the TB-interface was significantly lower in the MMP13-ASO treated group as compared to the control-ASO treated group (**Figure 3D**). We observed very low levels of MMP-13 expression in the tumor alone area which was not altered by MMP13-ASO treatment (**Figure 3D**).

Inhibition of MMP-13 decreases RANKL expression and regulates the RANK/OPG ratio at the TB-interface

Previous observations from our laboratory have shown the upregulation of RANKL at the TB-interface in mammary tumor-induced osteolysis (Nannuru *et al.*, 2009; Futakuchi *et al.*, 2009). RANKL interacts with its receptor RANK and activates osteoclasts. We evaluated RANKL mRNA levels in MMP13-ASO and Control-ASO treated mice and observed a significant decrease in RANKL expression at the TB-interface in the MMP13-ASO treatment group (**Appendix 1**).

The RANKL/OPG axis has been shown to play a pivotal role in osteolytic bone metastasis (Dougall and Chaisson, 2006). We examined how the RANKL:OPG ratio at the TB-interface was altered due to MMP-13 ASO treatment. RANKL levels were significantly reduced due to MMP13-ASO treatment (**Appendix 1**), whereas we did not observe any significant difference in OPG levels between the two treatment groups (**Appendix 1**). With the decrease in the RANKL levels, we observed a significant decrease in the RANKL:OPG at the TB-interface in the MMP13-ASO treatment group (**Appendix 1**). These observations suggest a functional role for MMP-13 in tumor-induced osteolysis mediated by the regulation of the RANKL/OPG axis.

Targeting MMP-13 inhibits MMP-9 activation and TGF β signaling

Previously, we have shown that MMP-9 is also upregulated at the TB-interface in mammary tumor implanted mice (Wilson *et al.*, 2008). We observed a decrease in MMP-9 mRNA expression at the TB-interface in the MMP13-ASO treated group as compared to the control-ASO treated group (**Appendix 1**). We evaluated the activity of MMP-9 at the TB-interface of Cl66 tumor bearing mice treated with MMP13-ASO compared to Control-ASO. We observed a significant decrease in gelatinolytic activity (at 92kDa) in the MMP13-ASO treated mice. We observed a significant decrease in active:pro MMP-9 enzyme levels in MMP13-ASO treated mice (**Appendix 1**).

We have previously reported that, upregulation of TGF β signaling during tumor-bone interaction promotes tumor-induced osteolysis (Futakuchi *et al.*, 2009). We observed a significant decrease in tumor-induced osteolysis with MMP-13 ASO treatment. To examine whether MMP-13 acts via TGF β signaling in mammary induced osteolysis, we evaluated TGF β expression and activity at the TB-interface of MMP13-ASO and control-ASO treated mice. We observed downregulation of TGF β mRNA expression in MMP13-ASO treated mice (**Figure 4B**). We evaluated TGF β signaling using immunohistochemistry for p-Smad2 (Nakao *et al.*, 1997). We observed a significant decrease in the pSmad-2 staining index and TGF β signaling at the TB-interface of mice with MMP13-ASO treatment (**Figure 4A & C**).

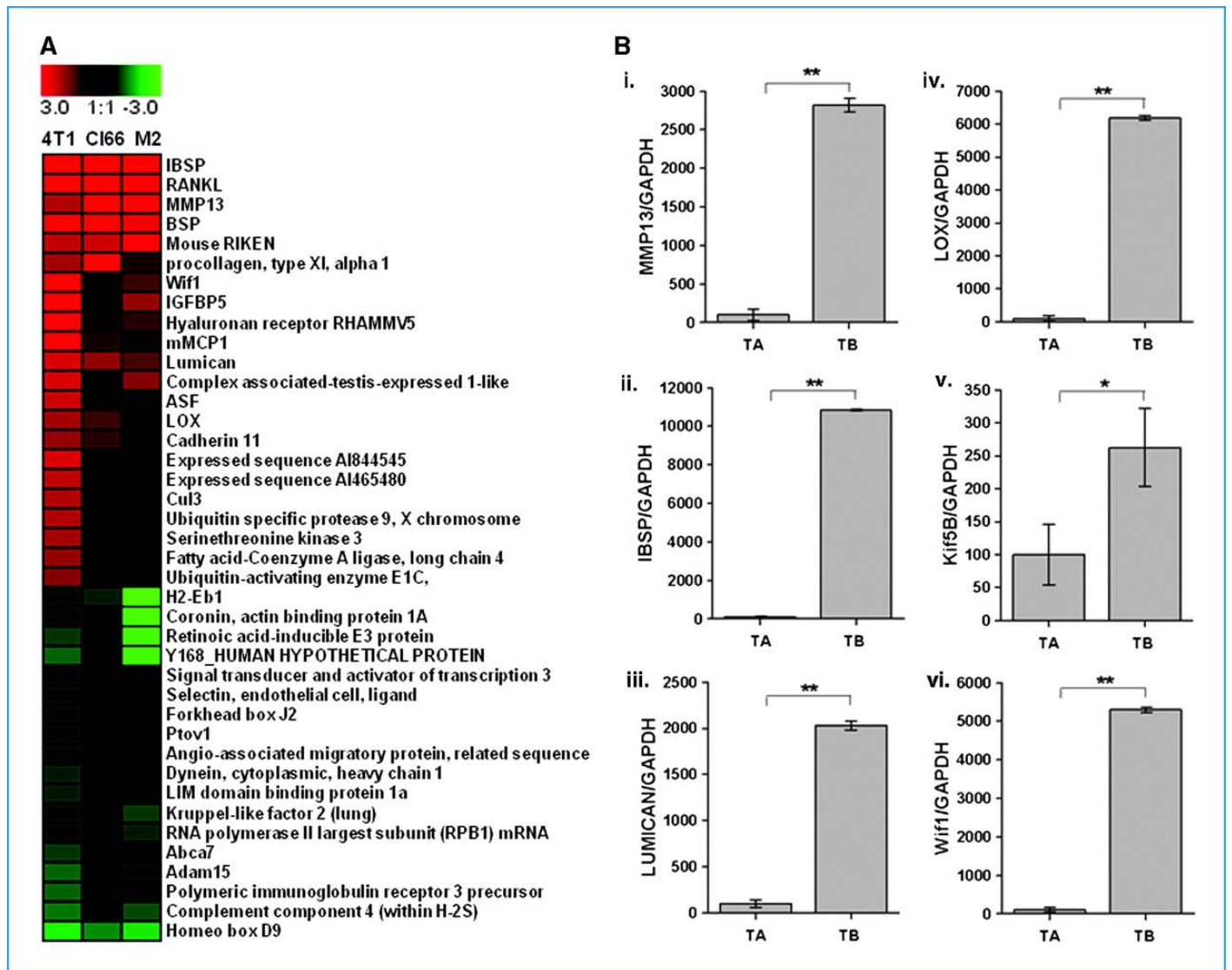


Figure 1. Gene expression profile at the TB interface. A, changes in the gene expression profile at the TB interface in comparison with the tumor alone area were determined using cDNA microanalysis using week 4 samples from 4T1, Cl66, and Cl66M2 tumors. B, i-vi, mRNA expression of MMP13, IBSP, Lumican, LOX, Kif5b, and Wif1 was confirmed by real-time PCR analysis with gene-specific primers. Relative expression of these genes from tumor alone and TB interface samples were normalized to GAPDH expression. Real-time gene expression data presented are representative of all three cell lines done in triplicate. Bars, SEM. **, $P < 0.0$

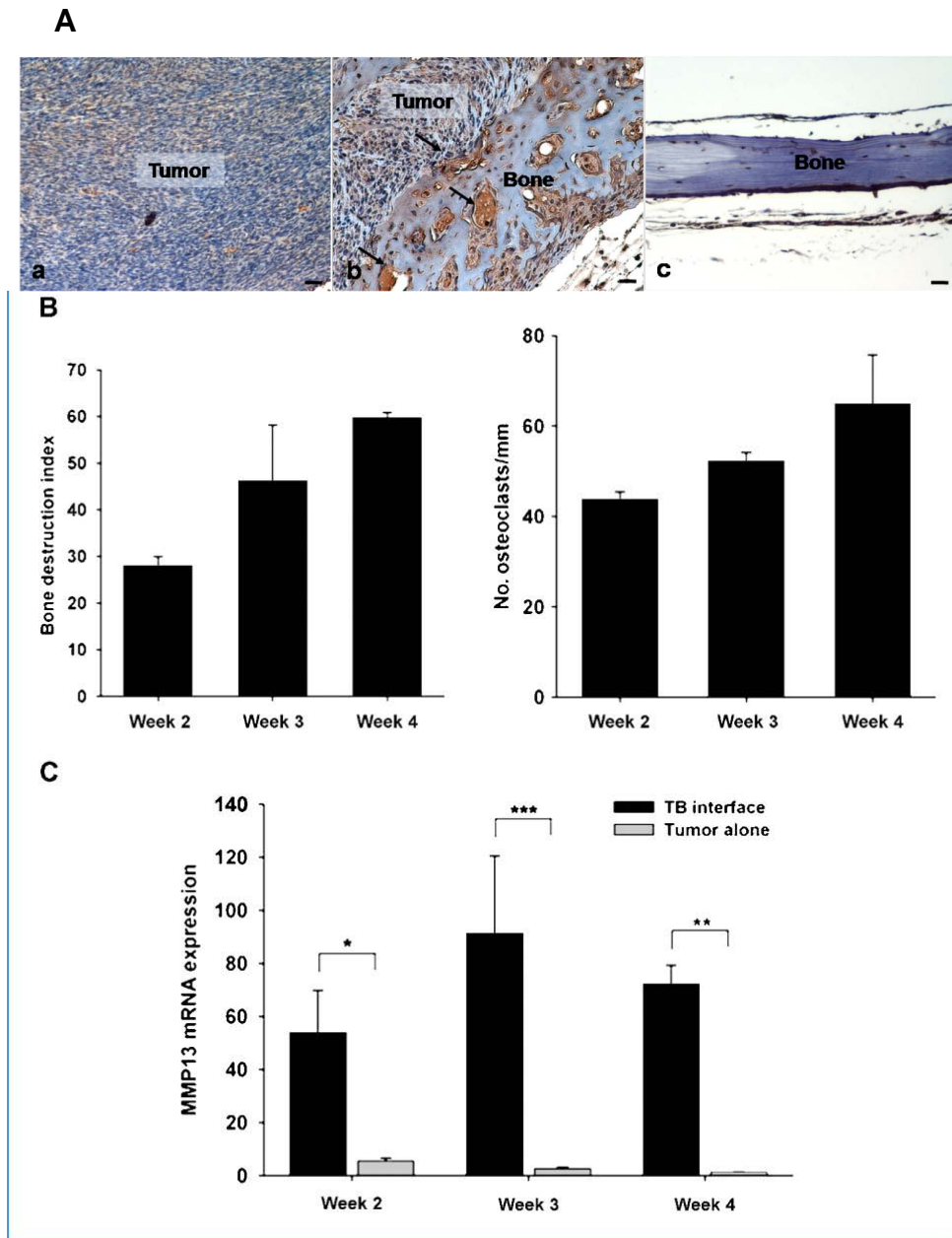


Figure 2. MMP13 expression at TB interface is associated with tumor-induced osteolysis. A, expression of MMP13 at the TB interface. Immunohistochemistry for MMP13 was done on sections from Cl66 tumor-bearing mice and non-tumor-bearing mice. b, tumor cells, osteoblasts, and stromal cells at the TB interface were stained positive for the MMP13 (arrows). a, tumor cells in the tumor alone area did not stain for MMP13. c, immunostaining of normal bone showing very low MMP13 expression. Bar, 0.01 mm. B, severity of tumor-induced osteolysis was computed by measuring the BDI on sections from Cl66 tumor-bearing mice at weeks 2, 3, and 4 after tumor implantation. We observed an increase in the BDI with time and an association with osteoclast homing at the TB interface. Bars, SD ($n = 5$). C, kinetics of MMP13 expression at different time points after tumor implantation by RT-PCR. TB interface and tumor alone area samples from Cl66 tumor-bearing mice were analyzed for MMP13 expression, and an increase in expression was observed at the TB interface at all time points. Relative MMP13 expression was normalized to GAPDH expression. Bars, SD. *, $P < 0.05$; **, $P < 0.01$; ***, $P < 0.005$.

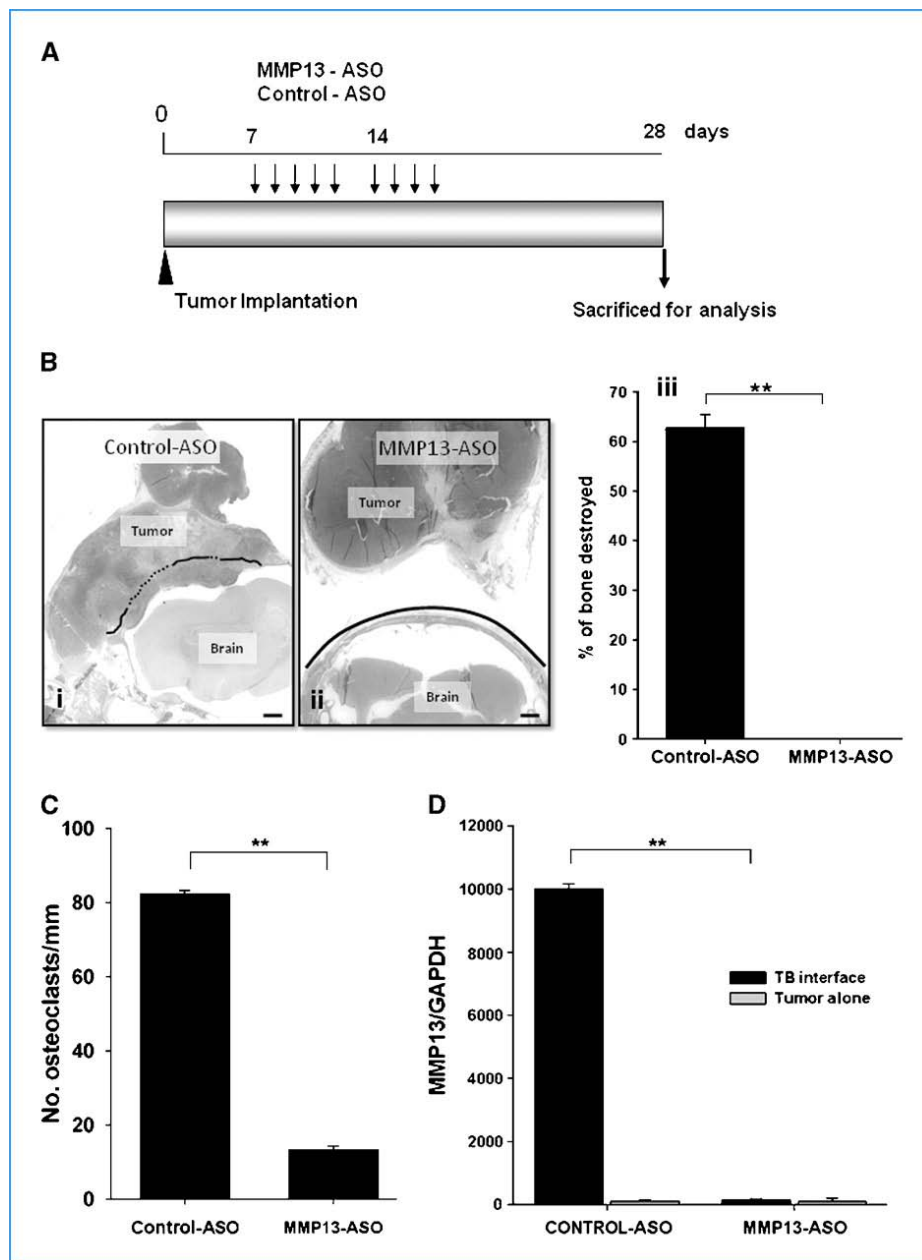


Figure 3. Inhibition of MMP13 in vivo reduces tumor-induced osteolysis. A, experimental strategy for treatment of Cl66 tumor-bearing mice with MMP13-ASO and control-ASO. B, H&E-stained sections (magnification, 20 \times) of tumors from control-ASO-treated (i) and MMP13-ASO-treated (ii) mice. Solid line, the intact bone; dotted line, the bone resorbed. iii, severity of the osteolytic lesion was measured by calculating the BDI; a significant reduction in the BDI was observed in MMP13-ASO-treated mice compared with control-ASO-treated mice. Bars, SD (n = 5 per group, and the study was repeated with same number of mice in each group). C, number of TRAP-positive osteoclasts in MMP13-ASO-treated and control-ASO-treated mice. D, expression of MMP13 at the TB interface of MMP13-ASO-treated animal is significantly reduced compared with control-ASO-treated mice. MMP13 expression was determined by RT-PCR and normalized to GAPDH expression. The values are mean \pm SEM. This is a representative of three experiments with similar results. Scale bar, 0.01 mm.

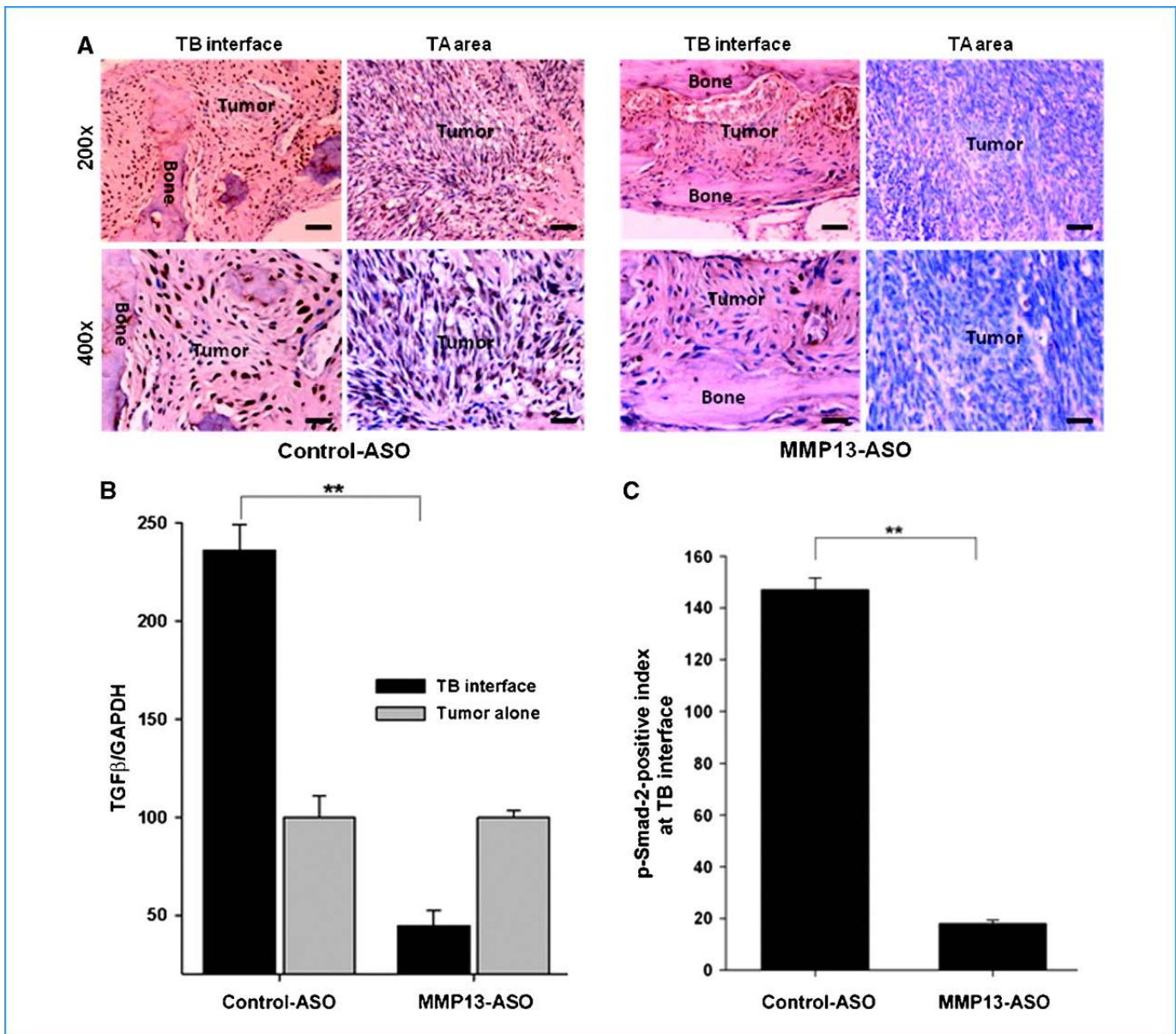


Figure 4. Inhibition of MMP13 blocks TGFβ signaling at the TB interface. A and C, sections from MMP13-ASO–treated mice showed a significantly reduced p-Smad-2 staining index at the TB interface. Scale bars, 0.01 mm (n = 5). B, qRT-PCR showed a significant decrease in TGFβ mRNA expression at the TB interface in MMP13-ASO–treated mice compared with control-ASO–treated mice. The values are mean ± SEM. This is representative of three experiments with similar results. **, P < 0.05.

- **Key Research Accomplishments:**

- In our research effort to elucidate the molecular mechanisms that regulated osteolytic bone metastasis, we observed that,
- Tumor cells in the bone microenvironment promote bone resorption and osteolysis. Three different mammary adenocarcinoma cell lines (4T1, Cl66 and Cl66M2) were implanted on calvaria. Though these tumor cells differ in their metastatic potential, once they are in the bone microenvironment they promote osteoclast activation and induce similar levels of osteolysis.
- Interaction of mammary tumor cells with bone microenvironment alters the gene expression profile at the tumor-bone interface.
- In our experimental osteolytic bone metastasis model RANKL, MMP13, IBSP, Lox, Lumican, IGFBP5 and WIF1 genes were highly upregulated at the TB interface.
- During the tumor-bone interaction, we found that not only RANKL mRNA and protein levels were upregulated at the TB interface, but also we have observed solubilization of membrane bound RANKL to form soluble RANKL (sRANKL).
- Levels of RANKL and sRANKL in TB interface samples and TA samples from Cl66 tumors were analyzed by western blot using an antibody that detects a moiety at the c-terminal of RANKL. Soluble RANKL levels were also higher in TB interface samples.
- Generation of sRANKL bypasses requirement of cell-cell interaction between RANKL expressing osteoblasts and RANK expressing osteoclasts for their activation. Soluble RANKL generation is higher in tumor-bone lysates compared tumor alone samples.
- Soluble RANKL is generated from proteolytic cleavage of full length RANKL near the NH₂ terminus within the extracellular domain by Cathepsin G.
- Increased expression of RANKL and subsequent generation of sRANKL at the TB interface during mammary tumor cell interaction in bone microenvironment led to increased osteoclast activation, which is responsible for increased bone resorption and tumor-induced osteolysis.
- Activated osteoclasts at the TB interface were analyzed using TRAP staining, which specifically stains multinucleated alkaline phosphatase producing activated osteoclasts.
- Targeting RANKL expression with antisense oligonucleotides (ASO) in Cl66 tumor bearing mice significantly reduced RANKL expression at TB interface, thereby reduced osteoclast activation and significantly inhibited tumor-induced osteolysis. Whereas in Control-ASO treated group significant levels of bone destruction due to tumor growth was observed.
- RANKL protein levels were lower in RANKL-ASO treated group compared to Control-ASO treated group. OPG levels were not altered due to ASO treatment, but OPG:RANKL ratio is elevated at the TB interface in RANKL-ASO treated group. This eventually resulted in decreased activated osteoclasts at the TB interface and inhibition of tumor-induced osteolysis.

- No significant difference in tumor growth in RANKL-ASO and Control-ASO treated groups was observed. Number of proliferating cells observed by PCNA staining showed a significantly higher number of proliferating tumor cells in control tumors compared to RANKL targeted tumors.
- MMP13 expression at the TB interface was upregulated both at mRNA and protein level. Increased MMP13 expression levels were associated with increase in osteolysis observed in tumor bearing mice.
- Inhibition of MMP13 in Cl66 tumor-bearing mice with ASO significantly reduced MMP13 expression and tumor-induced osteolysis.
- Incubation of RANKL with MMP13 *in vitro* has shown that MMP13 cannot cleave RANKL to form soluble RANKL.
- The ratio of active MMP-9 to ProMMP-9 levels was significantly reduced in MMP13 ASO treated mice compared Control-ASO treated mice. MMP13 might be involved in activation of pro-MMP-9 to active MMP-9. MMP-9 is a known osteoclast recruiter and decrease in Active MMP-9 levels with MMP13 ASO treatment may be responsible for the decreased osteoclast number observed at the TB interface.
- A significant decrease in TGF β signaling (pSAMD2 staining) at the TB interface was observed in MMP13-ASO treated group compared to Control-ASO group.
- Upregulation of MMP13 expression during tumor-bone interaction in mammary tumor growth in bone microenvironment promotes osteolysis through activation MMP-9 and TGF β signaling.

Reportable Outcomes:

Findings from this research work were published in the following articles in peer-reviewed journals.

Publications:

Nannuru KC, Futakuchi M, Varney ML, Vincent TM, Marcusson EG, Singh RK. MMP-13 regulates mammary tumor-induced osteolysis by activating MMP9 and TGF β signaling at the tumor-bone interface. *Cancer Res* 2010; 70(9) 3494 - 504

Nannuru KC, Futakuchi M, Sadanandam A, Wilson TJ, Varney ML, Myers KJ, et al. Enhanced expression and shedding of receptor activator of NF-kappaB ligand during tumor-bone interaction potentiates mammary tumor-induced osteolysis. *Clin Exp Metastasis* 2009;26:797-808

Wilson TJ, **Nannuru KC**, Futakuchi M, Sadanandam A, Singh RK. Cathepsin G enhances mammary tumor-induced osteolysis by generating soluble receptor activator of nuclear factor-kappaB ligand. *Cancer Res* 2008;68:5803-11.

Meeting Abstracts:

Nannuru K.C., Futakuchi M, Sadanandam A, Varney M, Vincent T, Marcusson E, et al. Up-regulation of Matrix metalloproteinase (MMP-13) expression at the tumor-bone interface favors mammary tumor-induced osteolysis. 99th AACR annual meeting 2008, San Diego, CA. Poster presentation.

Nannuru, K.C., Futakuchi.M, Wilson.T.J, Varney. M.L, Vincent. T.M, Marcusson. E.G, and Singh.R.K. Up-regulation of Matrix metalloproteinase (MMP-13) expression at the tumor-bone interface favors mammary tumor-induced osteolysis. 39th Midwest Student Biomedical Research Forum, Omaha, NE, Feb 29- Mar 1, 2008. Poster presentation.

Nannuru, K.C. and Singh, R.K. Up-regulation of soluble RANKL at the tumor-bone interface is critical for osteolytic bone metastasis in breast cancer. International Student Forum at IMSUT, Tokyo, Japan, June 24th – 27th, 2007

Nannuru, K.C., Futakuchi.M, Wilson.T.J, Varney. M.L, Vincent. T.M, Marcusson. E.G, and Singh.R.K. Up-regulation of soluble RANKL at tumor-bone interface is critical for mammary tumor-induced osteolysis. American Association for Cancer Research Annual meeting 2007, Los Angeles, CA Apr 14-18, 2007

Nannuru, K.C., Futakuchi.M, Wilson.T.J, Varney. M.L, Vincent. T.M, Marcusson. E.G, and Singh.R.K. Breast cancer bone metastasis: Mechanisms of mammary tumor-induced osteolysis. 2007 Midwest Student Biomedical Research Forum, Omaha, NE, Feb 24, 2007

Conclusions:

In our study, we sought to determine the functional significance of RANKL during tumor-stromal interaction in mammary tumor-induced osteolytic lesions. Our data demonstrate upregulation of RANKL and MMP13 expression and generation of sRANKL at the TB-interface in tumor-induced osteolysis. Moreover, we showed that cathepsin G is capable of shedding the extracellular domain of RANKL, generating active sRANKL that is capable of inducing differentiation and activation of osteoclast precursors. Targeting RANKL expression using antisense-RANKL oligonucleotide decreased RANKL levels and RANKL:OPG ratio at the TB- interface and significantly reduced tumor-induced osteolysis. Furthermore our findings delineate the potential role of MMP-13 as one of the key regulators, commonly upregulated at the TB-interface, during tumor bone interaction in osteolytic bone metastasis. MMP-13 expression contributes to the osteolytic process by regulating RANKL:OPG levels, activating MMP-9 and increasing TGF β signaling (**Figure 23**). Our study provides data for understanding the mechanistic role of MMP-13 in osteolysis observed during bone metastasis. Additional studies are required to understand the regulation of MMP-13 expression during osteolytic bone metastasis and the development of targeted therapeutics.

List of personnel received pay from this research effort:

Kalyan C. Nannuru

Reference List:

Birkedal-Hansen H (1987) Catabolism and turnover of collagens: collagenases. *Methods Enzymol* **144:140-71**. 140-171

Boyce BF, Yoneda T, Guise TA (1999) Factors regulating the growth of metastatic cancer in bone. *Endocr Relat Cancer* **6** (3): 333-347

Cazorla M, Hernandez L, Nadal A, Balbin M, Lopez JM, Vizoso F, Fernandez PL, Iwata K, Cardesa A, Lopez-Otin C, Campo E (1998) Collagenase-3 expression is associated with advanced local invasion in human squamous cell carcinomas of the larynx. *J Pathol* **186** (2): 144-150

Chesneau V, Becherer JD, Zheng Y, Erdjument-Bromage H, Tempst P, Blobel CP (2003) Catalytic properties of ADAM19. *J Biol Chem* **278** (25): 22331-22340

Coleman RE (1997) Skeletal complications of malignancy. *Cancer* **80** (8 Suppl): 1588-1594

Dallas SL, Rosser JL, Mundy GR, Bonewald LF (2002) Proteolysis of latent transforming growth factor-beta (TGF-beta)-binding protein-1 by osteoclasts. A cellular mechanism for release of TGF-beta from bone matrix. *J Biol Chem* **277** (24): 21352-21360

Djonov V, Cresto N, Aebersold DM, Burri PH, Altermatt HJ, Hristic M, Berclaz G, Ziemiecki A, Andres AC (2002) Tumor cell specific expression of MMP-2 correlates with tumor vascularisation in breast cancer. *Int J Oncol* **21** (1): 25-30

Dougall WC, Chaisson M (2006) The RANK/RANKL/OPG triad in cancer-induced bone diseases. *Cancer Metastasis Rev* **25** (4): 541-549

Dunne AA, Sesterhenn A, Gerisch A, Teymoortash A, Kuropkat C, Werner JA (2003) Expression of MMP-2, -9 and -13 in cell lines and fresh biopsies of squamous cell carcinomas of the upper aerodigestive tract. *Anticancer Res* **23** (3B): 2233-2239

Freije JM, Diez-Itza I, Balbin M, Sanchez LM, Blasco R, Tolivia J, Lopez-Otin C (1994) Molecular cloning and expression of collagenase-3, a novel human matrix metalloproteinase produced by breast carcinomas. *J Biol Chem* **269** (24): 16766-16773

Futakuchi M, Nannuru KC, Varney ML, Sadanandam A, Nakao K, Asai K, Shirai T, Sato SY, Singh RK (2009) Transforming growth factor-beta signaling at the tumor-bone interface promotes mammary tumor growth and osteoclast activation. *Cancer Sci* **100** (1): 71-81

Guisse TA, Yin JJ, Taylor SD, Kumagai Y, Dallas M, Boyce BF, Yoneda T, Mundy GR (1996) Evidence for a causal role of parathyroid hormone-related protein in the pathogenesis of human breast cancer-mediated osteolysis. *J Clin Invest* **98** (7): 1544-1549

Hsu CP, Shen GH, Ko JL (2006) Matrix metalloproteinase-13 expression is associated with bone marrow microinvolvement and prognosis in non-small cell lung cancer. *Lung Cancer* **52** (3): 349-357

Jemal A, Siegel R, Ward E, Hao Y, Xu J, Thun MJ (2009) Cancer Statistics, 2009. *CA Cancer J Clin Oncol*

Johansson N, Airola K, Grenman R, Kariniemi AL, Saarialho-Kere U, Kahari VM (1997) Expression of collagenase-3 (matrix metalloproteinase-13) in squamous cell carcinomas of the head and neck. *Am J Pathol* **151** (2): 499-508

Johansson N, Vaalamo M, Grenman S, Hietanen S, Klemi P, Saarialho-Kere U, Kahari VM (1999) Collagenase-3 (MMP-13) is expressed by tumor cells in invasive vulvar squamous cell carcinomas. *Am J Pathol* **154** (2): 469-480

John A, Tuszynski G (2001) The role of matrix metalloproteinases in tumor angiogenesis and tumor metastasis. *Pathol Oncol Res* **7** (1): 14-23

Kakonen SM, Mundy GR (2003) Mechanisms of osteolytic bone metastases in breast carcinoma. *Cancer* **97** (3 Suppl): 834-839

Kitazawa S, Kitazawa R (2002) RANK ligand is a prerequisite for cancer-associated osteolytic lesions. *J Pathol* **198** (2): 228-236

Kondratiev S, Gnepp DR, Yakirevich E, Sabo E, Annino DJ, Rebeiz E, Laver NV (2008) Expression and prognostic role of MMP2, MMP9, MMP13, and MMP14 matrix metalloproteinases in sinonasal and oral malignant melanomas. *Hum Pathol* **39** (3): 337-343

Lacey DL, Tan HL, Lu J, Kaufman S, Van G, Qiu W, Rattan A, Scully S, Fletcher F, Juan T, Kelley M, Burgess TL, Boyle WJ, Polverino AJ (2000) Osteoprotegerin ligand modulates murine osteoclast survival in vitro and in vivo. *Am J Pathol* **157** (2): 435-448

Lacey DL, Timms E, Tan HL, Kelley MJ, Dunstan CR, Burgess T, Elliott R, Colombero A, Elliott G, Scully S, Hsu H, Sullivan J, Hawkins N, Davy E, Capparelli C, Eli A, Qian YX, Kaufman S, Sarosi I, Shalhoub V, Senaldi G, Guo J, Delaney J, Boyle WJ (1998) Osteoprotegerin ligand is a cytokine that regulates osteoclast differentiation and activation. *Cell* **93** (2): 165-176

Lynch CC, Hikosaka A, Acuff HB, Martin MD, Kawai N, Singh RK, Vargo-Gogola TC, Begtrup JL, Peterson TE, Fingleton B, Shirai T, Matrisian LM, Futakuchi M (2005) MMP-7 promotes prostate cancer-induced osteolysis via the solubilization of RANKL. *Cancer Cell* **7** (5): 485-496

- Mauviel A (1993) Cytokine regulation of metalloproteinase gene expression. *J Cell Biochem* **53** (4): 288-295
- Morony S, Capparelli C, Sarosi I, Lacey DL, Dunstan CR, Kostenuik PJ (2001) Osteoprotegerin inhibits osteolysis and decreases skeletal tumor burden in syngeneic and nude mouse models of experimental bone metastasis. *Cancer Res* **61** (11): 4432-4436
- Morrissey C, Kostenuik P, Brown L, Vessella R, Corey E (2007) Host-derived RANKL is responsible for osteolysis in a C4-2 human prostate cancer xenograft model of experimental bone metastases. *BMC Cancer* **7** (1): 148, doi:10.1186/1471-2407-7-148
- Mundy GR (2002) Metastasis to bone: causes, consequences and therapeutic opportunities. *Nat Rev Cancer* **2** (8): 584-593
- Nakao A, Imamura T, Souchelnytskyi S, Kawabata M, Ishisaki A, Oeda E, Tamaki K, Hanai J, Heldin CH, Miyazono K, ten DP (1997) TGF-beta receptor-mediated signalling through Smad2, Smad3 and Smad4. *EMBO J* **16** (17): 5353-5362
- Nannuru KC, Futakuchi M, Sadanandam A, Wilson TJ, Varney ML, Myers KJ, Li X, Marcusson EG, Singh RK (2009) Enhanced expression and shedding of receptor activator of NF-kappaB ligand during tumor-bone interaction potentiates mammary tumor-induced osteolysis. *Clin Exp Metastasis* **26** (7): 797-808
- Nelson AR, Fingleton B, Rothenberg ML, Matrisian LM (2000) Matrix Metalloproteinases: Biologic Activity and Clinical Implications. *J Clin Oncol* **18** (5): 1135
- Overall CM, Blobel CP (2007) In search of partners: linking extracellular proteases to substrates. *Nat Rev Mol Cell Biol* **8** (3): 245-257
- Pinto CA, Carvalho PE, Antonangelo L, Garippo A, Da Silva AG, Soares F, Younes R, Beyruti R, Takagaki T, Saldiva P, Vollmer RT, Capelozzi VL (2003) Morphometric evaluation of tumor matrix metalloproteinase 9 predicts survival after surgical resection of adenocarcinoma of the lung. *Clin Cancer Res* **9** (8): 3098-3104
- Powell GJ, Southby J, Danks JA, Stillwell RG, Hayman JA, Henderson MA, Bennett RC, Martin TJ (1991) Localization of Parathyroid Hormone-related Protein in Breast Cancer Metastases: Increased Incidence in Bone Compared with Other Sites. *Cancer Res* **51** (11): 3059-3061
- Roodman GD (2004a) Mechanisms of bone metastasis. *N Engl J Med* **350** (16): 1655-1664
- Roodman GD (2004b) Mechanisms of bone metastasis. *N Engl J Med* **350** (16): 1655-1664
- Roodman GD, Dougall WC (2008) RANK ligand as a therapeutic target for bone metastases and multiple myeloma. *Cancer Treatment Reviews* **34** (1): 92-101

- Ruokolainen H, Paakko P, Turpeenniemi-Hujanen T (2004) Expression of matrix metalloproteinase-9 in head and neck squamous cell carcinoma: a potential marker for prognosis. *Clin Cancer Res* **10** (9): 3110-3116
- Schlondorff J, Lum L, Blobel CP (2001) Biochemical and pharmacological criteria define two shedding activities for TRANCE/OPGL that are distinct from the tumor necrosis factor alpha convertase. *J Biol Chem* **276** (18): 14665-14674
- Selak MA, Chignard M, Smith JB (1988) Cathepsin G is a strong platelet agonist released by neutrophils. *Biochem J* **251** (1): 293-299
- Selvamurugan N, Fung Z, Partridge NC (2002) Transcriptional activation of collagenase-3 by transforming growth factor-beta1 is via MAPK and Smad pathways in human breast cancer cells. *FEBS Lett* **532** (1-2): 31-35
- Stetler-Stevenson WG (2001) The role of matrix metalloproteinases in tumor invasion, metastasis, and angiogenesis. *Surg Oncol Clin N Am* **10** (2): 383-92, x
- Tanaka S, Nakamura K, Takahashi N, Suda T (2005) Role of RANKL in physiological and pathological bone resorption and therapeutics targeting the RANKL-RANK signaling system. *Immunol Rev* **208:30-49**. 30-49
- Uria JA, Jimenez MG, Balbin M, Freije JM, Lopez-Otin C (1998) Differential effects of transforming growth factor-beta on the expression of collagenase-1 and collagenase-3 in human fibroblasts. *J Biol Chem* **273** (16): 9769-9777
- Van Wart HE, Birkedal-Hansen H (1990) The cysteine switch: a principle of regulation of metalloproteinase activity with potential applicability to the entire matrix metalloproteinase gene family. *Proc Natl Acad Sci U S A* **87** (14): 5578-5582
- Wilson TJ, Nannuru KC, Futakuchi M, Sadanandam A, Singh RK (2008) Cathepsin G enhances mammary tumor-induced osteolysis by generating soluble receptor activator of nuclear factor-kappaB ligand. *Cancer Res* **68** (14): 5803-5811
- Wilson TJ, Singh RK (2008) Proteases as modulators of tumor-stromal interaction: primary tumors to bone metastases. *Biochim Biophys Acta* **1785** (2): 85-95
- Yoneda T, Hiraga T (2005) Crosstalk between cancer cells and bone microenvironment in bone metastasis. *Biochemical and Biophysical Research Communications* **328** (3): 679-687, doi:doi: DOI: 10.1016/j.bbrc.2004.11.070
- Zhang J, Dai J, Qi Y, Lin DL, Smith P, Strayhorn C, Mizokami A, Fu Z, Westman J, Keller ET (2001) Osteoprotegerin inhibits prostate cancer-induced osteoclastogenesis and prevents prostate tumor growth in the bone. *J Clin Invest* **107** (10): 1235-1244
- Zhang J, Dai J, Yao Z, Lu Y, Dougall W, Keller ET (2003) Soluble receptor activator of nuclear factor kappaB Fc diminishes prostate cancer progression in bone. *Cancer Res* **63** (22): 7883-7890

Appendices:

1. **Nannuru KC**, Futakuchi M, Varney ML, Vincent TM, Marcusson EG, Singh RK. MMP-13 regulates mammary tumor-induced osteolysis by activating MMP9 and TGF β signaling at the tumor-bone interface. *Cancer Res* 2010; 70(9) 3494 - 504
2. **Nannuru KC**, Futakuchi M, Sadanandam A, Wilson TJ, Varney ML, Myers KJ, et al. Enhanced expression and shedding of receptor activator of NF-kappaB ligand during tumor-bone interaction potentiates mammary tumor-induced osteolysis. *Clin Exp Metastasis* 2009;26:797-808
3. Wilson TJ, **Nannuru KC**, Futakuchi M, Sadanandam A, Singh RK. Cathepsin G enhances mammary tumor-induced osteolysis by generating soluble receptor activator of nuclear factor-kappaB ligand. *Cancer Res* 2008;68:5803-11.
4. Curriculum Vitae – Kalyan C. Nannuru.

Enhanced expression and shedding of receptor activator of NF- κ B ligand during tumor–bone interaction potentiates mammary tumor-induced osteolysis

Kalyan C. Nannuru · Mitsuru Futakuchi · Anguraj Sadanandam · Thomas J. Wilson · Michelle L. Varney · Kathleen J. Myers · Xiaodong Li · Eric G. Marcusson · Rakesh K. Singh

Received: 28 April 2009 / Accepted: 23 June 2009
© Springer Science+Business Media B.V. 2009

Abstract The bone microenvironment plays a critical role in tumor-induced osteolysis and osteolytic metastasis through tumor–bone (TB)-interaction. Receptor activator of nuclear factor- κ B (RANK) ligand (RANKL) is one of the critical signaling molecules involved in osteolysis and bone metastasis. However, the regulation and functional significance of RANKL at the TB-interface in tumor-induced osteolysis remains unclear. In this report, we examined the role of tumor–stromal interaction in the regulation of RANKL expression and its functional significance in tumor-induced osteolysis. Using a novel mammary tumor model, we identified that RANKL expression was upregulated at the TB-interface as compared to the tumor alone area. We demonstrate increased generation of sRANKL at the TB-interface, which is associated with tumor-induced osteolysis. The ratio of RANKL to osteoprotegerin (OPG), a decoy receptor for RANKL, at the TB-interface was also increased. Targeting RANKL expression with antisense oligonucleotides (RANKL-ASO), significantly abrogated tumor-induced

osteolysis, decreased RANKL expression and the RANKL:OPG ratio at the TB-interface. Together, these results demonstrate that upregulation of RANKL expression and sRANKL generation at the TB-interface potentiates tumor-induced osteolysis.

Keywords Bone metastasis · RANKL · Soluble RANKL · Tumor–bone interaction · Tumor-induced osteolysis · Anti-sense therapeutics

Introduction

Breast cancer is the most common cancer among women in the United States. Annually, breast cancer is responsible for over 40,000 deaths, making it the second leading cause of cancer death [1]. A large portion of breast cancer-related mortality is due to metastatic disease rather than the primary tumor itself. Breast cancer cells demonstrate strong predilection for metastasis to bone resulting in lesions that are predominantly osteolytic. These lesions significantly reduce the quality of life of the patient by causing intractable bone pain, anemia, hypercalcemia, increasing the risk of pathologic fracture and dramatically increase the risk of mortality [2–4].

Malignant breast cancer cells entry to bone microenvironment initiates a vicious cycle of bidirectional communication between tumor and stromal cells that promotes osteolytic metastases [2, 5, 6]. One of the critical signaling molecules involved in this cycle is receptor activator of NF- κ B ligand (RANKL). RANKL is a membrane-bound protein expressed on the cell surface of osteoblasts and bone marrow stromal cells [6–9]. Binding of RANKL to its receptor, RANK, expressed on the surface of osteoclast precursors leads to their differentiation into mature

K. C. Nannuru · A. Sadanandam · T. J. Wilson · M. L. Varney · R. K. Singh (✉)
Department of Pathology and Microbiology, 985845 Nebraska Medical Center, University of Nebraska Medical Center, Omaha, NE 68198-5845, USA
e-mail: rsingh@unmc.edu

M. Futakuchi
Department of Molecular Toxicology, Nagoya City University, Nagoya City, Nagoya, Japan

K. J. Myers · X. Li · E. G. Marcusson
Isis Pharmaceuticals, Carlsbad, CA, USA

osteoclasts [7, 8, 10]. Another molecule intimately tied to the RANKL-RANK signaling axis is osteoprotegerin (OPG) which is a soluble, decoy receptor of RANKL that prevents RANKL from engaging RANK and initiating signaling [7, 8, 11]. Malignant cells secrete soluble factors such as parathyroid hormone related peptide (PTHrP) that up-regulates RANKL expression [12] and enhanced RANKL signaling appears to be the driving force behind tumor-induced osteolytic lesions [12–17]. However, very little is known about the role of tumor–bone interaction in regulation of RANKL expression.

While RANKL-RANK signaling is critical to the osteolytic metastasis, it is also the rate limiting step of the cycle since signaling requires cell to cell contact to bring both membrane-bound proteins into contact. One mechanism by which this requirement can be bypassed is the generation of a soluble form of RANKL (sRANKL) that allows widespread osteoclast activation. Recently, Cathepsin G was identified as a protein that is upregulated at the TB-interface of mammary tumor-induced osteolytic lesions and was shown to be capable of generating sRANKL [18, 19]. Other proteases known to be capable of generating sRANKL include matrix metalloproteinase (MMP)3, MMP7, a disintegrin and metalloproteinase (ADAM)-17, and ADAM-19 [20–22]. Inhibition of Cathepsin G significantly reduced mammary tumor-induced osteolysis suggesting the importance of sRANKL [18]. However, while the centrality of RANKL-RANK signaling has been clearly established the relative contributions of RANKL and sRANKL during TB-interactions remain unclear.

In the present study, we sought to determine the functional significance of RANKL during tumor–stromal interaction in mammary tumor-induced osteolytic lesions. Our data demonstrate upregulation of RANKL expression and generation of sRANKL at the TB-interface in tumor-induced osteolysis. Furthermore, targeting RANKL expression using antisense-RANKL oligonucleotide decreased RANKL levels and RANKL:OPG ratio at the TB-interface and significantly reduced tumor-induced osteolysis.

Materials and methods

Animal model and tissue sample processing

4T1 (highly metastatic), Cl66 (moderately metastatic), and Cl66M2 (low metastatic), three murine mammary adenocarcinoma cell lines with different metastatic potentials [23–29] syngeneic to BALB/c mice, were used in this study. All cell lines were maintained in Dulbecco's Modified Eagle Media (DMEM) (Mediatech, Hendon, VA) with 5% serum supreme (Biowhitaker, Walkersville, MD), 1%

vitamins, 1% L-glutamine, and 0.08% gentamicin (Invitrogen, Carlsbad, CA).

Six to eight week old female BALB/c mice (NCI, Bethesda, MD) were used in this study. All mice were maintained in accordance with the Institutional Animal Use and Care Committee of the University of Nebraska Medical Center. Mammary tumor cells (5×10^4 cells/50 μ l) mixed in growth-factor reduced Matrigel (BD Biosciences, San Jose, CA) were injected directly onto the calvaria to mimic the close association of tumor cells and cells of the bone microenvironment [12, 18, 20]. Tumor growth was monitored and animals were sacrificed at 4 weeks post-implantation. The tumor and the underlying bone tissues were dissected into two halves, one half being used for histology sections and the other half used for micro-dissecting the tumor alone area and the TB interface for further analysis.

For histological examination and immunohistochemistry, the samples were fixed with periodate-lysine-paraformaldehyde at 4°C for 48 h. The tissues were then transferred into a decalcification solution (15% EDTA with glycerol, pH 7.4) for 4 weeks and were subsequently paraffin embedded and processed for histology.

Total RNA was extracted using Trizol (Invitrogen, Carlsbad, CA) following the manufacturer's instructions. The RNA concentration was quantified using a NANO drop ND-1000 Spectrophotometer (Nano Drop Technologies, Wilmington, DE).

Protein was extracted from the samples using T-PER tissue protein extractor solution (Pierce, Rockford, IL) following the manufacturer's provided protocol. Protein samples were quantified using a BCA protein assay kit (Pierce, Rockford, IL).

Microarray analysis and quantitative real time PCR (qRT-PCR)

Calcified frozen sections were serially sectioned in 10- μ m thick slices and at least ten slides per mouse were micro-dissected with careful separation of the TB-interface and the tumor alone areas. Total RNA was extracted from each micro-dissected population, pooled and an equal amount of RNA was amplified using a probe amplification kit (Affymetrix, Santa Clara, CA). An Affymetrix Mouse Expression Array 430 was used for comparing gene expression profiles between the TB-interface and the tumor alone areas. A complete detection and analysis of signals for each chip was performed using Affymetrix GeneChip[®] Operating Software to generate raw expression data. A signal log ratio algorithm was used to estimate the magnitude of change of a transcript when two arrays are compared (experimental versus baseline). It is calculated by comparing each probe pair on the

experimental array, here the TB-interface, to the corresponding probe pair on the baseline array, here the tumor alone area, and considering the mean of the log ratios of probe pair intensities across the two arrays. The change is expressed as the \log_2 ratio. Thus, a signal log ratio of 1.0 indicates an increase of transcript level by twofold and -1.0 indicates a decrease by twofold. For each set of tissue from 4T1, Cl66 and Cl66M2, the signal log ratio of the TB-interface versus the tumor alone area was calculated, and the genes were ordered from highest to lowest expression levels.

Gene expression analysis was confirmed using qRT-PCR for the TB-interface and tumor alone area samples. 5 μg of RNA from each sample was used to synthesize first strand cDNA. 2 μl of 1:100 diluted first strand cDNA were amplified in a 20 μl reaction with SYBR green master mix (Roche, Indianapolis IN) and 10 mM primer mix using a Bio-Rad iCycler (Bio-Rad, Hercules, CA). The following reaction conditions were used: initial denaturation at 95°C for 3 min, followed by amplification cycles with denaturation at 95°C for 60 s, annealing at 60°C for 60 s, and extension at 72°C for 60 s, and finally a long extension at 72°C for 2 min. Primers used for RANKL were 5'-TTA GCA TTC AGG TGT CCA ACC-3' and 5'-CGT GGG CCA TGT CTC TTA GTA-3'; and for glyceraldehyde-3-phosphate dehydrogenase (GAPDH) were 5'-AGC CTC GTC CCG TAG ACA AAA-3' and 5'-GAT GAC AAG CTT CCC ATT CTC G-3'. The fluorescence intensity of double-strand specific SYBR Green, reflecting the amount of formed PCR-product, was monitored at the end of each elongation step. The *ct* value for each gene was normalized with GAPDH expression for relative gene expression analysis.

Immunohistochemistry and TRAP staining

RANKL protein expression was evaluated by immunohistochemistry on tumor sections using a RANKL-specific antibody (Santa Cruz Biotechnology, Santa Cruz, CA). The sections were deparaffinized using EZ dewax solution (Biogenex, San Ramon, CA). For antigen retrieval, the sections were boiled in 0.1 M citrate buffer (pH 6.0) for 10 min and endogenous peroxidase activity was blocked using 3% H_2O_2 for 5 min. The sections were then blocked in antibody diluent for 1 h at room temperature. RANKL antibody was diluted 1:100 in blocking solution and sections were incubated overnight at 4°C. After washing, the slides were incubated with anti-goat biotinylated antibody for 30 min at room temperature. After washing, immunoreactivity was detected using Vectastain ABC and DAB substrate kits (Vector Laboratories, Burlingame, CA). Sections were counterstained with hematoxylin, dehydrated, and permanently mounted.

Tartrate resistant acid phosphatase (TRAP) staining was performed to detect activated osteoclasts in vivo according to the manufacturer's instructions (Sigma Chemicals, St. Louis, MO). For quantitative analysis, immunostained sections were examined under a Nikon light microscope. The number of positive cells was assessed at a magnification of 400 \times for each lesion.

Enzyme linked immunosorbent assay (ELISA) for RANKL and OPG

Quantitative determination of RANKL and OPG levels at the TB-interface and tumor alone area was performed using a commercially available ELISA kit (Biomedica, Vienna, Austria: Cat:BI20522) according to the manufacturer's instructions. Briefly, pre-coated wells were incubated with samples or recombinant standard and biotinylated antibody for 3 h. After washing, the reactivity was detected using streptavidin-HRP conjugate and tetramethylbenzidine substrate solution. The reaction was stopped and absorbance was determined at 450 nm, with correction at 540 nm using an ELx800 ELISA plate reader (BioTek, Winooski, VT). The sensitivity of these kits were 0.4 pmol/l for sRANKL and 0.14 pmol/l for OPG.

Western blot analysis

Tissue lysates (50 μg) from microdissected tumor alone area and TB-interface were separated on a 12% SDS-polyacrylamide gel and then electrotransferred to a PVDF membrane. The membrane was then washed with 0.1% Tween-Tris-buffered saline (TTBS). The membrane was then blocked overnight in 5% bovine serum albumin (BSA) in phosphate buffered saline (PBS) and blotted with 1:500 anti-RANKL antibody that recognizes an epitope near the C-terminus of RANKL (Santa Cruz Biotechnology, Santa Cruz, CA) and anti-GAPDH antibody (Cell Signaling Technology Inc, Danvers, MA) diluted in TTBS. After washing in TTBS, the membrane was incubated for 60 min with 1:1500 anti-goat-HRP diluted in TTBS. Finally, after washing with TTBS, the membrane was developed using an ECL Plus Western Blotting Detection System (GE Healthcare) per manufacturer's protocol and imaged using a Typhoon 9410 Variable Mode Imager (GE Healthcare). The bands for RANKL, sRANKL and GAPDH were quantified and compared using ImageQuant 5.1 (GE Healthcare).

Treatment with antisense oligonucleotides for inhibition of RANKL expression and osteolysis

Antisense oligonucleotides (ASO) used in the therapeutic protocol were obtained from Isis Pharmaceuticals,

Carlsbad, CA. These ASOs, used throughout this study, were designed specific to RANKL. 2'-methoxyethyl modified chimeric ASOs are synthesized as previously described [30]. These oligonucleotides are modified at the 2' sugar position of the five bases at both the 3' and 5' ends with a methoxyethyl group. This modification greatly increases the stability of the oligonucleotides and the affinity for its target mRNA while reducing the amount of immune stimulatory and inflammatory effects that can be seen with oligonucleotides in mice [31]. Active ASOs were identified by screening 46 ASOs designed to be specific for RANKL. These ASOs were transfected into cells and RNA was isolated 24 h later. RANKL mRNA levels were determined by RT-PCR and the most effective ASOs were identified. The efficacy of these ASOs was confirmed in concentration-response experiments and the most potent ASO was used for further experiments. The sequence of this ASO is GTC TTA CAC ATG TAT AGA CA. As a negative control, we used an oligonucleotide with the same chemical modifications, but a sequence, TCT TAT GTT TCC GAA CCG TT, that did not match any known mRNA in the mouse genome.

To determine the effect of inhibition of RANKL expression using ASOs, animals bearing Cl66 mammary tumors were randomly divided into two treatment groups (control-ASO and RANKL-ASO). The oligonucleotides were dissolved in normal saline (0.9% NaCl) and were administered by intraperitoneal (i.p.) injection at a dose of 50 mg/kg/day starting at day 7 following tumor implantation for 5 days with 2 days off followed by another 4 days (see Fig. 5A). Tumor growth was monitored and mice were sacrificed on day 28. Tumor alone and TB-interface samples were collected and processed for further analysis.

Statistical analysis

The significance of the *in vitro* data was determined by Student's *t*-test (two-tailed) using SPSS software (SPSS, Chicago, IL). *In vivo* analysis was performed using Wilcoxon signed rank test and Mann-Whitney *U*-test of significance. A value of $P < 0.05$ was deemed significant.

Results

Osteoclast activation and osteolysis is similar between cell lines

Mammary tumor cells 4T1, Cl66, and Cl66M2, were transplanted onto the calvaria of BALB/c mice and tumor growth was monitored. Histochemical analysis demonstrated that all tumors exhibited tumor-induced osteolysis

and osteoclast activation similar to that observed in breast cancer bone metastasis (Fig. 1). The degree of osteolysis was assessed by calculating the bone destruction index (BDI), calculated by comparing the ratio of the length of bone completely destroyed by the tumor cells to the total length of the bone at the tumor-bone interface (Fig. 1B). We did not observe any difference in bone destruction index between the three cell lines with the BDI being 45–50% for all three cell lines (Fig. 1B). Similarly, we observed no significant difference in the number of TRAP-positive osteoclasts at the tumor-bone interface among tumors from the three different cell lines (Fig. 1C, D). Furthermore, the number of osteoclasts at the TB-interface was associated with the bone destruction index (Fig. 1B, D).

RANKL is upregulated at the tumor-bone interface

We utilized microarray analysis to examine the gene expression pattern at the TB-interface compared to the tumor alone area in tumors derived from all three cell lines (Fig. 2). We observed a set of 414 genes commonly upregulated among the three cell lines and 27 genes commonly down-regulated among the three cell lines at the TB-interface compared to the tumor alone area. Three highly upregulated genes included integrin binding bone sialoprotein, RANKL, and MMP13. From these genes, we selected RANKL for further analysis (Fig. 2A, B). We did not observe any significant difference in RANK expression at the TB-interface compared to the tumor alone area (data not shown). We validated the microarray data using qRT-PCR. We observed upregulation of RANKL mRNA at the TB-interface compared to the tumor alone area in all three groups (Fig. 2C).

We further validated upregulation of RANKL at the tumor-bone interface by using immunohistochemical analysis to demonstrate upregulation of RANKL at the protein level. In agreement with the mRNA expression data, we observed higher expression of RANKL protein at the TB-interface (Fig. 2D). Osteoblasts, stromal cells and tumor cells at the TB-interface stained strongly positive for RANKL [Fig. 2D-ii (lower magnification); 2D-iii (higher magnification)]. In contrast, low expression of RANKL was observed in the tumor alone area (Fig. 2D-i).

RANKL, sRANKL and OPG expression at the TB-interface

To attempt to decipher the relative contributions of membrane-bound RANKL and sRANKL at the tumor-bone interface, we next analyzed expression of sRANKL, the cleaved form of membrane-bound RANKL in mice bearing Cl66 tumors. In addition, we also analyzed the expression of OPG, a soluble decoy receptor of RANKL. Expression

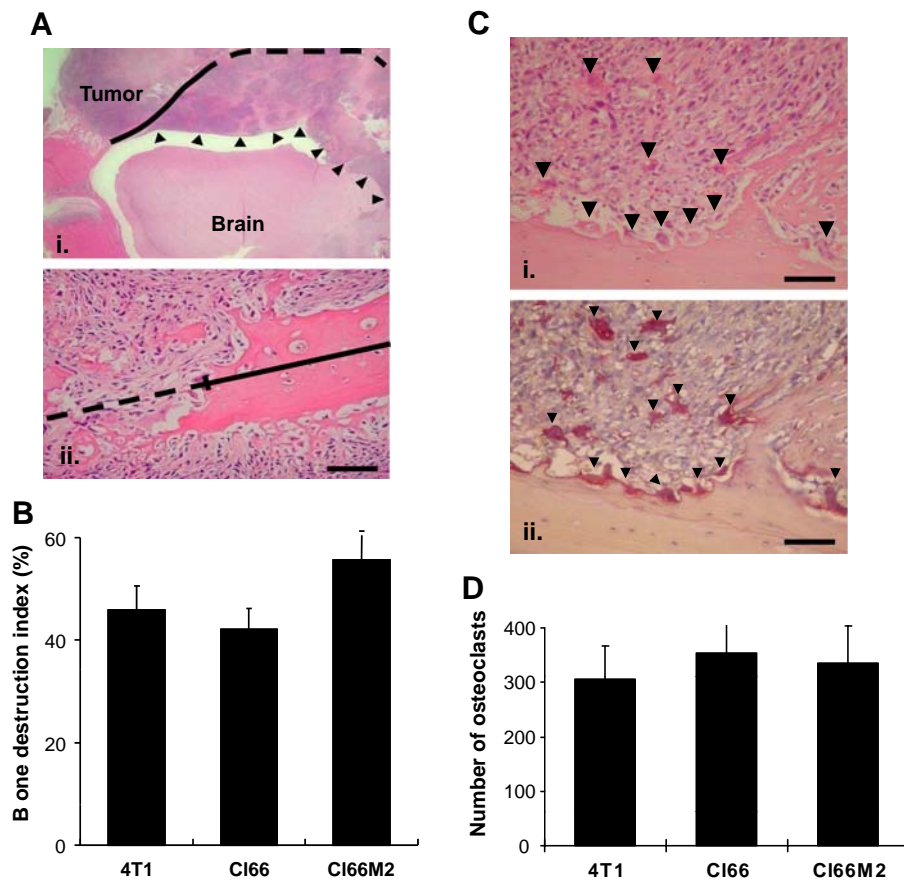


Fig. 1 Mammary tumor-induced osteolytic changes. **A** H&E staining of the tumor bone interface from Cl66 tumors implanted mice; **i** low magnification (20×); **ii** higher magnification (200×) to demonstrate the tumor-bone interface. The levels of tumor-induced osteolysis in H&E-stained sections were measured by comparing length of the completely resorbed bone (*dotted line*) and areas of no bone destruction (*solid lines*). Arrows indicate cranial invasion and growth of tumors. **B** The bone destruction index in 4T1, Cl66 and Cl66M2 tumors. BDI was measured on at least two different sections for each

mice and average value of BDI calculated from the measurements of all the mice in the group. **C** **i** H&E-stained section to demonstrate the presence of osteoclasts at the Tumor Bone interface during intracranial penetration and growth of tumor (*arrows heads*); **ii** TRAP-positive multinucleated cells as osteoclasts counted along the total length of the TB-interface (*arrow heads*). **D** The number of TRAP-positive osteoclasts in 4T1, Cl66 and Cl66M2 tumors. The values are mean ± SEM ($n = 5$ mice per group). *Scale bars* represent 0.01 mm

of both proteins was analyzed using ELISA specific for OPG and RANKL. Similar to RANKL mRNA expression, the levels of RANKL at the TB-interface were significantly higher compared to the tumor alone area in all tumors examined (Fig. 3A). We did not observe any significant difference in the level of OPG at the TB-interface compared to the tumor alone area (data not shown).

We then examined the ratio of RANKL to OPG at the TB-interface and tumor alone area. Results shown in Fig. 3B demonstrate an increased RANKL:OPG ratio at the TB-interface compared to the tumor alone area for all tumors. Together, these data demonstrate upregulation of RANKL and likely upregulation of free, active sRANKL during tumor-induced osteolysis.

We further examined the proportions of RANKL and sRANKL at the TB-interface using Western blot analysis

with an antibody capable of detecting both full-length, membrane-bound RANKL (~36 kDa) and sRANKL (~24kDa) (Fig. 4A). Similar to ELISA results, a significant difference in the levels of RANKL and sRANKL were observed at the TB-interface compared with the tumor alone area (Fig. 4B). These data further confirmed that in addition to upregulation of RANKL expression, there was also increased generation of sRANKL at the TB-interface of mammary tumor-induced osteolytic lesions.

Inhibiting RANKL expression abrogates mammary tumor-induced osteolysis

Next, we evaluated the functional significance of enhanced RANKL expression and increased soluble

RANKL levels during tumor–bone interaction. To determine the functional role of RANKL and soluble RANKL in tumor induced osteolysis, we used ASOs to knock down RANKL expression in Cl66 tumor bearing mice. We did not observe any weight loss or toxicity in any of the treatment groups (data not shown). In addition, we did not observe any significant difference in tumor growth between RANKL-ASO and control-ASO groups (data not shown).

H&E staining of tumor sections demonstrated severe bone destruction in control-ASO treated tumors (Fig. 5B-i) whereas RANKL-ASO treated tumors showed very little or no osteolysis (Fig. 5B-ii). We observed a significant inhibition in RANKL expression at the TB-interface in RANKL-ASO treated group as compared to control-ASO treated group (Fig. 5F). We quantified the severity of lesion by measuring bone destruction index and observed a significant decrease in osteolysis in the RANKL-ASO treated group compared to the control-ASO treated group (Fig. 5C). Activated osteoclasts are responsible for osteolysis, hence we analyzed whether RANKL targeting has any effect on osteoclast activation and number at the tumor bone interface. TRAP staining was used to enumerate activated osteoclasts at the TB interface (Fig. 5D). We observed a significant decrease in activated osteoclasts per microscopic field at the TB interface in RANKL-ASO treated mice compared to control-ASO treated group (Fig. 5E). Decreased osteoclast number observed in RANKL-ASO treated group is in association with inhibition of tumor induced osteolysis.

We then examined the expression of RANKL in tumors from RANKL-ASO and control-ASO treated animals using qRT-PCR. The expression of RANKL at the TB-interface was significantly lower in the RANKL-ASO treated group as compared to the control-ASO treated group (Fig. 5F). We observed low levels of RANKL expression in the tumor alone area which was not altered by RANKL-ASO treatment (Fig. 5F).

Next, we analyzed the effect of RANKL-ASO on the levels of RANKL and OPG proteins in tumors. Similar to RANKL mRNA expression, knocking down expression of RANKL using RANKL-ASO inhibited RANKL protein levels at the TB-interface (Fig. 6A). We also observed a concomitant increase (but not significantly different) in the level of OPG at the TB-interface in the RANKL-ASO treated group compared to the control-ASO treatment (Fig. 6B).

With a decrease in RANKL at the TB-interface of RANKL-ASO treated animals, there was a significant decrease in the RANKL:OPG ratio following RANKL-ASO treatment (Fig. 6C). These studies demonstrate that knocking down RANKL expression at the TB-interface inhibits generation of RANKL, decreases RANKL to

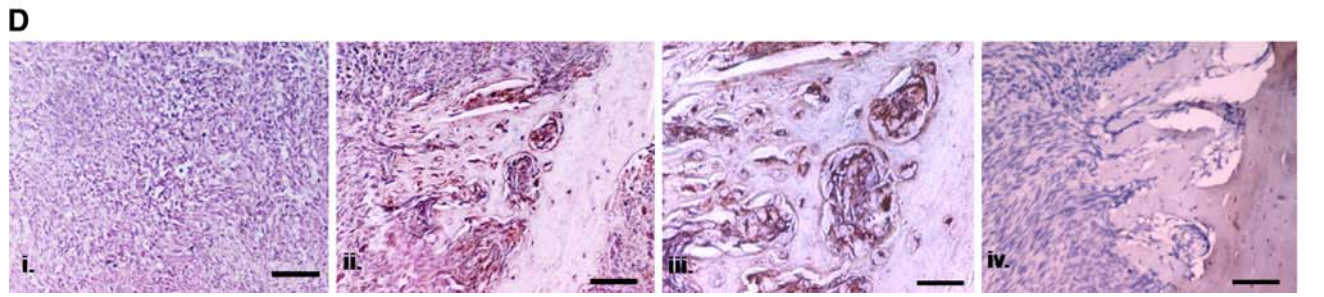
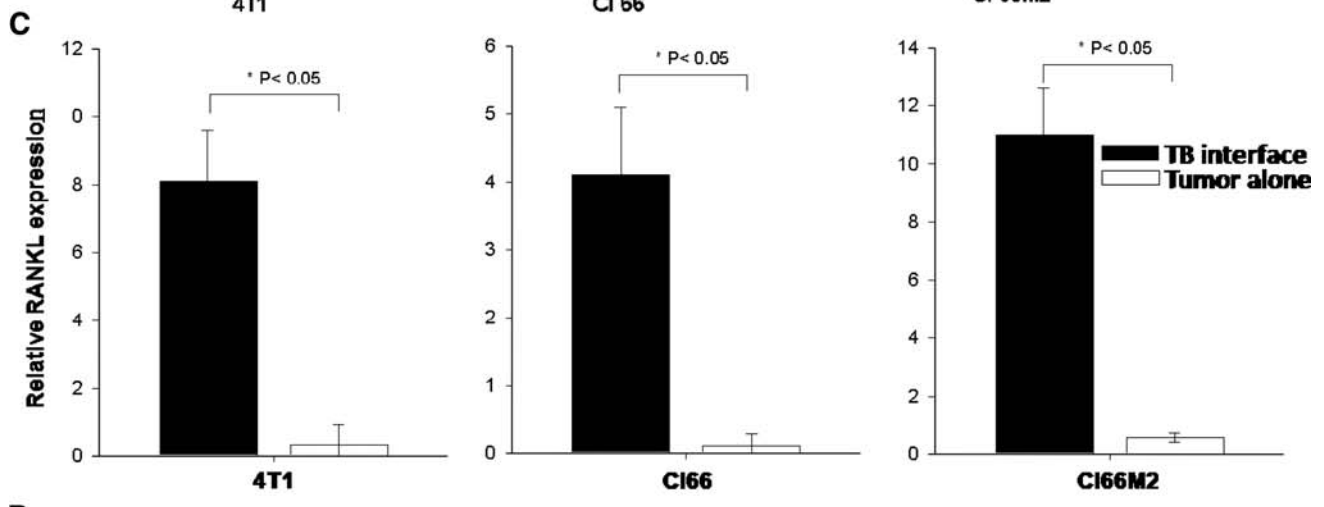
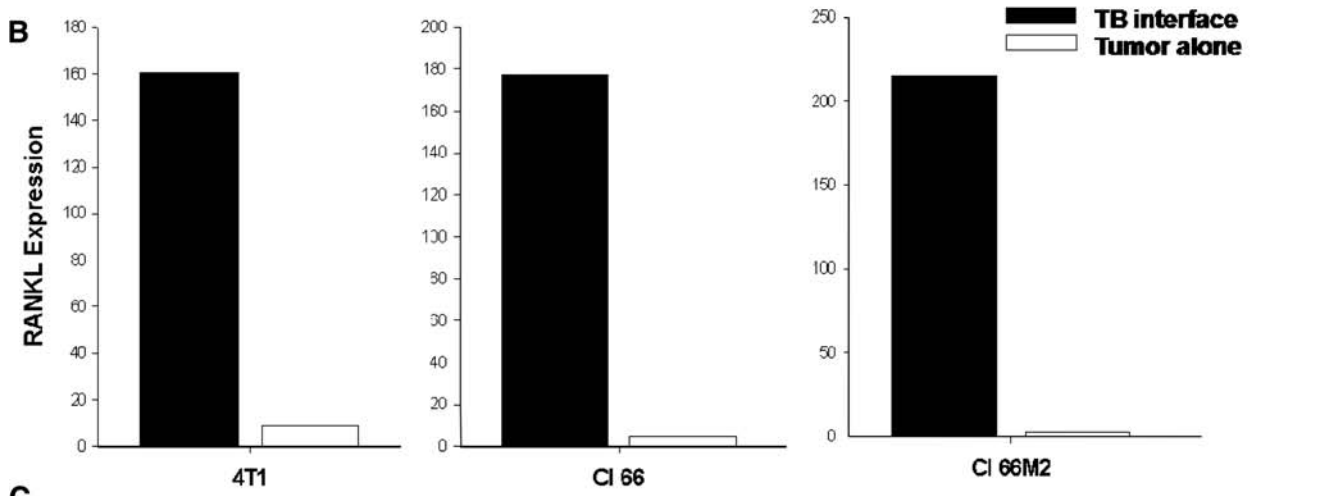
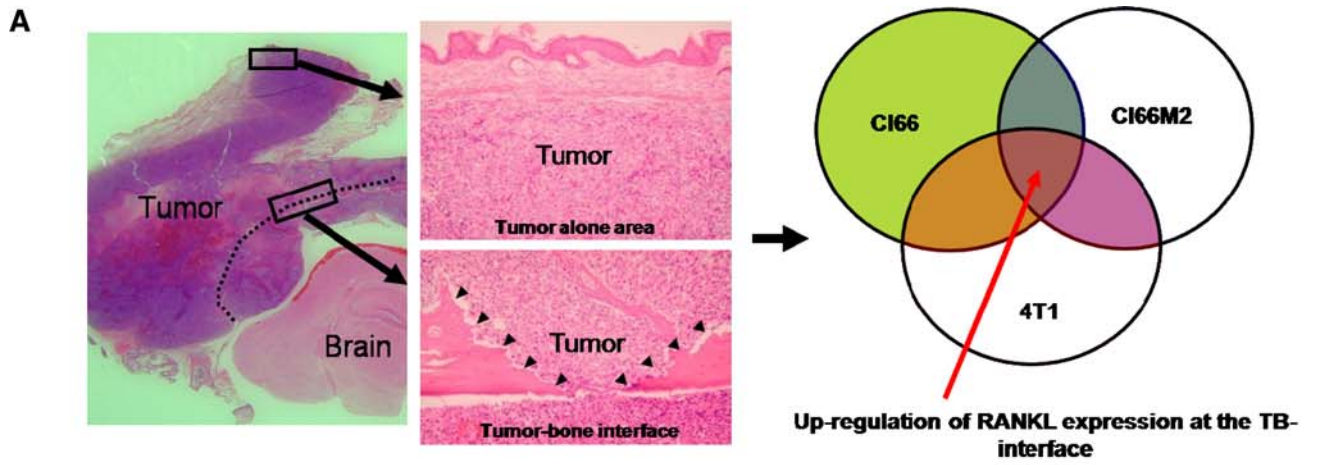
OPG ratios, and inhibits mammary tumor-induced osteolysis.

Discussion

Breast cancer bone metastasis depends on the interaction of tumor cells with the bone microenvironment which triggers a ‘vicious cycle’ leading to osteoclast activation and bone destruction [5, 32, 33]. The cellular and molecular regulators of tumor–stromal interaction in osteolytic bone metastasis remain unclear. Understanding the bidirectional communication that occurs between tumor cells and bone stromal cells has the potential to reveal potential therapeutic targets that would abrogate osteolysis and significantly improve the quality of life for breast cancer patients.

Using a syngeneic murine model and three mammary tumor cell lines, we demonstrated that RANKL expression was commonly up-regulated at the TB-interface as compared to the tumor alone area. Several studies have implicated the role of RANKL in the vicious cycle of osteolytic bone metastasis [34]. RANKL is the key stimulator of bone resorption; however, the relative abundance and importance of RANKL produced by malignant cells and host cells during tumor–bone interaction remains unclear. In the present study, we demonstrated that RANKL is predominantly expressed at the TB-interface. Both tumor cells and bone stromal cells, including osteoblasts at the TB-interface, expressed RANKL. This data agrees with a recent report in a prostate cancer model that utilized a xenograft model of human tumor cells into a murine host to decipher the relative contributions of RANKL from the tumor cells versus the bone stromal cells [9]. In contrast, we observed very little RANKL expression in the tumor alone areas. The expression of RANKL at the TB-interface coincided

Fig. 2 Upregulation of RANKL expression at the tumor-bone interface. **A** Samples were microdissected to separate the tumor alone area from the tumor-bone interface for each of the three mammary tumor cell lines. Analysis of Affymetrix Gene Arrays from these samples identified upregulated genes. RANKL was among the genes commonly upregulated at the tumor-bone interface in all three cell lines. **B** Microarray analysis demonstrated that RANKL is upregulated at the tumor-bone interface in all three cell lines. **C** qRT-PCR confirmed that RANKL is upregulated at the tumor-bone interface in all three cell lines. The values are mean \pm SEM. This is a representative of three experiments with similar results. **D** Immunohistochemistry of tumor sections stained with RANKL specific antibody depicts increased RANKL staining at the tumor-bone interface (**ii** 200 \times ; **iii** 400 \times) compared to the tumor alone area (**i** 200 \times), antibody control shows no non specific staining (**iv** 200 \times). Scale bars represent 0.01 mm



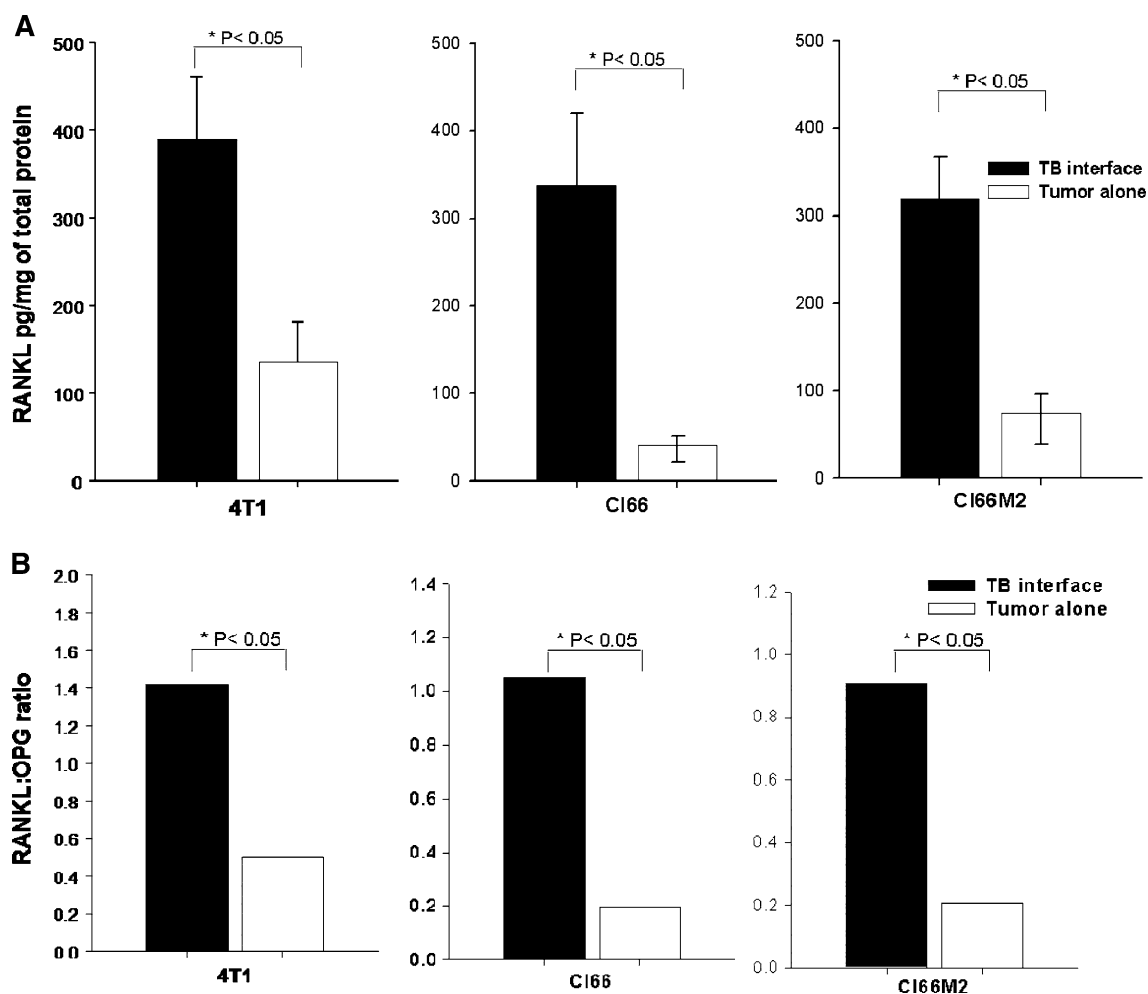


Fig. 3 RANKL and OPG levels at the tumor-bone interface. RANKL was upregulated at the tumor-bone interface compared to the tumor alone area (A) as demonstrated by ELISA. B The RANKL:OPG ratio was significantly increased at the tumor-bone interface compared to

the tumor alone area in all three cell lines used. The values are mean \pm SEM. This is a representative of three experiments with similar results

with increased osteolysis and numbers of activated osteoclasts, suggesting that tumor–stromal interactions regulate RANKL-mediated osteoclast activation and tumor-induced osteolysis.

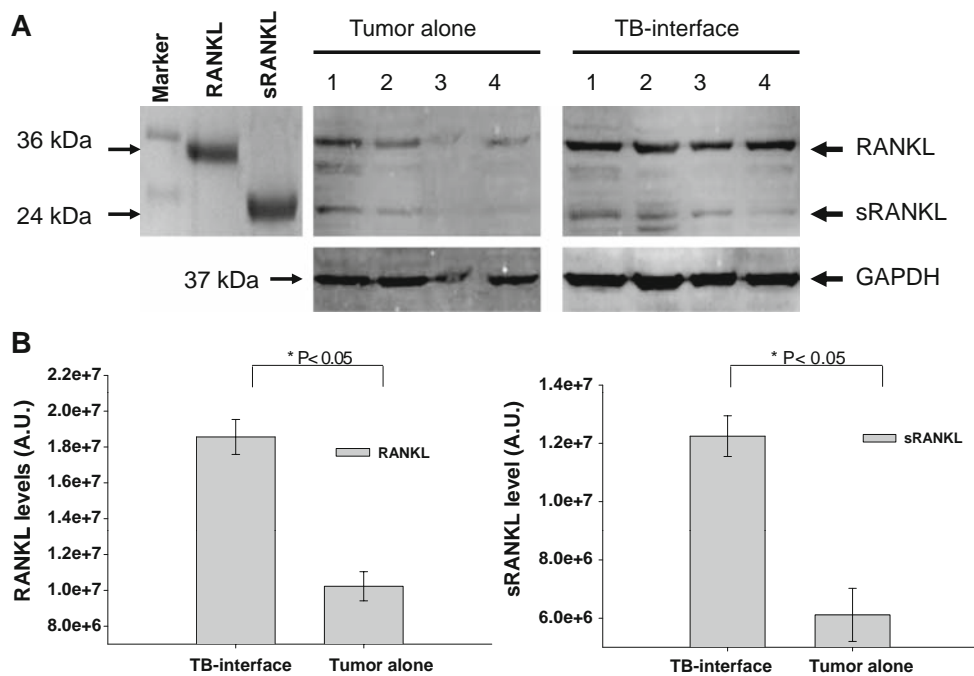
A major barrier to progress in identifying the molecular mechanism(s) of osteolytic breast cancer bone metastasis is the lack of appropriate animal models that fully reflect the biology of human breast cancer metastasis to bone [35, 36]. These models of human bone metastasis of breast cancer produce mixed osteolytic lesions which make it difficult to examine the tumor–stromal interactions. In this study, we used a bone invasion model that mimics the osteolytic changes associated with human cancer [12, 18, 20]. This model allows focused study of the molecular mechanisms governing osteolysis by creating a distinct TB-interface. We used three murine mammary tumor cell lines 4T1, C166 and C166M2, which are derived from a spontaneous

mammary carcinoma in a BALB/c mouse and that exhibit different patterns of spontaneous and experimental lung metastasis [23, 37]. While these three cell lines demonstrate markedly different metastatic potential, we found that each of the three cell lines establish osteolytic lesions in bone when directly implanted and do not differ in their osteolytic potential.

The importance of RANKL signaling at the tumor-bone interface remains unclear [12]. Suppression of the RANKL-RANK signaling axis abrogates both tumor-induced osteolysis and osteolysis associated with arthritis [13–17]. However, little is known about the relative importance of the soluble form of RANKL (sRANKL) in tumor-induced osteolysis. Both MMP7 and Cathepsin G have been shown to be capable of shedding the extracellular domain of RANKL, generating active sRANKL that is capable of inducing widespread osteoclast

Fig. 4 RANKL and sRANKL proteins during tumor-induced osteolysis. **A** Tissue lysates from tumor alone areas and TB-interface from four different mice (indicated as 1,2,3 and 4) bearing Cl66 tumors were examined for RANKL and sRANKL levels using Western blot analysis. The antibody used in the analysis detects ~36 kDa (membrane bound RANKL) and ~24 kDa (sRANKL).

B Quantitation of the levels of RANKL and sRANKL was performed using ImageQuant analysis software (GE Biosciences). The levels of RANKL and sRANKL were determined as presented as arbitrary units (A.U.). The values are mean \pm SEM. This is a representative of three experiments with similar results



activation [18, 19]. Both RANKL and RANK are membrane-bound proteins and thus require cell to cell contact between RANKL-expressing cells and RANK-expressing cells in order to initiate signaling. Thus, osteoclast activation via RANK activation is limited spatially to the area surrounding RANKL-expressing cells. The significance of the generation of sRANKL lies in the ability to bypass this cell-cell contact requirement and trigger widespread osteoclast activation without any spatial limitation. Accordingly, in these models, inhibition of MMP7 or Cathepsin G significantly reduced tumor-induced osteolysis providing indirect evidence for the importance of sRANKL [18–20]. For the first time, we demonstrate that sRANKL is upregulated at the TB-interface of mammary tumor-induced osteolytic lesions. Importantly, we did not observe a concomitant increase in OPG levels at the tumor-bone interface. Furthermore, the elevated RANKL:OPG ratio that we observed at the tumor-bone interface suggests that not only is there an elevation in absolute RANKL levels but there is also an elevation in the level of free, functional sRANKL that is capable of binding to RANK yielding osteoclast differentiation and activation.

Inhibition of RANKL expression using RANKL-ASO inhibited tumor-induced osteolysis demonstrating the centrality of RANKL signaling in mammary tumor-induced osteolysis. RANKL levels were significantly reduced at the TB-interface of RANKL-ASO treated mice. Interestingly, OPG levels were increased at the TB-interface in these mice. The combination of decreased RANKL expression at the TB-interface and increased OPG led to a significantly

decreased RANKL:OPG ratio. Previous studies have suggested the importance of the sRANKL:OPG ratio in serum as a prognostic indicator in osteolytic bone metastasis [38–41]. Our report suggests that this serum prognostic factor is likely a reflection of what is occurring in the bone micro-environment at the TB-interface.

Studies in the animal model of bone metastasis suggest that malignant breast cancer cells and clinical data demonstrate that bone resorption is associated with progression of bone metastases [2, 5, 6, 42–45]. Preclinical studies demonstrate that animals pretreated with bisphosphonate prior to bone colonization of breast cancer cells, showed significant reduction in the number and progression of bone metastases [46–48]. However, bisphosphonate treatment in animals with established bone metastasis did not consistently inhibit disease progression, despite a substantial anti-osteolytic effect, which could be due to elimination of bone forming osteoblasts by the tumor cells [46–49]. Furthermore, in human patients bisphosphonates have been shown to affect bone density, but not overall survival of breast cancer patients [44, 50, 51]. These studies suggest that the vicious cycle might be critical for initial steps during bone metastasis and later on malignant cells become independent of bone-derived growth factors [48]. Therefore, novel therapeutic strategies to prevent and treat breast cancer bone metastases are required.

In summary, the present study demonstrated the importance of RANKL signaling at the TB-interface of mammary tumor-induced osteolytic lesions, supporting

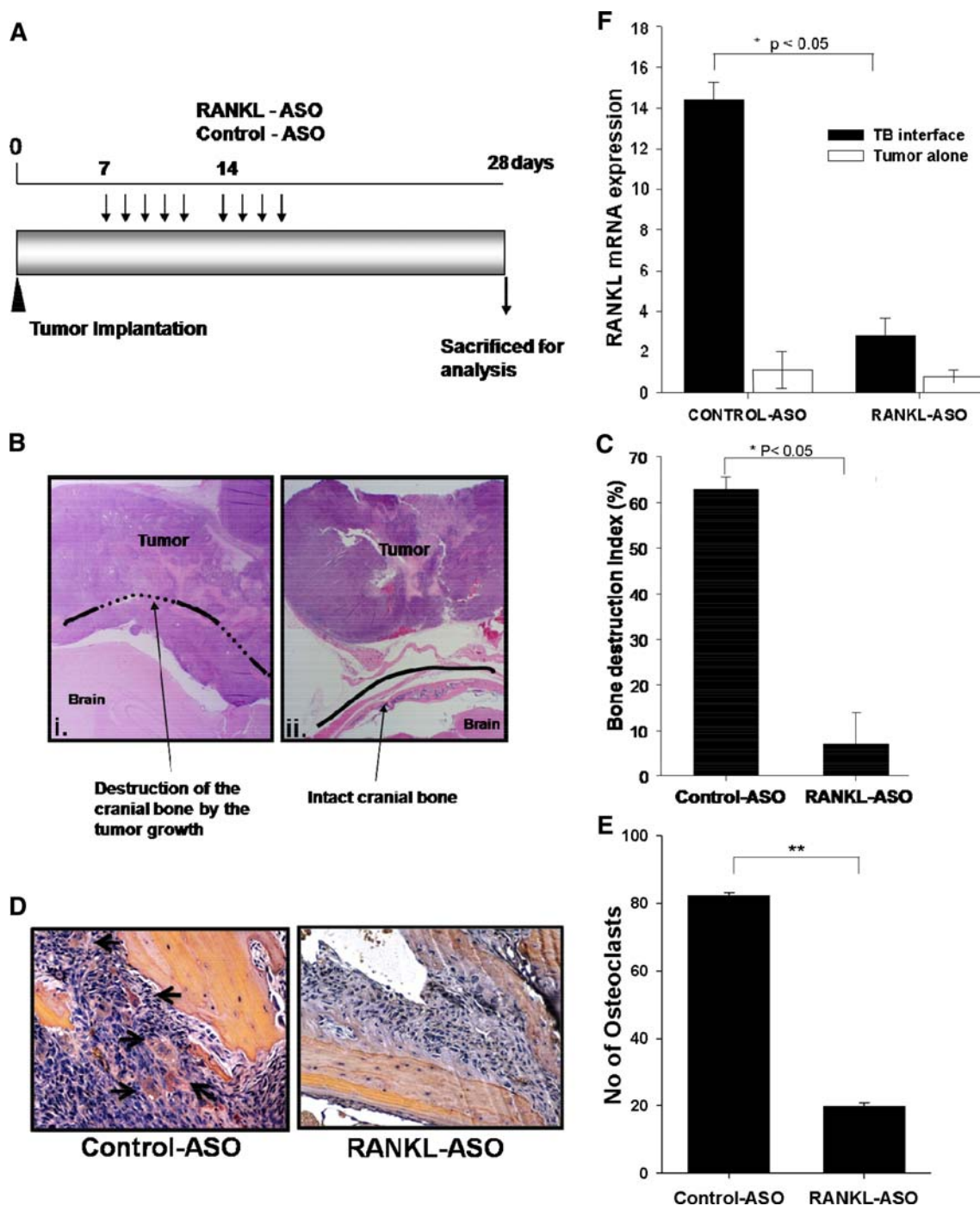


Fig. 5 Inhibition of RANKL expression abrogated tumor-induced osteolysis. **A** Experimental strategy for treatment of Cl66 tumor bearing mice with RANKL-ASO and control-ASO. **B** H&E-stained section (20 \times magnification) of tumors from control-ASO (i) and RANKL-ASO (ii) treated animals. *Solid line* represents intact bone and the *dotted line* shows the osteolytic lesion induced by the tumor. **C** The bone destruction index was significantly reduced in RANKL-

previous studies [12, 14–16]. In addition, our data demonstrated increased sRANKL generation at the TB-interface and suggested that the RANKL:OPG ratio is positively associated with the degree of osteolysis. Together, these

ASO treated animals compared to control-ASO treated animals. **F** qRT-PCR demonstrated that RANKL mRNA expression was significantly reduced at the tumor-bone interface of RANKL-ASO treated animals demonstrating the efficacy of the RANKL-ASO. **D**, **E** Number of TRAP positive osteoclasts in RANKL-ASO and control treated animals. The values are mean \pm SEM. This is a representative of three experiments with similar results.

results demonstrated that not only upregulation of RANKL but also generation of sRANKL at the TB-interface is an important mediator of RANKL-dependent tumor-induced osteolysis.

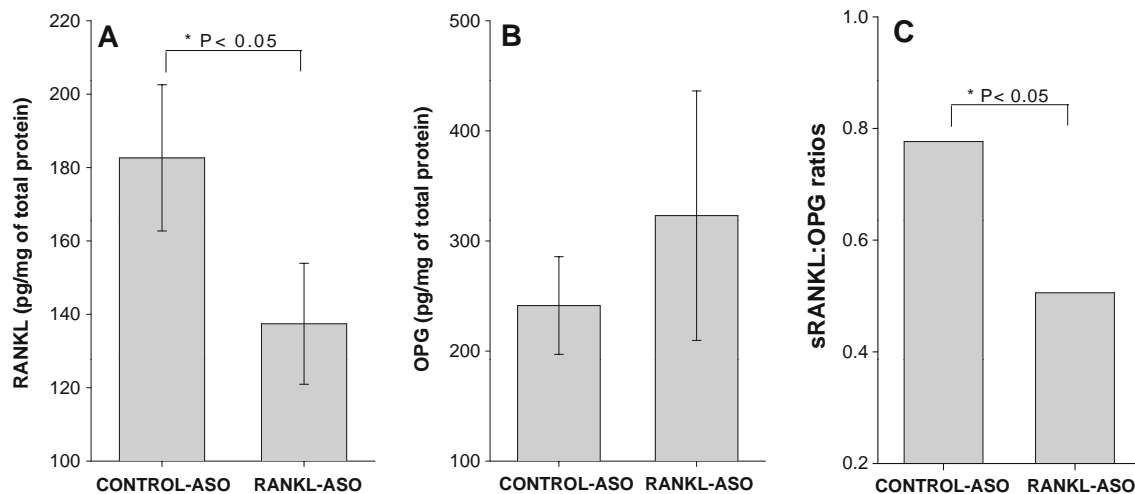


Fig. 6 Inhibiting RANKL expression regulates RANKL and OPG production at the TB interface. RANKL levels at the TB-interface of RANKL-ASO treated animals were significantly reduced compared to control-ASO animals. Five mice were used in each group and the experiment was repeated twice. **A** While OPG levels were concomitantly increased (but not significantly different) in RANKL-ASO

treated animals (**B**) as demonstrated by ELISA. **C** The RANKL:OPG ratio was decreased significantly at the tumor-bone interface of RANKL-ASO treated animals compared to control-ASO treated animals. The values are mean \pm SEM. This is a representative of three experiments with similar results

Acknowledgments This work was supported in part by grants CA72781 (R.K.S.) and Cancer Center Support Grant (P30CA036727) from National Cancer Institute, National Institutes of Health, Susan G. Komen for the Cure grant KG090860 and Nebraska Research Initiative Program in Cancer Glycobiology (R.K.S.), Department of Defense Breast Cancer Research Program Predoctoral traineeship award (K.C.N) and the Howard Hughes Medical Institute Research Training Fellowship (T.J.W.). We thank Dr. James Eudy and the UNMC DNA Microarray Core Facility for help in microarray analysis.

References

- Jemal A, Siegel R, Ward E, Hao Y, Xu J, Murray T et al (2008) Cancer statistics, 2008. *CA Cancer J Clin* 58(2):71–96
- Mundy GR (2002) Metastasis to bone: causes, consequences and therapeutic opportunities. *Nat Rev Cancer* 2(8):584–593
- Boyce BF, Yoneda T, Guise TA (1999) Factors regulating the growth of metastatic cancer in bone. *Endocr Relat Cancer* 6(3):333–347
- Coleman RE (1997) Skeletal complications of malignancy. *Cancer* 80(8 Suppl):1588–1594
- Kakonen SM, Mundy GR (2003) Mechanisms of osteolytic bone metastases in breast carcinoma. *Cancer* 97(3 Suppl):834–839
- Roodman GD (2004) Mechanisms of bone metastasis. *N Engl J Med* 350(16):1655–1664
- Lacey DL, Tan HL, Lu J, Kaufman S, Van G, Qiu W et al (2000) Osteoprotegerin ligand modulates murine osteoclast survival in vitro and in vivo. *Am J Pathol* 157(2):435–448
- Dougall WC, Chaisson M (2006) The RANK/RANKL/OPG triad in cancer-induced bone diseases. *Cancer Metastasis Rev* 25(4):541–549
- Morrissey C, Kostenuik P, Brown L, Vessella R, Corey E (2007) Host-derived RANKL is responsible for osteolysis in a C4-2 human prostate cancer xenograft model of experimental bone metastases. *BMC Cancer* 7(1):148
- Dallas SL, Rosser JL, Mundy GR, Bonewald LF (2002) Proteolysis of latent transforming growth factor-beta (TGF-beta)-binding protein-1 by osteoclasts. A cellular mechanism for release of TGF-beta from bone matrix. *J Biol Chem* 277(24):21352–21360
- Lacey DL, Timms E, Tan H-L, Kelley MJ, Dunstan CR, Burgess T et al (1998) Osteoprotegerin ligand is a cytokine that regulates osteoclast differentiation and activation. *Cell* 93(2):165–176
- Kitazawa S, Kitazawa R (2002) RANK ligand is a prerequisite for cancer-associated osteolytic lesions. *J Pathol* 198(2):228–236
- Tanaka S, Nakamura K, Takahashi N, Suda T (2005) Role of RANKL in physiological and pathological bone resorption and therapeutics targeting the RANKL-RANK signaling system. *Immunol Rev* 208:30–49
- Roodman GD, Dougall WC (2008) RANK ligand as a therapeutic target for bone metastases and multiple myeloma. *Cancer Treat Rev* 34(1):92–101
- Zhang J, Dai J, Qi Y, Lin DL, Smith P, Strayhorn C et al (2001) Osteoprotegerin inhibits prostate cancer-induced osteoclastogenesis and prevents prostate tumor growth in the bone. *J Clin Invest* 107(10):1235–1244
- Zhang J, Dai J, Yao Z, Lu Y, Dougall W, Keller ET (2003) Soluble receptor activator of nuclear factor kappaB Fc diminishes prostate cancer progression in bone. *Cancer Res* 63(22):7883–7890
- Morony S, Capparelli C, Sarosi I, Lacey DL, Dunstan CR, Kostenuik PJ (2001) Osteoprotegerin inhibits osteolysis and decreases skeletal tumor burden in syngeneic and nude mouse models of experimental bone metastasis. *Cancer Res* 61(11):4432–4436
- Wilson TJ, Nannuru KC, Futakuchi M, Sadanandam A, Singh RK (2008) Cathepsin G enhances mammary tumor-induced osteolysis by generating soluble receptor activator of nuclear factor- κ B ligand. *Cancer Res* 68(14):5803–5811
- Wilson TJ, Singh RK (2008) Proteases as modulators of tumor-stromal interaction: primary tumors to bone metastases. *Biochimica et Biophysica Acta (BBA) Rev Cancer* 1785(2):85–95

20. Lynch CC, Hikosaka A, Acuff HB, Martin MD, Kawai N, Singh RK et al (2005) MMP-7 promotes prostate cancer-induced osteolysis via the solubilization of RANKL. *Cancer Cell* 7(5):485–496
21. Chesneau V, Becherer JD, Zheng Y, Erdjument-Bromage H, Tempst P, Blobel CP (2003) Catalytic properties of ADAM19. *J Biol Chem* 278(25):22331–22340
22. Schlondorff J, Lum L, Blobel CP (2001) Biochemical and pharmacological criteria define two shedding activities for TRANCE/OPGL that are distinct from the tumor necrosis factor alpha convertase. *J Biol Chem* 276(18):14665–14674
23. Aslakson CJ, Miller FR (1992) Selective events in the metastatic process defined by analysis of the sequential dissemination of subpopulations of a mouse mammary tumor. *Cancer Res* 52(6):1399–1405
24. Chen Z, Varney ML, Backora MW, Cowan K, Solheim JC, Talmadge JE et al (2005) Down-regulation of vascular endothelial cell growth factor-C expression using small interfering RNA vectors in mammary tumors inhibits tumor lymphangiogenesis and spontaneous metastasis and enhances survival. *Cancer Res* 65(19):9004–9011
25. Heppner GH, Miller FR, Shekhar PM (2000) Nontransgenic models of breast cancer. *Breast Cancer Res* 2(5):331–334
26. Huang X, Wong MK, Yi H, Watkins S, Laird AD, Wolf SF et al (2002) Combined therapy of local and metastatic 4T1 breast tumor in mice using SU6668, an inhibitor of angiogenic receptor tyrosine kinases, and the immunostimulator B7.2-IgG fusion protein. *Cancer Res* 62(20):5727–5735
27. Lelekakis M, Moseley JM, Martin TJ, Hards D, Williams E, Ho P et al (1999) A novel orthotopic model of breast cancer metastasis to bone. *Clin Exp Metastasis* 17(2):163–170
28. Murphy BO, Joshi S, Kessinger A, Reed E, Sharp JG (2002) A murine model of bone marrow micrometastasis in breast cancer. *Clin Exp Metastasis* 19(7):561–569
29. Sloan EK, Stanley KL, Anderson RL (2004) Caveolin-1 inhibits breast cancer growth and metastasis. *Oncogene* 23(47):7893–7897
30. Bennett CF, Cowser LM (1999) Antisense oligonucleotides as a tool for gene functionalization and target validation. *Biochim Biophys Acta* 1489(1):19–30
31. Henry SP, Geary RS, Yu R, Levin AA (2001) Drug properties of second-generation antisense oligonucleotides: how do they measure up to their predecessors? *Curr Opin Invest Drugs* 2(10):1444–1449
32. Kingsley LA, Fournier PGJ, Chirgwin JM, Guise TA (2007) Molecular biology of bone metastasis. *Mol Cancer Ther* 6(10):2609–2617
33. Siclari VA, Guise TA, Chirgwin JM (2006) Molecular interactions between breast cancer cells and the bone microenvironment drive skeletal metastases. *Cancer Metastasis Rev* 25(4):621–633
34. Blair JM, Zhou H, Seibel MJ, Dunstan CR (2006) Mechanisms of disease: roles of OPG, RANKL and RANK in the pathophysiology of skeletal metastasis. *Nat Clin Pract Oncol* 3(1):41–49
35. Kuperwasser C, Dessain S, Bierbaum BE, Garnet D, Sperandio K, Gauvin GP et al (2005) A mouse model of human breast cancer metastasis to human bone. *Cancer Res* 65(14):6130–6138
36. Reddi AH, Roodman D, Freeman C, Mohla S (2003) Mechanisms of tumor metastasis to the bone: challenges and opportunities. *J Bone Miner Res* 18(2):190–194
37. Varney ML, Singh S, Backora M, Chen Z, Singh RK (2008) Lymphangiogenesis and anti-tumor immune responses. *Curr Mol Med* (In Press)
38. Grimaud E, Soubigou L, Couillaud S, Coipeau P, Moreau A, Passuti N et al (2003) Receptor activator of nuclear factor kappaB ligand (RANKL)/osteoprotegerin (OPG) ratio is increased in severe osteolysis. *Am J Pathol* 163(5):2021–2031
39. Jung K, Stephan C, Semjonow A, Lein M, Schnorr D, Loening SA (2003) Serum osteoprotegerin and receptor activator of nuclear factor-kappa B ligand as indicators of disturbed osteoclastogenesis in patients with prostate cancer. *J Urol* 170(6 Pt 1):2302–2305
40. Seidel C, Hjertner O, Abildgaard N, Heickendorff L, Hjorth M, Westin J et al (2001) Serum osteoprotegerin levels are reduced in patients with multiple myeloma with lytic bone disease. *Blood* 98(7):2269–2271
41. Terpos E, Szydlo R, Apperley JF, Hatjiharissi E, Politou M, Meletis J et al (2003) Soluble receptor activator of nuclear factor kappaB ligand-osteoprotegerin ratio predicts survival in multiple myeloma: proposal for a novel prognostic index. *Blood* 102(3):1064–1069
42. Kostenuik PJ, Singh G, Suyama KL, Orr FW (1992) Stimulation of bone resorption results in a selective increase in the growth rate of spontaneously metastatic Walker 256 cancer cells in bone. *Clin Exp Metastasis* 10(6):411–418
43. Schneider A, Kalikin LM, Mattos AC, Keller ET, Allen MJ, Pienta KJ et al (2005) Bone turnover mediates preferential localization of prostate cancer in the skeleton. *Endocrinology* 146(4):1727–1736
44. Brown JE, Cook RJ, Major P, Lipton A, Saad F, Smith M et al (2005) Bone turnover markers as predictors of skeletal complications in prostate cancer, lung cancer, and other solid tumors. *JNCI J Natl Cancer Inst* 97(1):59–69
45. Costa L, Demers LM, Gouveia-Oliveira A, Schaller J, Costa EB, de Moura MC et al (2002) Prospective evaluation of the peptide-bound collagen type I cross-links N-telopeptide and C-telopeptide in predicting bone metastases status. *J Clin Oncol* 20(3):850–856
46. Sasaki A, Boyce BF, Story B, Wright KR, Chapman M, Boyce R et al (1995) Bisphosphonate risedronate reduces metastatic human breast cancer burden in bone in nude mice. *Cancer Res* 55(16):3551–3557
47. van der Pluijm G, Que I, Sijmons B, Buijs JT, Lowik CWGM, Wetterwald A et al (2005) Interference with the microenvironmental support impairs the de novo formation of bone metastases in vivo. *Cancer Res* 65(17):7682–7690
48. Buijs JT, Que I, Lowik CW, Papapoulos SE, Van der Pluijm G (2009) Inhibition of bone resorption and growth of breast cancer in the bone microenvironment. *Bone* 44(2):380–386
49. Phadke PA, Mercer RR, Harms JF, Jia Y, Frost AR, Jewell JL et al (2006) Kinetics of metastatic breast cancer cell trafficking in bone. *Clin Cancer Res* 12(5):1431–1440
50. Michaelson MD, Smith MR (2005) Bisphosphonates for treatment and prevention of bone metastases. *J Clin Oncol* 23(32):8219–8224
51. Saarto T, Vehmanen L, Virkkunen P, Blomqvist C (2004) Ten-year follow-up of a randomized controlled trial of adjuvant clodronate treatment in node-positive breast cancer patients. *Acta Oncol* 43(7):650–656

Cathepsin G Enhances Mammary Tumor–Induced Osteolysis by Generating Soluble Receptor Activator of Nuclear Factor- κ B Ligand

Thomas J. Wilson,¹ Kalyan C. Nannuru,¹ Mitsuru Futakuchi,² Anguraj Sadanandam,¹ and Rakesh K. Singh¹

¹Department of Pathology and Microbiology, University of Nebraska Medical Center, Omaha, Nebraska and ²Department of Experimental Pathology and Tumor Biology, Graduate School of Medical Sciences, Nagoya City University, Nagoya, Japan

Abstract

Breast cancer commonly causes osteolytic metastases in bone, a process that is dependent on tumor-stromal interaction. Proteases play an important role in modulating tumor-stromal interactions in a manner that favors tumor establishment and progression. Whereas several studies have examined the role of proteases in modulating the bone microenvironment, little is currently known about their role in tumor-bone interaction during osteolytic metastasis. In cancer-induced osteolytic lesions, cleavage of receptor activator of nuclear factor- κ B ligand (RANKL) to a soluble version (sRANKL) is critical for widespread osteoclast activation. Using a mouse model that mimics osteolytic changes associated with breast cancer–induced bone metastases, we identified cathepsin G, cathepsin K, matrix metalloproteinase (MMP)-9, and MMP13 to be proteases that are up-regulated at the tumor-bone interface using comparative cDNA microarray analysis and quantitative reverse transcription-PCR. Moreover, we showed that cathepsin G is capable of shedding the extracellular domain of RANKL, generating active sRANKL that is capable of inducing differentiation and activation of osteoclast precursors. The major source of cathepsin G at the tumor-bone interface seems to be osteoclasts that up-regulate production of cathepsin G via interaction with tumor cells. Furthermore, we showed that *in vitro* osteoclastogenesis is reduced by inhibition of cathepsin G in a coculture model and that *in vivo* inhibition of cathepsin G reduces mammary tumor–induced osteolysis. Together, our data indicate that cathepsin G activity at the tumor-bone interface plays an important role in mammary tumor–induced osteolysis and suggest that cathepsin G is a potentially novel therapeutic target in the treatment of breast cancer bone metastasis. [Cancer Res 2008;68(14):5803–11]

Introduction

As the most common type of cancer in women in the United States and the second leading cause of cancer-related death, breast cancer represents a serious health problem (1). Metastatic disease

is responsible for most of breast cancer–related mortality, accounting for the sharp decline in 5-year survival observed as breast cancer progresses from regional to distant metastasis (1). In patients that ultimately succumb to breast cancer, nearly all are found to have bone metastases, showing the tropism of breast cancer cells to bone. These metastatic bone lesions, predominantly osteolytic in nature, carry severe consequences including hypercalcemia, pathologic fracture, and leukoerythroblastic anemia (2). As a result, bone metastasis dramatically increases the risk of mortality as well as significantly reduces the quality of life.

The mechanisms involved in breast cancer–induced osteolytic bone metastases have been extensively studied but remain unclear. As breast cancer cells establish secondary colonies in the bone microenvironment, a vicious cycle ensues (2). Tumor cells secrete soluble factors such as interleukin (IL)-1, IL-8, and parathyroid hormone–related peptide that activate osteoblasts and induce expression of receptor activator of nuclear factor- κ B ligand (RANKL). RANKL expressed by osteoblasts can then interact with its receptor (RANK) on the cell surface of osteoclast precursors, leading to osteoclast differentiation and activation. Activated osteoclasts then mediate bone degradation through the release of proteases including matrix metalloproteinases (MMP) and cathepsins. As bone is degraded, sequestered growth factors are released that serve as growth and survival factors as well as chemoattractants for tumor cells, promoting the establishment of bone metastases (2). Thus, tumor-stromal interactions play a significant role in the establishment and regulation of osteolytic bone metastases.

Proteases play a major role in tumor-stromal interactions by modifying the bidirectional communication to favor tumor establishment and growth at both the primary tumor site and metastatic site (3–5). In a prostate cancer model, we have previously shown that MMP7 is capable of cleaving membrane-bound RANKL into a soluble version (sRANKL), which relieves the contact-dependent nature of osteoblast-osteoclast interaction, bypasses the rate-limiting step of the vicious cycle, and enhances osteoclast activation and subsequent osteolysis (6). To date, however, no such mechanism has been described in breast cancer.

In the present study, we examined the patterns of expression of proteases at the tumor-bone interface of mammary tumor–induced osteolytic lesions and investigated their functional significance in modulating RANKL-RANK signaling in osteoclast activation and osteolysis. We identified cathepsin G, cathepsin K, MMP9, and MMP13 to be proteases that are up-regulated at the tumor-bone interface. Moreover, we showed that cathepsin G is capable of shedding the extracellular domain of RANKL, generating active sRANKL that is capable of inducing differentiation and activation of osteoclast precursors. Furthermore, we

Note: Supplementary data for this article are available at Cancer Research Online (<http://cancerres.aacrjournals.org/>).

T.J. Wilson is a Howard Hughes Medical Institute Research Training Fellow.

Requests for reprints: Rakesh K. Singh, Department of Pathology and Microbiology, University Nebraska Medical Center, 985845 Nebraska Medical Center, Omaha, NE 68198-5845. Phone: 402 559 9949; Fax: 402 559 4077; E-mail: rsingh@unmc.edu.

©2008 American Association for Cancer Research.

doi:10.1158/0008-5472.CAN-07-5889

showed that *in vitro* osteoclastogenesis is reduced by inhibition of cathepsin G in a coculture model and subsequently showed that *in vivo* inhibition of cathepsin G reduces mammary tumor-induced osteolysis. Thus, we have shown for the first time a role for cathepsin G at the tumor-bone interface of mammary tumor-induced osteolytic lesions and have uncovered a potential therapeutic target.

Materials and Methods

Animal model and tissue preparation. 4T1, Cl66, and Cl66M2 murine breast adenocarcinoma cell lines were used in this study. Tumor cells (1×10^6) mixed with growth factor-reduced Matrigel were implanted on the dorsal skin flap over the calvaria of female BALB/c mice. Tumor growth was monitored twice a week. Mice were sacrificed and necropsied for examination of osteolytic lesions at 4 wk postimplantation. At that time, the tumor and the underlying bone were divided into two pieces. One piece was used for separation of the tumor-bone interface from the tumor alone area for further analysis and the other piece was used for histology sections. All studies were done in accordance with the Institutional Animal Use and Care Committee of the University of Nebraska Medical Center. For histologic examination, tissues were fixed with periodate-lysine-paraformaldehyde at 4°C for 48 h. The tissues were then transferred into a decalcification solution (15% EDTA with glycerol, pH 7.4–7.5) for 4 wk. The tissue was then paraffin embedded and processed for further analysis.

Microarray analysis and real-time PCR. Calcified frozen sections were serially sectioned into 10- μ m slices. Sections were then microdissected to separate the tumor-bone interface from the tumor alone area (Fig. 1A). Total RNA was extracted from both the tumor-bone interface and the tumor alone area and then amplified by using a probe amplification kit (Affymetrix). Genetic expression at the tumor-bone interface was compared with the tumor alone area using an Affymetrix Mouse Expression Array (430A). Analysis was done using Affymetrix Gene Chip Operating Software to generate raw expression data. A signal log algorithm was used to compare the quantity of a given transcript in two arrays: a baseline array, here the tumor alone area, and an experimental array, here the tumor-bone interface. The signal log ratio is calculated by comparing each probe pair on the experimental array to the corresponding probe pair on the baseline array and then considering the mean of the log ratios of probe pair intensities across the two arrays. The change in transcript level is then expressed as a log 2 ratio. Using this system, a signal log ratio of 1.0 indicates a 2-fold increase at the tumor-bone interface whereas a ratio of -1.0 indicates a 2-fold decrease. For each set of tissue from 4T1, Cl66, and Cl66M2, the fold change at the tumor-bone interface with respect to the tumor alone area was calculated and the genes were ranked from highest to lowest expression.

For real-time quantitative reverse transcription-PCR (RT-PCR) analysis, total RNA was isolated from tissue at the tumor-bone interface and tumor alone area using Trizol reagent (Invitrogen). Five micrograms of total RNA were used for reverse transcription. First-strand cDNA was generated using oligo(dT)₁₈ (Fermentas) and Superscript II RT (Invitrogen). Two microliters of the resulting cDNA (1:10 dilution) were used in the real-time reactions with gene-specific primers. The following gene-specific primers were used: cathepsin G, 5'-GAGTCCAGAAGGGCTGAGTG-3' and 5'-CCTTCTCGCA-TTTGGATGT-3'; cathepsin K, 5'-CCAGTGGGAGCTATGGAAGA-3' and 5'-CTCCAGGTTATGGCCAGAGA-3'; MMP9, 5'-CATTCCGCTGGATAAG-GAGT-3' and 5'-TCACACGCCAGAAGAATTG-3'; MMP12, 5'-AATGGG-CAACTGGACAAC-3' and 5'-ACCGCTTCATCCATCTTGAC-3'; MMP13, 5'-TCCCTGCCCTTCCCTATGG-3' and 5'-CTCGGAGCTGTCAACTGTG-G-3'; and glyceraldehyde-3-phosphate dehydrogenase (GAPDH), 5'-AGCCT-CGTCCCGTAGACAAA-3' and 5'-GATGACAAGCTTCCATCTCG-3'. Quantitative RT-PCR reactions were carried out with FastStart SYBR Green Master mix (Roche) and MyIQ iCycler (Bio-Rad). Fluorescence intensity was measured at the end of each elongation step as a means to evaluate the amount of formed PCR product. GAPDH was used as a reference to normalize the samples.

Generation of RANKL protein. Full-length RANKL cDNA (NM_003701) with an NH₂-terminal His-tag sequence cloned in pReceiver-B01 (Gene-Copoeia) plasmid was used to generate RANKL protein using a TnT Quick Coupled Transcription/Translation system (Promega) per manufacturer's protocol using translation grade [³⁵S]methionine (1,175 Ci/mmol at 10 mCi/mL). Two microliters of the reaction mixture were separated on a 12% SDS-polyacrylamide gel and subsequently visualized and photographed with a Typhoon 9410 Variable Mode Imager (GE Healthcare). The resulting translation product was purified with a His-Trap Crude 1-mL column (GE Healthcare) per manufacturer's protocol. The purified protein was then concentrated by using a Centrprep YM-10 spin column (Omicron) and quantified with the BCA Protein Assay kit per manufacturer's protocol (Pierce).

Protease function assays. To test the activity of each of the proteases, colorimetric substrates were used. One hundred nanograms of cathepsin G or cathepsin K were incubated with 500 μ mol/L Suc-AAPF-pNA substrate (Biomol International) in enough buffer to make a 50- μ L reaction. The 10 \times buffer contained 100 mmol/L CaCl₂, 500 mmol/L HEPES, 10 mmol/L DTNB, and 0.5% Brij-35. Similar reactions were done for MMP9 and MMP13 with chromogenic MMP substrate (Biomol International). Reaction mixtures were incubated at 37°C for 60 min. Readings were taken on a BioTek ELx800 microplate reader every 15 min at 405 nm.

Protease-mediated cleavage of RANKL. Three micrograms of full-length RANKL were incubated overnight at 37°C alone or with 100 ng of cathepsin G, cathepsin K, MMP9, or MMP13 in enough buffer to make a 25- μ L reaction. Reactions were terminated by adding EDTA to a final concentration of 10 mmol/L. The reaction mixture was then separated on a 12% SDS-polyacrylamide gel. The gel was then stained with 0.025% Coomassie brilliant blue (Bio-Rad) and photographed by using a Multi-Image Light Cabinet (Alpha Innotech Corporation). Cathepsin G inhibition was tested by adding Na-Tosyl-Phe-chloromethylketone (TPCK; Sigma-Aldrich) at a final concentration of 1 mmol/L. TPCK was incubated with enzyme and buffer for 30 min at 37°C before adding RANKL. The reaction mixture was then incubated, separated, and analyzed.

Similar reactions were carried out and subsequently used for Western blot analysis. Reaction mixtures were separated on a 12% SDS-polyacrylamide gel and then transferred onto a polyvinylidene difluoride (PVDF) membrane (GE Healthcare) at 100 V for 1 h. The membrane was then washed with 0.1% Tween-TBS. The membrane was then blocked overnight in 5% bovine serum albumin in PBS. The next day, the membrane was incubated for 90 min with 1:500 anti-RANKL antibody that recognizes an epitope near the COOH terminus of RANKL (Santa Cruz Biotechnology) diluted in 0.1% Tween-TBS. After washing in 0.1% Tween-TBS, the membrane was incubated for 60 min with 1:1,500 anti-goat-horseradish peroxidase diluted in 0.1% Tween-TBS. Finally, after washing with 0.1% Tween-TBS, the membrane was developed with an enhanced chemiluminescence (ECL) Plus Western Blotting Detection System (GE Healthcare) per manufacturer's protocol and imaged with a Typhoon 9410 Variable Mode Imager (GE Healthcare).

Osteoclast differentiation and activation assay. RAW 264.7 cells were seeded onto eight-well chambered slides at a density of 3,000 per chamber. Cells were grown in DMEM plus 10% fetal bovine serum (FBS), 1% vitamins, 1% L-glutamine, and 0.08% gentamicin (DMEM complete medium). The cells were incubated overnight at 37°C. The following day, the medium was changed and the cells were treated with medium alone, 50 ng/mL sRANKL, or 50 ng/mL cathepsin G-generated sRANKL. The cells were then allowed to incubate for 7 d with medium changes every other day. On the 7th day, cells were stained for tartrate-resistant acid phosphatase (TRAP) per manufacturer's protocol (Sigma-Aldrich). The number of osteoclasts per 250- μ m field was counted for five fields per treatment per replicate. Fully mature, TRAP-positive multinucleated cells were counted as osteoclasts.

BD BioCoat Osteologic Coverslips (BD Biosciences) were placed in 24-well plates. RAW 264.7 cells were then seeded onto the plates at a density of 5,000/cm². Cells were grown in DMEM complete medium. The cells were incubated overnight at 37°C. The following day, the medium was changed and the cells were treated with medium alone, 50 ng/mL sRANKL, or

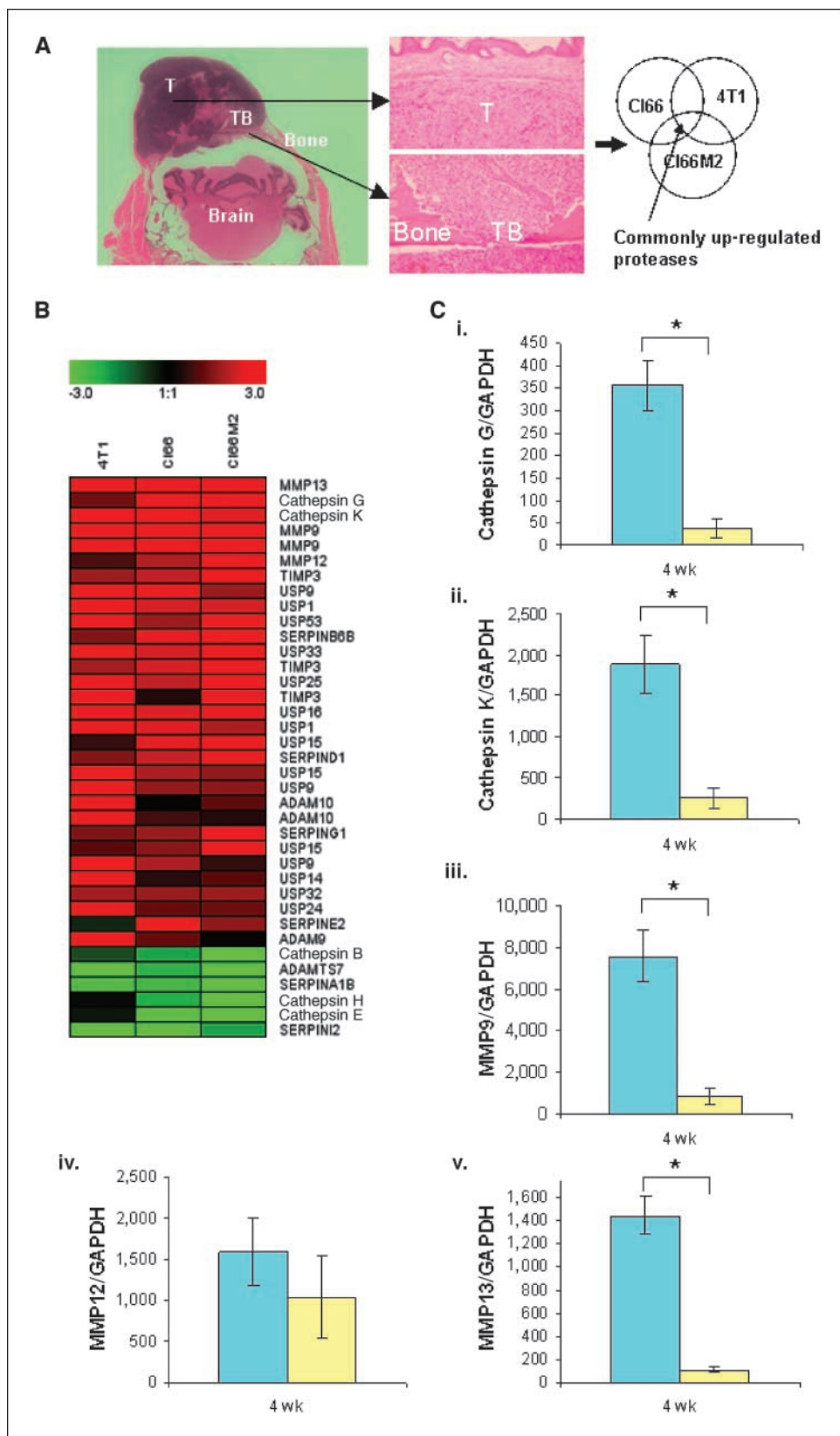


Figure 1. Protease gene expression at the tumor-bone interface. *A*, H&E-stained section of tumor-bone interface (TB) and tumor alone (T) area. Tumors (Cl66, Cl66M2, and 4T1) were microdissected to separate the tumor alone area from the tumor-bone interface ($n = 3$). Total RNA and protein were collected from these two regions of the lesions to determine what proteases are up-regulated as tumor cells engage in bidirectional communication with the bone microenvironment. *B*, gene expression at the tumor-bone interface was compared with the tumor alone area by comparative cDNA microarray analysis using week 4 samples from Cl66, Cl66M2, and 4T1 tumors. Protease-specific analysis of the data was conducted. *C*, *i* to *v*, expression of cathepsin G, cathepsin K, MMP9, MMP12, and MMP13 was confirmed by real-time PCR. *Columns*, average mRNA expression of the specific gene normalized to GAPDH. *Blue columns*, tumor-bone interface; *yellow columns*, tumor alone area. Representative data of all three cell lines done in triplicate. *Bars*, SD. *, $P < 0.05$.

50 ng/mL cathepsin G-generated sRANKL. The cells were then allowed to incubate for 7 d with medium changes every other day. On the 7th day, the medium was aspirated and 1 mL of bleach was added to each well. After 5 min, the bleach was aspirated and the coverslips were washed thrice with

distilled water. The coverslips were then stained with hematoxylin for 2 min and then rinsed with running tap water for 10 min. Finally, the number and area of calcium phosphate matrix resorption pits (clear areas) on each 12-mm coverslip were measured.

Immunoblotting for cathepsin G. Fifty micrograms of protein from the tumor-bone interface and tumor alone area for each of the animals injected with Cl66 cells were separated on a 12% SDS-polyacrylamide gel and then was transferred onto a PVDF membrane (GE Healthcare). The membranes were immunoblotted with anti-cathepsin G antibody that recognizes an epitope near the NH₂ terminus of cathepsin G (1:200; Santa Cruz Biotechnology) and anti-β-actin antibody (1:2,000; Santa Cruz Biotechnology) and developed with an ECL Plus Western Blotting Detection System (GE Healthcare) per manufacturer's protocol and imaged with a Typhoon 9410 Variable Mode Imager (GE Healthcare). The bands for both cathepsin G and β-actin were then quantified and compared using ImageQuant 5.1 (Molecular Dynamics).

Immunohistochemistry for cathepsin G. For the *in vivo* detection of cathepsin G, sections were deparaffinized and processed for antigen retrieval. Following nonspecific blocking, sections were then incubated with anti-cathepsin G antibody (Santa Cruz Biotechnology; 1:50 dilution) overnight at 4°C. The sections were then washed and subsequently incubated with biotinylated anti-goat IgG antibody diluted to 1:500 for 1 h. Sections were then washed and incubated with avidin-biotin complex (Vector Laboratories) for 45 min. Next, the slides were developed with diaminobenzidine tetrahydrochloride substrate (Vector Laboratories) and counterstained with hematoxylin for 30 s. Anti-goat IgG was added in lieu of primary antibody as control and no detectable staining was observed in these sections.

Cathepsin G inhibition coculture model. RAW 264.7 cells were seeded at a density of 3,000/cm² on gelatin-coated six-well plates in DMEM plus 10% FBS, 1% vitamins, 1% L-glutamine, and 0.08% gentamicin (DMEM complete medium). Following overnight incubation, cells were incubated with DMEM complete medium alone, DMEM complete medium plus 25% (v/v) Cl66-conditioned medium with or without TPCK at a final concentration of 1 mmol/L, TPCK at a final concentration of 1 mmol/L plus commercially available sRANKL at 50 ng/mL, or DMEM complete medium containing Cl66 cells at a density of 3000/cm² with or without TPCK. In the TPCK-treated groups, TPCK was added to a final concentration of 1 mmol/L every 24 h. After 4 d, the coverslips were stained for TRAP per manufacturer's instructions (Sigma-Aldrich) and multinucleated, TRAP-positive osteoclasts were counted.

***In vivo* inhibition of cathepsin G.** Cl66 tumor cells (1×10^5) mixed with growth factor-reduced Matrigel were implanted on the dorsal skin flap over the calvaria of female BALB/c mice. Tumor growth was monitored twice a week. Beginning 7 d after tumor implantation, mice were injected s.c. with TPCK (Sigma-Aldrich) at 50 mg/kg/d ($n = 6$) or 50-μL DMSO as control ($n = 6$) for 21 d. Mice were sacrificed at day 31 postimplantation and necropsied for examination of osteolytic lesions. To calculate the bone destruction index, sections were stained with H&E. The bone destruction index was calculated by dividing the length of bone destruction by the length of the tumor-bone interface and multiplying by 100. All studies were done in accordance with the Institutional Animal Use and Care Committee of the University of Nebraska Medical Center.

Statistical analysis. For *in vivo* studies, the Wilcoxon signed rank test was used to analyze data. For *in vitro* studies, the Student *t* test was used. $P < 0.05$ was considered significant.

Results

Protease gene expression at the tumor-bone interface. Mammary tumor cells with different metastatic potentials, 4T1 (high), Cl66 (moderate), and Cl66M2 (low), were transplanted into the calvaria of BALB/c mice. Histochemical analysis showed that all tumors exhibited tumor-induced osteolysis and osteoclast activation similar to that observed in breast cancer bone metastasis. Using cDNA microarray analysis, we examined the gene expression patterns at the tumor-bone interface compared with the tumor alone area (Fig. 1A). A whole-genome microarray was used and subsequently analyzed by sorting out proteases and protease inhibitors. The five most up-regulated protease

genes were *cathepsin G*, *cathepsin K*, *MMP9*, *MMP12*, and *MMP13* (Fig. 1B). The common up-regulation of these five genes in all three cell lines further suggested that they may play an important role at the tumor-bone interface.

We then used quantitative RT-PCR to confirm the up-regulation of these five genes at the tumor-bone interface. We confirmed the up-regulation of cathepsin G (Fig. 1C-*i*), cathepsin K (Fig. 1C-*ii*), MMP9 (Fig. 1C-*iii*), and MMP13 (Fig. 1C-*v*), but not MMP12 (Fig. 1C-*iv*), at the tumor-bone interface.

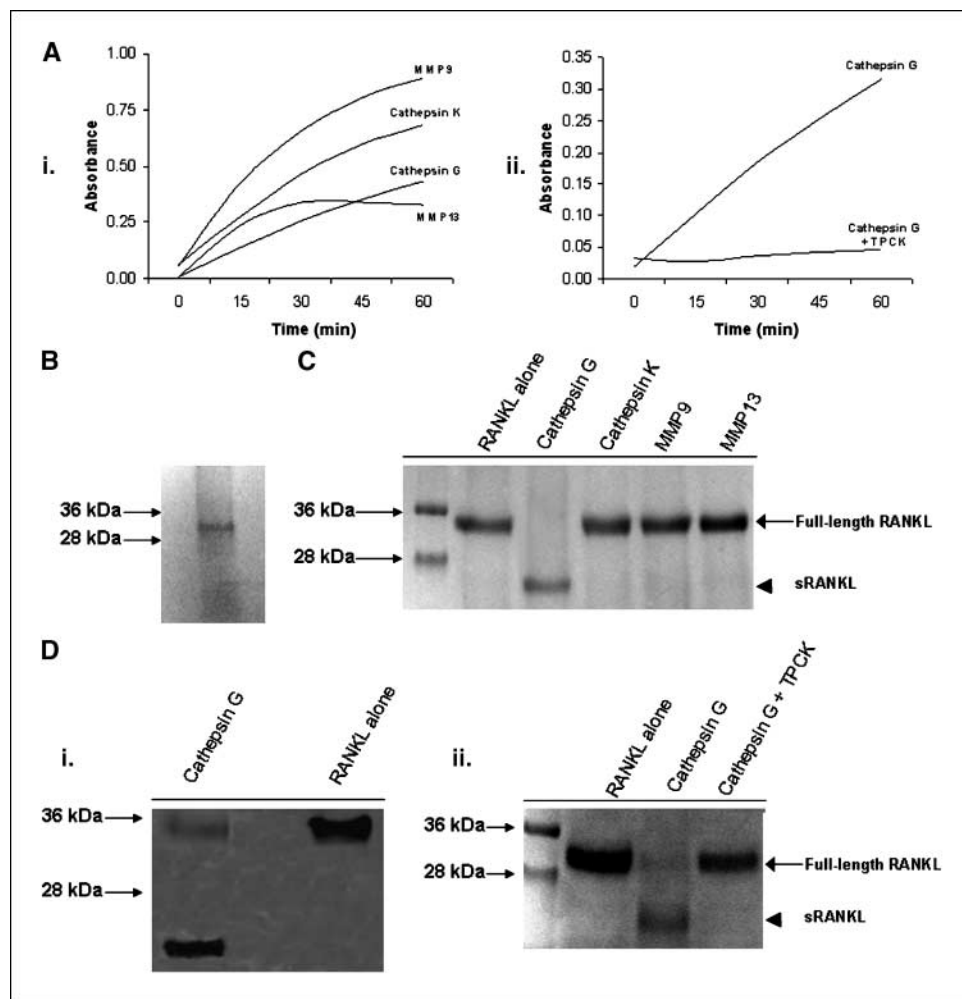
Cathepsin G cleaves RANKL to generate sRANKL. We previously reported that MMP7 plays a role in prostate tumor-induced osteolysis through the cleavage of cell-surface RANKL into a soluble form of RANKL that is capable of enhancing osteoclast differentiation and subsequent osteolysis (6). To determine if any of the proteases that we observed to be up-regulated at the tumor-bone interface play a similar role in mammary tumor-induced osteolysis, the activity of each protease against full-length RANKL was assessed.

Full-length RANKL protein was generated by using an *in vitro* transcription/translation kit. The product was visualized and the expected ~34-kDa protein was seen (Fig. 2B). Although activity against the native substrate of each protease was observed (Fig. 2A-*i*), only cathepsin G generated a soluble version of RANKL (~24 kDa; Fig. 2C). To confirm cathepsin G-mediated cleavage of RANKL, we used TPCK, a cathepsin G inhibitor, before incubation with full-length RANKL protein. TPCK is an inhibitor of the chymotrypsin-like group of proteases and is a potent inhibitor of cathepsin G (7, 8). We first confirmed the ability of TPCK to inhibit cathepsin G activity against its native substrate, and TPCK effectively inhibited cathepsin G activity (Fig. 2A-*ii*). Similarly, cathepsin G preincubated with TPCK did not cleave RANKL (Fig. 2D-*ii*). Finally, Western blot analysis with an anti-RANKL antibody that recognizes an epitope near the COOH terminus confirmed that the cleaved protein was RANKL and that the soluble product generated was derived from full-length RANKL cleaved near the NH₂ terminus within the extracellular domain (Fig. 2D-*i*).

Cathepsin G-generated sRANKL induces osteoclast differentiation and activation. The ability of cathepsin G-generated sRANKL to induce osteoclast differentiation and activation was assessed using the murine monocyte/macrophage cell line RAW 264.7. Fully mature, TRAP-positive multinucleated cells were counted as osteoclasts (Fig. 3B-*ii*). Commercially available sRANKL (positive control) induced significantly higher osteoclast differentiation than medium alone (negative control; Fig. 3A). Numerous TRAP-positive cells were seen in the control sample but most were mononuclear (Fig. 3B-*i*). Similar to the commercial sRANKL, cathepsin G-generated sRANKL induced significantly higher osteoclast formation than control (Fig. 3A). Although osteoclast differentiation was higher in the sRANKL-treated group, it did not differ statistically from the cathepsin G-generated sRANKL-treated group.

We then examined whether or not the osteoclasts produced by treatment with cathepsin G-generated sRANKL are active. Osteoclast activation was assessed by counting the number of calcium phosphate matrix resorption pits formed per BD BioCoat Osteologic Coverslip. Commercially available sRANKL (positive control) induced activation of osteoclasts with a significantly higher number of resorptive pits compared with medium alone (negative control; Fig. 3C and D). Similarly, cathepsin G-generated sRANKL yielded a significantly higher number of pits compared

Figure 2. Cathepsin G-dependent generation of sRANKL. *A, i*, the activity of each of the proteases was tested against colorimetric substrates to ensure appropriate reaction conditions. Each of the proteases showed activity against the substrate over a 60-min period. *ii*, TPCK, an inhibitor of cathepsin G, effectively inhibited the action of cathepsin G against the substrate at a concentration of 1 mmol/L. *B*, RANKL was generated by using an *in vitro* transcription/translation kit and then purified. A single band at ~34 kDa is appropriate for RANKL and shows the purity of the sample. *C*, cathepsin G incubated with full-length RANKL (arrow) generated a soluble ~24-kDa product (arrowhead). *D, i*, Western blot with anti-RANKL antibody directed at an epitope at the COOH terminus confirms that cathepsin G cleaves RANKL near the NH₂ terminus. *ii*, TPCK, a cathepsin G inhibitor, blocked cleavage of RANKL, confirming that cathepsin G is responsible for the generation of sRANKL.



with control and was statistically indistinguishable from commercially available sRANKL (Fig. 3C and D). Together, these results indicate that cathepsin G-generated sRANKL is capable of inducing osteoclast differentiation and activation and suggest that increased cathepsin G activity at the tumor-bone interface can lead to increased osteoclast differentiation and subsequent osteolysis.

Up-regulation of cathepsin G at the tumor-bone interface. Recognizing that cathepsin G may make a significant contribution to the vicious cycle, we reexamined cathepsin G expression at the tumor-bone interface and further confirmed its up-regulation at the protein level by Western blot analysis comparing the tumor-bone interface to the tumor alone area. Cl66 tumors showed significant up-regulation of cathepsin G at the tumor-bone interface as compared with the tumor alone area (Fig. 4A and B). This protein level analysis confirmed the earlier cDNA microarray and quantitative RT-PCR analyses.

Osteoclasts/osteoclast precursors are the major source of cathepsin G. To determine the source of cathepsin G at the tumor-bone interface, immunohistochemistry was used to assess the source of cathepsin G *in vivo*. Osteoclasts and osteoclast precursors stained strongly positive for cathepsin G (Fig. 4C-i), whereas tumor cells at the tumor-bone interface stained moderately positive (Fig. 4C-i). Tumor cells away from the tumor-bone interface in the tumor alone area stained weakly positive (Fig. 4C-ii). Normal bone did not show any immunoreactivity to cathepsin G (Fig. 4C-iii).

These data agree with our *in vitro* data (Supplementary data) that tumor cells have minimal baseline expression of cathepsin G that is up-regulated as they interact with osteoclast precursors, but osteoclasts are the major source of cathepsin G at the tumor-bone interface.

Inhibition of cathepsin G blocks osteoclastogenesis *in vitro*. RAW 264.7 cells treated with 25% Cl66-conditioned medium showed significantly higher osteoclast differentiation compared with control (Fig. 5A), suggesting that a soluble factor produced by Cl66 cells is capable of inducing osteoclast differentiation. To determine whether cathepsin G is responsible for the generation of this soluble factor, Cl66 cells were treated with TPCK while collecting conditioned medium. Cl66-conditioned medium from cells treated with TPCK induced significantly lower osteoclast differentiation compared with Cl66-conditioned medium from untreated cells (Fig. 5A). Importantly, RAW 264.7 cells treated with both TPCK and sRANKL showed significant osteoclast formation, showing that reduction in osteoclast formation in the TPCK-treated samples is not merely due to death of osteoclasts secondary to TPCK toxicity (Fig. 5A). Similarly, RAW 264.7 cells cocultured with Cl66 cells showed significantly higher osteoclast differentiation than RAW 264.7 cells alone (Fig. 5B). TPCK also reduced osteoclastogenesis in the coculture but did not eliminate it (Fig. 5B). Taken together, these results indicate that cathepsin G is responsible for the generation of a soluble factor capable of

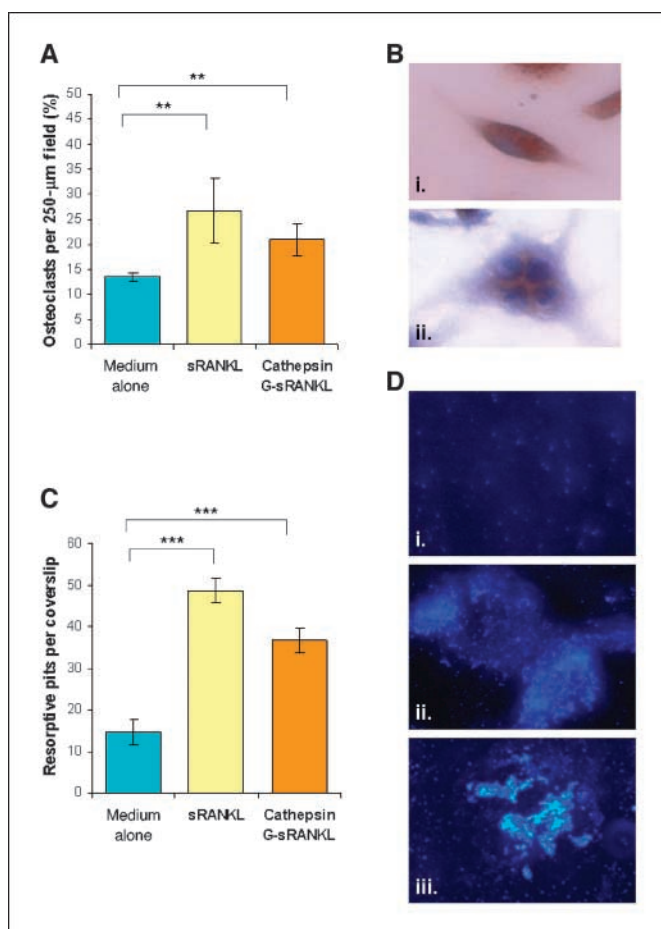


Figure 3. Cathepsin G-generated sRANKL induces osteoclast differentiation and activation. *A*, cathepsin G-generated sRANKL is an active product capable of inducing osteoclast differentiation. RAW 264.7 cells were treated with medium alone (negative control), commercially available sRANKL (positive control), or cathepsin G-generated sRANKL. Cells were stained for TRAP. Fully mature, TRAP-positive multinucleated cells were counted as osteoclasts. The number of osteoclasts per 250-µm field was counted. Bars, SD. **, $P < 0.01$. *B*, *i*, numerous TRAP-positive cells were seen in the medium-alone treatment group but most were mononuclear. *ii*, fully mature, TRAP-positive multinucleated osteoclast typical of sRANKL and cathepsin G-generated sRANKL groups. *C*, RAW 264.7 cells overlaid on coverslips containing artificial bone matrix were treated with medium alone (negative control), commercially available sRANKL (positive control), or cathepsin G-generated sRANKL. The number of calcium phosphate matrix resorption per coverslip was counted. Bars, SD. ***, $P < 0.001$. *D*, *i* to *iii*, typical 250-µm field from medium-alone, sRANKL, and cathepsin G-generated sRANKL groups, respectively. sRANKL and cathepsin G-generated sRANKL induced osteoclast differentiation and activation.

inducing osteoclast differentiation and that inhibition of cathepsin G reduces osteoclast differentiation.

Inhibition of cathepsin G reduces osteolysis *in vivo*. *In vitro* inhibition of cathepsin G reduced osteoclastogenesis, and thus we sought to determine whether inhibition of cathepsin G *in vivo* would reduce mammary tumor-induced osteolysis. No difference was observed in tumor growth or growth kinetics between TPCK-treated mice and negative control mice (data not shown). However, TPCK treatment significantly reduced tumor-induced osteolysis from an average bone destruction index of 35.3% in the DMSO-treated (negative control) mice to 13.2% in the TPCK-treated mice (Fig. 6*A*). Figure 6*B* shows the marked reduction in osteolysis at the tumor-bone interface of TPCK-treated mice compared with the control mice.

Discussion

Proteases play an important role in modulating tumor-stromal interactions in a manner that favors tumor establishment and progression. Although several studies have examined the role of proteases in modulating the bone microenvironment (9–12), little is currently known about their role in tumor-bone interaction during osteolytic metastasis. In this study, we have identified potentially important proteases in mammary tumor-induced osteolytic lesions, including cathepsin G, cathepsin K, MMP9, and MMP13.

Because RANKL is one of the key molecular players in a variety of osteolytic lesions that has previously been shown to be modified by proteases to favor tumor progression (6, 13, 14), we sought to determine if any of the up-regulated proteases were capable of modulating RANKL signaling. The importance of RANKL is in its ability to signal through RANK on preosteoclasts to induce differentiation and activation leading to bone resorption. The rate-limiting step to the vicious cycle is the RANKL-RANK signaling pathway. Because both RANKL and RANK are membrane-bound proteins, this interaction requires physical cell-to-cell contact between osteoblasts and osteoclast precursors in order to occur. Because RANKL, a member of the tumor necrosis factor family of cytokines, stimulates RANK via cell-to-cell contact between osteoblasts and osteoclast precursors, osteoclast differentiation and activation occurs with induction of TRAP activity, calcitonin binding, and actin-ring formation characteristic of osteoclasts (15, 16). The centrality of RANKL to the vicious cycle makes it a molecule that could potentially be up-regulated to establish osteolytic lesions, and in fact, we have found that RANKL is up-regulated at the tumor-bone interface of mammary tumor-induced osteolytic lesions.³ However, even with up-regulation of RANKL, the number of preosteoclasts that can be activated is spatially limited by their proximity to osteoblasts because cell-cell contact is required. In a prostate cancer model, our group has previously described a mechanism for cleavage of RANKL by MMP7 in a manner that releases it from the cell surface (6). The generation of sRANKL increases the number of preosteoclasts that can be activated and enhances osteolysis. Until now, no such mechanism has been described in mammary tumor-induced osteolytic lesions.

By identifying proteases differentially expressed as a result of tumor-bone interactions, we generated a list of proteases potentially involved in the modulation of RANKL-RANK signaling through the generation of sRANKL. We selected the top five proteases for further evaluation, which included cathepsin G, cathepsin K, MMP9, MMP12, and MMP13. Using quantitative RT-PCR to confirm up-regulation at the tumor-bone interface, we were able to eliminate MMP12 from the list, leaving four up-regulated proteases for further evaluation. Interestingly, RANKL has been shown to induce the expression of both cathepsin K and MMP9 in osteoclast precursor cells (17), and our data agree with this report (data not shown), suggesting that up-regulation of these two proteases may be an effect of enhanced RANKL signaling rather than a cause. Nonetheless, all four proteases were tested for their ability to cleave RANKL. Of these, only cathepsin G was capable of generating sRANKL. Western blot analysis suggests that the cleavage site is near the NH₂ terminus of the RANKL protein because the longer ~24-kDa fragment was detected with an

³ K.C. Nannuru, M. Futakuchi, A. Sadanandam, T.J. Wilson, M.L. Varney, L.J. Myers, X. Li, E.G. Marcusson, and R.K. Singh. Unpublished data.

anti-RANKL antibody that recognizes an epitope near the COOH terminus. The cleavage site and molecular weight of this larger fragment are similar to those observed in MMP7 cleavage of RANKL (6). Furthermore, the sRANKL generated by cathepsin G is an active product capable of inducing osteoclastogenesis. Osteoclasts are derived from the hematopoietic monocyte/macrophage lineage of cells. For this reason, we used the murine monocyte/macrophage cell line RAW 264.7 to test the activity of cathepsin G-generated sRANKL. Treatment of these cells with cathepsin G-generated sRANKL increased the number of differentiated and activated osteoclasts as shown by an increased number of multinucleated, TRAP-positive cells and the production of resorptive pits when cultured on artificial bone matrix.

The production of sRANKL by cathepsin G circumvents cell-cell contact-dependent signaling between membrane-bound RANKL and RANK, which allows increased osteoclastogenesis and subsequent bone resorption. Thus, cathepsin G can be added to the list of proteases known to be capable of cleaving RANKL, which includes MMP3, MMP7, a disintegrin and metalloproteinase

(ADAM)-17, and ADAM19 (6, 18, 19). The generation of sRANKL is one way that cathepsin G may make a significant contribution to the vicious cycle. However, outside of this report, little is currently known about cathepsin G in the pathologic microenvironment of bone metastases.

Although the functional role of cathepsin G is well characterized in a variety of pathologic conditions including rheumatoid arthritis (20), coronary artery disease (21), periodontitis (22), and ischemic reperfusion injury (23), this is the first report of its involvement in bone metastasis. Interestingly, however, the source of cathepsin G in rheumatoid arthritis is macrophages (20). Because osteoclasts are derived from the monocyte/macrophage lineage of cells, this represents a potential source for cathepsin G in the pathologic bone microenvironment. Currently, the other known source of cathepsin G is neutrophils. Cathepsin G is expressed at high levels on the plasma membrane of neutrophils bound to heparin and chondroitin sulfate after neutrophils degranulate (24). Whether or not neutrophils are an important source of cathepsin G at the tumor-bone interface is not currently known.

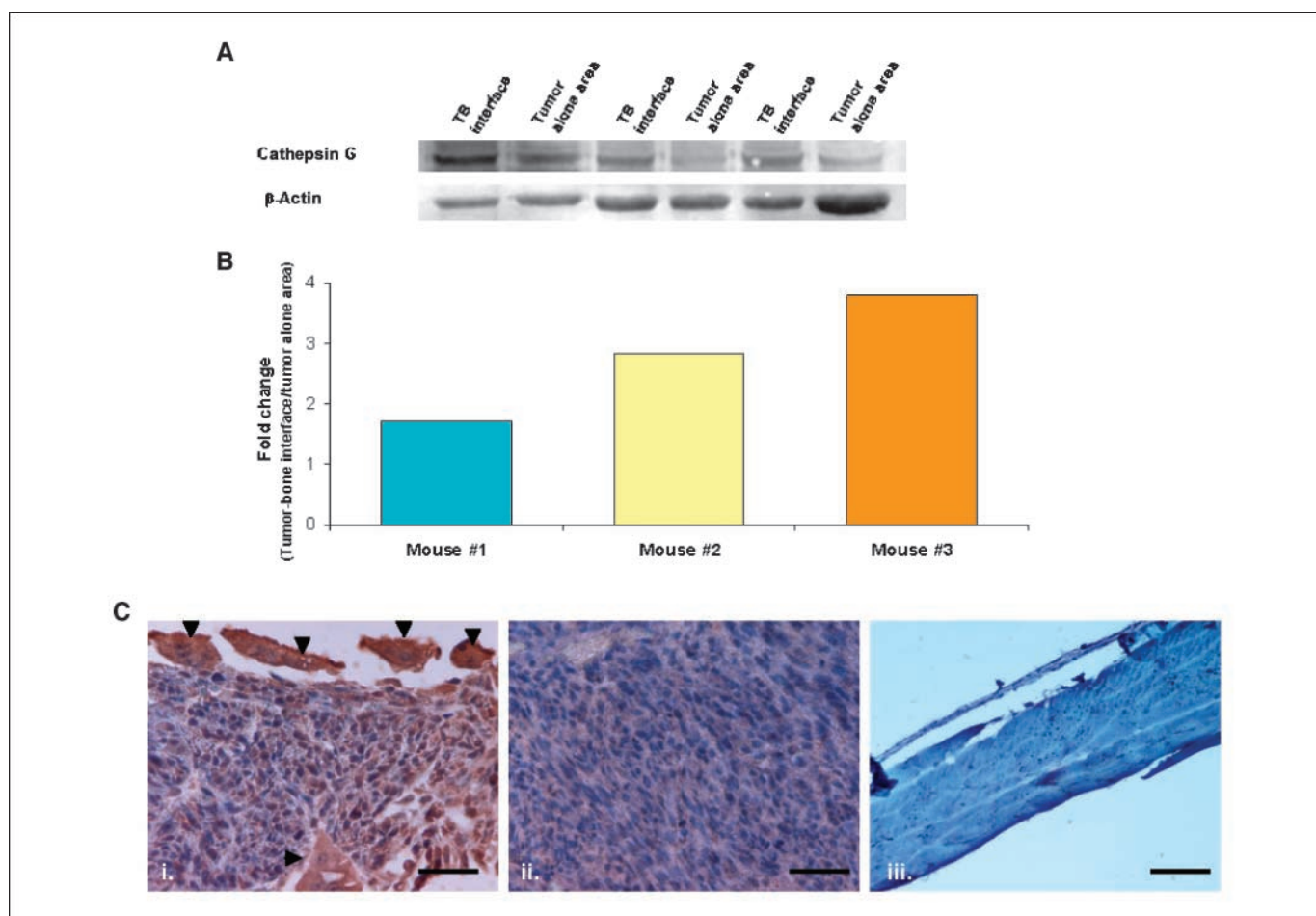


Figure 4. Expression of cathepsin G at the tumor-bone interface. *A*, Western blot analysis was done for mice bearing Cl66 tumors comparing cathepsin G expression at the tumor-bone interface to expression in the tumor alone area. Cathepsin G is up-regulated at the tumor-bone interface compared with the tumor-alone area. *B*, the expression of cathepsin G was quantified using ImageQuant gel analysis software (GE Healthcare). The expression indices for cathepsin G expression at the tumor-bone interface and tumor alone area were calculated by comparing the intensities of the cathepsin G and β -actin bands. The values are fold increase in cathepsin G expression at the tumor-bone area as compared with tumor alone area. Cathepsin G is increased at the tumor-bone interface compared with the tumor alone area in all three mice. *C*, immunohistochemistry for cathepsin G was done on sections from Cl66 tumor-bearing mice and non-tumor-bearing mice. *i*, osteoclasts (arrowheads) and osteoclast precursors stained strongly positive for cathepsin G and are the major source at the tumor-bone interface. Tumor cells near the tumor-bone interface stained moderately positive. *ii*, tumor cells in the tumor alone area stained weakly positive for cathepsin G. *iii*, immunostaining of normal bone showing no cathepsin G expression. Bar, 0.01 mm.

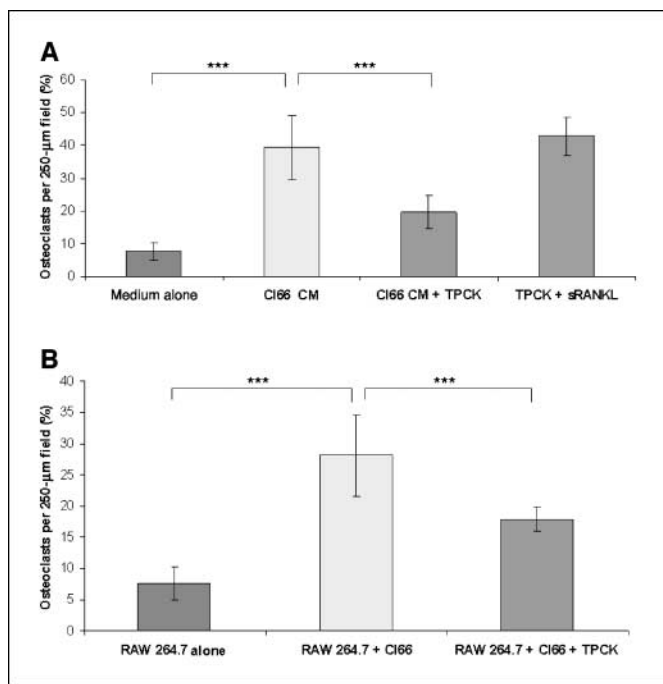


Figure 5. Inhibition of cathepsin G activity abrogates osteoclastogenesis. **A**, Cl66 conditioned medium (CM) induced higher osteoclastogenesis in RAW 264.7 cells compared with control (medium alone). TPCK treatment during collection of conditioned medium reduced osteoclastogenesis. Cl66 cells treated with TPCK plus commercially available sRANKL also showed higher osteoclastogenesis, showing that TPCK is not toxic to osteoclasts. **B**, Cl66 cells cocultured with RAW 264.7 cells induced higher osteoclastogenesis compared with RAW 264.7 cells alone. TPCK treatment reduced, but did not eliminate, this osteoclastogenesis. ***, $P < 0.001$.

To evaluate the source of cathepsin G in the bone microenvironment, immunohistochemistry was done. These studies supported the *in vitro* conclusion (Supplementary data) that osteoclasts likely make a significant contribution to the observed up-regulation of cathepsin G at the tumor-bone interface. Osteoclasts stained strongly positive for cathepsin G, whereas tumor cells at the tumor-bone interface showed moderate positivity. Osteoclast precursors that interspersed within the tumor cells also stained strongly positive. Further away from the tumor-bone interface in the tumor alone area, positivity for cathepsin G among the tumor cells became weaker and more sparse. Thus, this supports that tumor cells have low, baseline expression of cathepsin G that is up-regulated through interactions with osteoclast precursors but that osteoclasts are the major source of cathepsin G at the tumor-bone interface.

In addition to osteoblasts, all three cell lines (4T1, Cl66, and Cl66M2) used in this study express RANKL as well as cathepsin G (data not shown). The constitutive, low-level expression of cathepsin G by the tumor cells may be a mechanism by which they constitutively produce low levels of sRANKL. Thus, as tumor cells enter the bone microenvironment, they produce low levels of sRANKL, which triggers osteoclast differentiation and increased cathepsin G production. As the production of cathepsin G is then amplified, sRANKL production is increased, osteoclast differentiation is subsequently increased, and sequestered growth factors are released from the bone matrix that favor tumor progression. Thus, we are left with the potential for a new model of the osteolytic vicious cycle in which cathepsin G plays a central role.

Cathepsin G is potentially a central player in the vicious cycle, and thus, it represents an exciting potential therapeutic target in the treatment of mammary tumor-induced osteolysis. To test the effects of cathepsin G inhibition *in vitro*, we used a coculture model. Cl66-conditioned medium induced osteoclastogenesis in RAW 264.7 cells, suggesting that Cl66 cells produce a soluble factor capable of inducing osteoclastogenesis. Given that Cl66 cells express both cathepsin G and RANKL, this soluble factor is likely sRANKL. Thus, we would expect TPCK treatment to reduce the production sRANKL, which would reduce the concentration of sRANKL in the Cl66-conditioned medium and reduce osteoclastogenesis. As expected, TPCK abrogated the production of this soluble factor and reduced osteoclastogenesis, suggesting that cathepsin G is responsible for the generation of this soluble factor. Furthermore, Cl66 cells cocultured with RAW 264.7 cells also induced osteoclastogenesis that is reduced with TPCK treatment. Osteoclastogenesis is reduced but not eliminated because signaling via full-length, membrane-bound RANKL still occurs even with TPCK treatment. Thus, this is proof-in-principle that cathepsin G inhibition has the potential to reduce osteoclastogenesis and subsequent osteolysis *in vivo*. Based on these data, we subsequently sought to determine if inhibition of cathepsin G *in vivo* would reduce mammary tumor-induced osteolysis. TPCK treatment of mice significantly reduced osteolysis at the tumor-bone interface. In fact, TPCK-treated mice showed a 63% reduction in the bone destruction index. We did not observe a difference between TPCK-treated mice and control mice in terms of tumor growth or growth kinetics, suggesting that TPCK is not toxic to tumor cells and is not inducing apoptosis. In addition, our *in vitro* data suggest that

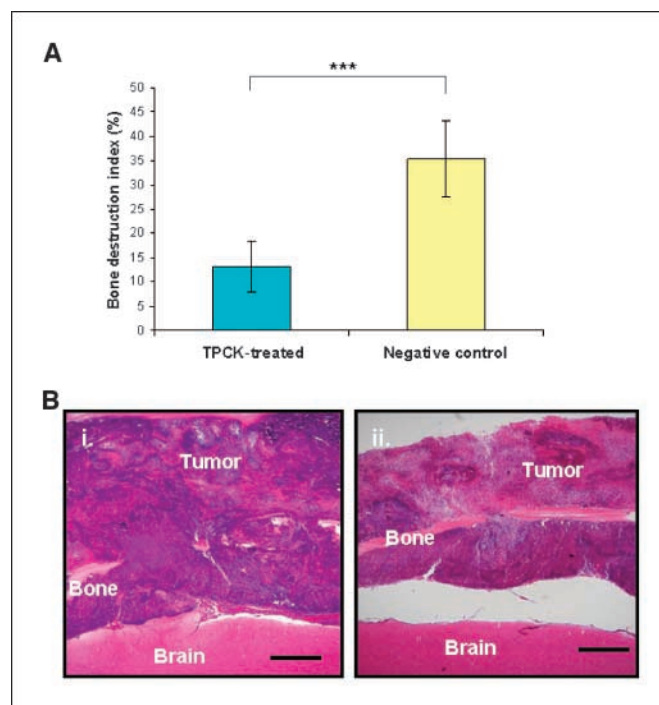


Figure 6. Inhibition of cathepsin G *in vivo* reduces osteolysis. **A**, TPCK treatment significantly reduced mammary tumor-induced osteolysis *in vivo* compared with DMSO-treated mice (negative control). Bars, SD. ***, $P < 0.001$. **B**, *i*, H&E-stained section of the tumor-bone interface from DMSO-treated mouse (negative control) showing significant osteolysis. *ii*, H&E-stained section of the tumor-bone interface from TPCK-treated mouse showing significantly reduced osteolysis. Bar, 2 mm.

TPCK is not toxic to osteoclasts. Thus, the mechanism by which TPCK inhibits osteolysis is likely via interruption of signaling between tumor cells and the bone microenvironment, and our data suggest that the pathway that is interrupted is the generation of sRANKL.

This reduction in osteolysis shows the central role that cathepsin G plays in mammary tumor-induced osteolysis *in vivo*. TPCK is a potent inhibitor of cathepsin G but is not specific to only cathepsin G (8). TPCK is also capable of inhibiting chymotrypsin, papain, bromelain, and ficin (7). Although TPCK is not specific for cathepsin G, given its ability to potently inhibit cathepsin G, taken with the lack of toxicity to tumor cells shown by no observable difference in tumor growth or growth kinetics, the lack of toxicity to osteoclasts as shown *in vitro* by treatment of RAW 264.7 cells with both TPCK and sRANKL, and the proposed mechanism by which inhibition of cathepsin G would reduce sRANKL and specifically decrease osteolysis, we believe that inhibition with TPCK adequately shows the role of cathepsin G in mammary tumor-induced osteolysis.

In conclusion, this study shows that cathepsin G plays an important role in mammary tumor-induced osteolytic lesions by contributing to the vicious cycle. It is significantly up-regulated at the tumor-bone interface and is capable of generating sRANKL,

which potentially enhances osteoclast activation and osteolysis. We have also shown that inhibition of cathepsin G *in vitro* and *in vivo* reduces osteoclastogenesis and subsequent osteolysis. Thus, we have shown a central role for cathepsin G in the establishment of mammary tumor-induced osteolytic lesions. Further studies are needed to reveal the potential subsequent roles of cathepsin G, in addition to generation of soluble RANKL, in the bone tumor microenvironment. This study reveals cathepsin G as an appealing therapeutic target in mammary tumor-induced osteolysis.

Disclosure of Potential Conflicts of Interest

No potential conflicts of interest were disclosed.

Acknowledgments

Received 10/18/2007; revised 3/10/2008; accepted 5/19/2008.

Grant support: Grant CA72781 and Cancer Center Support Grant P30CA036727 from the NIH (R.K. Singh), Nebraska Department of Health and Human Services, Nebraska Research initiative (R.K. Singh), and the Howard Hughes Medical Institute Research Training Fellowship (T.J. Wilson).

The costs of publication of this article were defrayed in part by the payment of page charges. This article must therefore be hereby marked *advertisement* in accordance with 18 U.S.C. Section 1734 solely to indicate this fact.

We thank Michelle Varney for careful review and critique of the manuscript.

References

- Jemal A, Siegel R, Ward E, Murray T, Xu J, Thun MJ. Cancer statistics, 2007. *CA Cancer J Clin* 2007;57:43–66.
- Mundy GR. Metastasis to bone: causes, consequences and therapeutic opportunities. *Nat Rev Cancer* 2002;2:584–93.
- Kajita M, Itoh Y, Chiba T, et al. Membrane-type 1 matrix metalloproteinase cleaves CD44 and promotes cell migration. *J Cell Biol* 2001;153:893–904.
- Eliceiri BP, Cheresch DA. Role of α_v integrins during angiogenesis. *Cancer J* 2000;6 Suppl 3:S245–9.
- Deryugina EI, Ratnikov BI, Postnova TI, Rozanov DV, Strongin AY. Processing of integrin α_v subunit by membrane type 1 matrix metalloproteinase stimulates migration of breast carcinoma cells on vitronectin and enhances tyrosine phosphorylation of focal adhesion kinase. *J Biol Chem* 2002;277:9749–56.
- Lynch CC, Hikosaka A, Acuff HB, et al. MMP-7 promotes prostate cancer-induced osteolysis via the solubilization of RANKL. *Cancer Cell* 2005;7:485–96.
- Overall CM, Blobel CP. In search of partners: linking extracellular proteases to substrates. *Nat Rev Mol Cell Biol* 2007;8:245–57.
- Selak MA, Chignard M, Smith JB. Cathepsin G is a strong platelet agonist released by neutrophils. *Biochem J* 1988;251:293–9.
- Yu Q, Stamenkovic I. Cell surface-localized matrix metalloproteinase-9 proteolytically activates TGF- β and promotes tumor invasion and angiogenesis. *Genes Dev* 2000;14:163–76.
- Ishikawa T, Kamiyama M, Tani-Ishii N, et al. Inhibition of osteoclast differentiation and bone resorption by cathepsin K antisense oligonucleotides. *Mol Carcinog* 2001;32:84–91.
- Nemeth JA, Yousif R, Herzog M, et al. Matrix metalloproteinase activity, bone matrix turnover, and tumor cell proliferation in prostate cancer bone metastasis. *J Natl Cancer Inst* 2002;94:17–25.
- Ishibashi O, Niwa S, Kadoyama K, Inui T. MMP-9 antisense oligodeoxynucleotide exerts an inhibitory effect on osteoclastic bone resorption by suppressing cell migration. *Life Sci* 2006;79:1657–60.
- Jimi E, Aoki K, Saito H, et al. Selective inhibition of NF- κ B blocks osteoclastogenesis and prevents inflammatory bone destruction *in vivo*. *Nat Med* 2004;10:617–24.
- Ohshiba T, Miyaura C, Inada M, Ito A. Role of RANKL-induced osteoclast formation and MMP-dependent matrix degradation in bone destruction by breast cancer metastasis. *Br J Cancer* 2003;88:1318–26.
- Yasuda H, Shima N, Nakagawa N, et al. Osteoclast differentiation factor is a ligand for osteoprotegerin/osteoclastogenesis-inhibitory factor and is identical to TRANCE/RANKL. *Proc Natl Acad Sci U S A* 1998;95:3597–602.
- Lacey DL, Timms E, Tan HL, et al. Osteoprotegerin ligand is a cytokine that regulates osteoclast differentiation and activation. *Cell* 1998;93:165–76.
- Fujisaki K, Tanabe N, Suzuki N, et al. Receptor activator of NF- κ B ligand induces the expression of carbonic anhydrase II, cathepsin K, and matrix metalloproteinase-9 in osteoclast precursor RAW264.7 cells. *Life Sci* 2007;80:1311–8.
- Chesneau V, Becherer JD, Zheng Y, Erdjument-Bromage H, Tempst P, Blobel CP. Catalytic properties of ADAM19. *J Biol Chem* 2003;278:22331–40.
- Schlondorff J, Lum L, Blobel CP. Biochemical and pharmacologic criteria define two shedding activities for TRANCE/OPGL that are distinct from the tumor necrosis factor α convertase. *J Biol Chem* 2001;276:14665–74.
- Szekanecz Z, Koch AE. Macrophages and their products in rheumatoid arthritis. *Curr Opin Rheumatol* 2007;19:289–95.
- Chavan V, Patil N, Karnik ND. Study of leukocytic hydrolytic enzymes in patients with acute stage of coronary heart disease. *Indian J Med Sci* 2007;61:73–82.
- Komine K, Kuroishi T, Ozawa A, et al. Cleaved inflammatory lactoferrin peptides in parotid saliva of periodontitis patients. *Mol Immunol* 2007;44:1498–508.
- Shimoda N, Fukazawa N, Nonomura K, Fairchild RL. Cathepsin g is required for sustained inflammation and tissue injury after reperfusion of ischemic kidneys. *Am J Pathol* 2007;170:930–40.
- Campbell EJ, Owen CA. The sulfate groups of chondroitin sulfate- and heparan sulfate-containing proteoglycans in neutrophil plasma membranes are novel binding sites for human leukocyte elastase and cathepsin G. *J Biol Chem* 2007;282:14645–54.

Matrix Metalloproteinase (MMP)-13 Regulates Mammary Tumor-Induced Osteolysis by Activating MMP9 and Transforming Growth Factor- β Signaling at the Tumor-Bone Interface

Kalyan C. Nannuru¹, Mitsuru Futakuchi², Michelle L. Varney¹, Thomas M. Vincent³, Eric G. Marcussos³, and Rakesh K. Singh¹

Abstract

The tropism of breast cancer cells for bone and their tendency to induce an osteolytic phenotype are a result of interactions between breast cancer cells and stromal cells and are of paramount importance for bone metastasis. However, the underlying molecular mechanisms remain poorly understood. We hypothesize that tumor-stromal interaction alters gene expression in malignant tumor cells and stromal cells creating a unique expression signature that promotes osteolytic breast cancer bone metastasis and that inhibition of such interactions can be developed as targeted therapeutics. Microarray analysis was performed to investigate gene expression profiling at the tumor-bone (TB) interface versus the tumor alone area from syngenic mice injected with three different syngenic mammary tumor cell lines that differ in their metastatic potential. We identified matrix metalloproteinase 13 (MMP13), receptor activator of NF- κ B ligand (RANKL), and integrins binding sialoprotein to be genes upregulated at the TB interface and validated. To determine the functional role of MMP13 in tumor-induced osteolysis, mice with Cl66 mammary tumors were treated with MMP13 antisense oligonucleotides (MMP13-ASO) or control scrambled oligonucleotides (control-ASO). Knockdown of MMP13 expression at the TB interface leads to significant reduction in bone destruction and in the number of activated osteoclasts at the TB interface. Further analysis to evaluate the mechanism of MMP13-dependent osteolytic bone metastasis revealed that MMP13-ASO treatment decreased active MMP9, RANKL levels, and transforming growth factor- β signaling at the TB interface. Together, our data indicate that upregulation of MMP13 at the TB interface is important in tumor-induced osteolysis and suggest that MMP13 is a potential therapeutic target for breast cancer bone metastasis. *Cancer Res*; 70(9); 3494-504. ©2010. AACR.

Introduction

Breast cancer is the most common cancer and the second leading cause of cancer-related death in women in the United States (1). Most complications of breast cancer are attributed to metastasis to distant organs, including lymph nodes, liver, lung, and bone (2, 3). In advanced stages of the disease, nearly all breast cancer patients suffer with bone metastasis. Bone metastases in breast cancer are predominantly osteolytic and also cause skeletal lesions including

pathologic fracture, intractable bone pain, nerve compression, and hypercalcemia (4, 5). These complications not only increase the risk of mortality but also cause a significant decrease in the quality of life (3).

Breast cancer cells show a strong predilection for bone (5). Arrival of tumor cells in the bone microenvironment initiates a "vicious cycle" of bidirectional interactions between tumor cells and stromal cells (3, 6). Tumor cells produce various factors such as parathyroid hormone-related peptide (7, 8), interleukin-8 (IL-8), and IL-1 to stimulate osteoblasts to induce expression of receptor activator of NF- κ B ligand (RANKL) to induce bone resorption (9). Increased bone resorption causes the release of sequestered factors that favor the growth of malignant tumor cells including bone-derived growth factor, fibroblast growth factor, and transforming growth factor β (TGF β ; ref. 3). The underlying molecular mechanisms of tumor-bone (TB) interaction are poorly understood. In this report, we hypothesize that tumor-stromal interaction in the bone microenvironment alters gene expression in malignant tumor cells and stromal cells creating a unique expression signature that promotes osteolytic bone metastasis and that inhibition of

Authors' Affiliations: ¹Department of Pathology and Microbiology, University of Nebraska Medical Center, Omaha, Nebraska; ²Department of Molecular Toxicology, Nagoya City University, Nagoya, Japan; and ³Isis Pharmaceuticals, Carlsbad, California

Note: Supplementary data for this article are available at Cancer Research Online (<http://cancerres.aacrjournals.org/>).

Corresponding Author: Rakesh K. Singh, Department of Pathology and Microbiology, University of Nebraska Medical Center, 985900 Nebraska Medical Center, Omaha, NE 68198-5900. Phone: 402-559-9949; Fax: 402-559-5900; E-mail: rsingh@unmc.edu.

doi: 10.1158/0008-5472.CAN-09-3251

©2010 American Association for Cancer Research.

such interactions can be targeted for development of novel therapeutics.

Extracellular matrix (ECM) degradation, mediated by matrix metalloproteinases (MMP), is an essential step in the growth, invasion, and metastasis of malignant tumors. MMPs are a family of human zinc endopeptidases that can degrade virtually all ECM components (10). Apart from their ECM degradation functionality, latest research in MMPs reveals their specific roles in cleaving several extracellular and membrane-associated proteins and regulating cellular signaling pathways. MMP7 promotes osteolytic bone metastasis in prostate cancer through generation of soluble RANKL (sRANKL) from membrane bound RANKL (11). MMP2 and MMP9 have been associated with tumor angiogenesis (12). Expression of these proteases is also associated with poor clinical outcome in various malignancies, such as bladder, breast, lung cancer and head and neck squamous cell carcinomas (SCC; refs. 13, 14).

MMP13 was first identified from overexpressing breast carcinomas (15). IL-1 α and IL-1 β are potential candidates for inducing expression of MMP13 in breast carcinomas (16). In case of SCC, MMP13 is predominantly expressed by the tumor cells at the invading front and to some extent by stromal fibroblasts surrounding tumor cells (17, 18). Expression of MMP13 in the head and neck SCCs correlates with the invasion and metastatic capacity (17, 18). In laryngeal and vulvar carcinomas, the expression of MMP13 colocalizes with the expression of MT1-MMP and MMP2, suggesting that these three MMPs form a proteolytic cascade that leads to potent extracellular collagenolytic activity (19). In non-small cell lung carcinoma, tumor cells expressing MMP13 have a potential to shed from the primary tumor and aggregate in the bone marrow and associated with poorer survival rates (20). But the specific role of MMP13 in malignant breast cancer remains unclear. Our study is focused on elucidating the role of MMP13 in the tumor-stromal interaction, with particular attention to the TB microenvironment.

We identified that MMP13, RANKL, and integrins binding sialoprotein (IBSP) were the genes upregulated at the TB interface. Moreover, we showed that knockdown of MMP13 expression at the TB interface leads to a significant reduction in bone destruction and in the number of activated osteoclasts at the TB interface. MMP13-ASO treatment decreased the RANKL/OPG ratio, active MMP9, and TGF β levels at the TB interface. Together, our data showed that upregulation of MMP13 at the TB interface is important for regulation of tumor-induced osteolysis and suggest that MMP13 might be a potential novel therapeutic target for breast cancer bone metastasis.

Materials and Methods

Cells and animals. Three murine mammary adenocarcinoma cell lines 4T1 (highly metastatic), Cl66 (moderately metastatic), and Cl66M2 (poorly metastatic), differing in their metastatic potential, were used in this study (21, 22). Cells were maintained in DMEM (Mediatech) with 5% serum

supreme (Biowhitaker), 1% vitamins, 1% L-glutamine, and 0.08% gentamicin (Invitrogen).

Animal experiments were approved by Institutional Animal Care and Use Committee of University of Nebraska Medical Center. Eight-week-old female BALB/c mice (National Cancer Institute) were used in this study. For *in vivo* experiments, tumor cells ($5 \times 10^4/50 \mu\text{L}$) mixed in growth factor-reduced Matrigel (BD Biosciences) were injected directly onto the calvaria to mimic the close association of tumor cells and bone. Four weeks after implantation of tumor cells, mice were sacrificed and tumor alone and TB interface samples were collected. For immunohistochemical analysis, the samples were fixed in 4% paraformaldehyde at 4°C for 48 hours. The tissues were then transferred into a decalcification solution [15% EDTA with glycerol (pH 7.4)] for 4 weeks and were subsequently paraffin embedded and processed for histology.

RNA and protein extraction were done by homogenization of tissue samples in liquid nitrogen. Total RNA was extracted using Trizol (Invitrogen) following the manufacturer's instructions. The RNA concentration was quantified using a NANO drop ND-1000 Spectrophotometer (Nano Drop Technologies).

Protein was extracted using T-PER tissue protein extractor solution (Pierce) following the manufacturer's provided protocol. Protein samples were quantified using a bicinchoninic acid protein assay kit (Pierce). Proteinase activity assays were performed with protein samples without protease inhibitors.

Microarray analysis and quantitative real-time PCR. Calcified frozen sections were serially sectioned in 10- μm -thick slices, and at least 10 slides per mouse were microdissected with careful separation of the TB interface and the tumor alone areas, as described earlier (22, 23). Total RNA was extracted from each microdissected population and pooled, and an equal amount of RNA was amplified using a probe amplification kit (Affymetrix). An Affymetrix Mouse Expression Array 430 was used for comparing gene expression profiles between the TB interface and the tumor alone areas. A complete detection and analysis of signals for each chip was performed using Affymetrix GeneChip Operating Software to generate raw expression data. A signal log ratio algorithm was used to estimate the magnitude of change of a transcript when two arrays were compared (experimental versus baseline). It was calculated by comparing each probe pair on the experimental array, the TB interface, with the corresponding probe pair on the baseline array, the tumor alone area, and considering the mean of the log ratios of probe pair intensities across the two arrays. The change is expressed as the log₂ ratio. Thus, a signal log ratio of 1.0 indicates an increase of transcript level by 2-fold and -1.0 indicates a decrease by 2-fold. For each set of tissues from 4T1, Cl66, and Cl66M2, the signal log ratio of the TB interface versus the tumor alone area was calculated, and the genes were ordered from highest to lowest expression levels.

Gene expression analysis was confirmed using quantitative real-time PCR (qRT-PCR) for the TB interface and tumor alone area samples. RNA (5 μg) from each sample was used to synthesize first-strand cDNA. Diluted first-strand cDNA

(1:100, 2 μ L) was amplified in a 20- μ L reaction with SYBR green master mix (Roche) and 10 mmol/L primer mix using a Bio-Rad iCycler (Bio-Rad). The following reaction conditions were used: initial denaturation at 95°C for 3 minutes, followed by amplification cycles with denaturation at 95°C for 60 seconds, annealing at 60°C for 60 seconds, extension at 72°C for 60 seconds, and finally a long extension at 72°C for 2 minutes. Primers used for validation of gene expression are included in Supplementary Table S1. The fluorescence intensity of double-strand specific SYBR green, reflecting the amount of formed PCR product, was monitored at the end of each elongation step. The Ct value for each gene was normalized with glyceraldehyde-3-phosphate dehydrogenase (GAPDH) expression for relative gene expression analysis.

Immunohistochemistry and tartrate-resistant acid phosphatase staining. MMP13 protein expression was evaluated by immunohistochemistry on tumor sections using a MMP13-specific antibody (Santa Cruz Biotechnology). The sections were deparaffinized using EZ dewax solution (Biogenex). For antigen retrieval, the sections were boiled in 10 mmol/L citrate buffer (pH 6.0) for 10 minutes, and endogenous peroxidase activity was blocked using 3% H₂O₂ for 5 minutes. The sections were then blocked in antibody diluent for 1 hour at room temperature. MMP13 antibody was diluted 1:100 in blocking solution, and sections were incubated overnight at 4°C. After washing, the slides were incubated with anti-goat biotinylated antibody for 30 minutes at room temperature. After washing, immunoreactivity was detected using Vectastain avidin-biotin complex method and 3,3'-diaminobenzidine substrate kits (Vector Laboratories). Sections were counterstained with hematoxylin, dehydrated, and permanently mounted.

For *in vivo* evaluation of TGF β signaling, we performed immunohistochemistry for phosphorylated Smad-2 (p-Smad-2; refs. 24, 25). Sections were blocked using goat serum diluted 1:500 for 1 hour at room temperature. Sections were then incubated overnight at 4°C with antibody directed against p-Smad-2 (Ser^{465/467}, Cell Signaling Technology) diluted 1:50 in blocking solution. After washing, sections were incubated for 1 hour at room temperature with biotinylated anti-rabbit IgG diluted 1:500. TRAP staining was performed to detect activated osteoclasts *in vivo* according to the manufacturer's instructions (Sigma Chemicals). Briefly, deparaffinized slides were rinsed with deionized water before incubating with TRAP containing buffer at 37°C for 1 hour, rinsed with deionized water, and counterstained with Gill3 hematoxylin solution for 2 minutes followed by aqueous mounting. Immunostained sections were examined under a Nikon light microscope, and the number of TRAP-positive multinucleated cells at the TB interface was assessed at a magnification of 400 \times for each lesion. The total number of osteoclasts was then divided by the length of the TB interface to get the number of osteoclasts per millimeter of TB interface.

Antisense oligonucleotide treatment for inhibition of tumor-induced osteolysis. Antisense oligonucleotides (ASO) used in the therapeutic protocol were obtained from Isis Phar-

maceuticals. ASOs designed specifically to target *MMP13* were used throughout this study. 2'-Methoxyethyl modified chimeric ASOs with a phosphorothioate backbone were synthesized as previously described (26). Briefly, these oligonucleotides are modified at the 2' sugar position of the five bases at both the 3' and 5' ends with a methoxyethyl group. This modification greatly increases the stability of the oligonucleotides and the affinity for its target mRNA while reducing the amount of immune stimulatory and inflammatory effects that can be seen with oligonucleotides in mice (27). Active ASOs were identified by screening 46 ASOs designed to be specific for *MMP13*. The efficacy of these ASOs was confirmed in concentration-response experiments, and the most potent ASO was used for further experiments. Control-ASO did not match any known mRNA in the mouse genome.

Animals bearing Cl66 mammary tumors were randomly divided into two treatment groups (control-ASO and MMP13-ASO). The oligonucleotides were dissolved in physiologic saline (0.9% NaCl) and were given by i.p. injection at a dose of 50 mg/kg/d starting at day 7 following tumor implantation for 5 days with 2 days off followed by another 4 days. Tumor growth was monitored, and mice were sacrificed on day 28. Tumor alone and TB interface samples were collected and processed for further analysis.

Gelatin zymography. Total protein (50 μ g) isolated from either the TB interface or tumor alone area from animals implanted with Cl66 tumors was subjected to electrophoresis on a 10% (w/v) polyacrylamide SDS gel containing 1 mg/mL porcine gelatin (Sigma-Aldrich). At the completion of electrophoresis, the gel was washed with 2.5% Triton X-100 buffer for 30 minutes. After rinsing, the gel was incubated for 12 hours at 37°C in incubation buffer containing 50 mmol/L Tris-HCl (pH 7.4), 150 mmol/L NaCl, 10 mmol/L CaCl₂, and 0.05% (w/v) Na₂S₂O₈. After rinsing, the gel was then stained using 0.025% Coomassie brilliant blue (Bio-Rad) and photographed using a Multi Image Light Cabinet (Alpha Innotech Corporation). The volume of gelatinolytic activity was evaluated using ImageQuant 5.1 (Molecular Dynamics).

Pro-MMP9 ELISA. TB lysates from control-ASO-treated and MMP13-ASO-treated mice (400 ng/ μ L) were used for analysis. The concentration of pro-MMP9 in these samples was determined by Quantikine Mouse pro-MMP9 ELISA according to the manufacturer's instructions (R&D Systems). This assay is a quantitative "sandwich" enzyme immunoassay. Based on a curve of the absorbance of samples to the standard curve (plotted using recombinant pro-MMP9 protein), we determined the concentrations of pro-MMP9 in the tumor lysates.

Statistical analysis. For *in vitro* studies, the Student's *t* test was used for statistical comparison. For *in vivo* studies, the Mann-Whitney *U* test was used for statistical comparison. A *P* < 0.05 was considered significant.

Results

Gene expression profile at the TB interface. We analyzed gene expression patterns at the TB interface compared with the tumor alone area using cDNA microarray. Mammary

tumor cells with different metastatic potential [4T1 (high), Cl66 (moderate), and Cl66M2 (low)] were transplanted onto the calvaria of BALB/c mice. Histologic analysis showed that all tumors exhibited tumor-induced osteolysis and osteoclast activation. Microarray analysis revealed the upregulation of 414 genes and the downregulation of 27 genes at the TB interface compared with the tumor alone area. The highly up-regulated genes were *IBSP*, *RANKL*, *MMP13*, *insulin growth factor binding protein 5*, *Lumican*, *Lysyl oxidase (Lox)*, *Kinesin family 5B (Kif5b)*, and *Wnt inhibitory factor 1 (Wif1)* (Fig. 1A). The common upregulation of these genes in all three cell lines further suggested that they may play an important role in mammary tumor-induced osteolysis.

We then used qRT-PCR with gene specific primers to confirm gene expression at the TB interface. Our data confirmed the upregulation of mRNA expression of *MMP13* (Fig. 1B, i),

IBSP (Fig. 1B, ii), *Lumican* (Fig. 1B, iii), *Lox* (Fig. 1B, iv), *Kif5b* (Fig. 1B, v), and *Wif1* (Fig. 1B, vi) at the TB interface.

Upregulation of MMP13 at the TB interface. Recognizing the important role of proteases in tumor progression, we further evaluated the functional role of MMP13 in mammary tumor-induced osteolysis. We examined MMP13 protein expression at the TB interface by immunohistochemistry. MMP13-specific antibody staining revealed a significant upregulation of MMP13 in Cl66 tumors at the TB interface (Fig. 2A, b) but not at the tumor alone area (Fig. 2A, a). We observed low levels of immunoreactivity in normal calvaria (Fig. 2A, c). Antibody controls did not show any non-specific staining (data not shown). This protein level analysis further confirmed the earlier observation of increased *MMP13* transcript levels by cDNA microarray and qRT-PCR analyses. In addition, our immunohistochemical

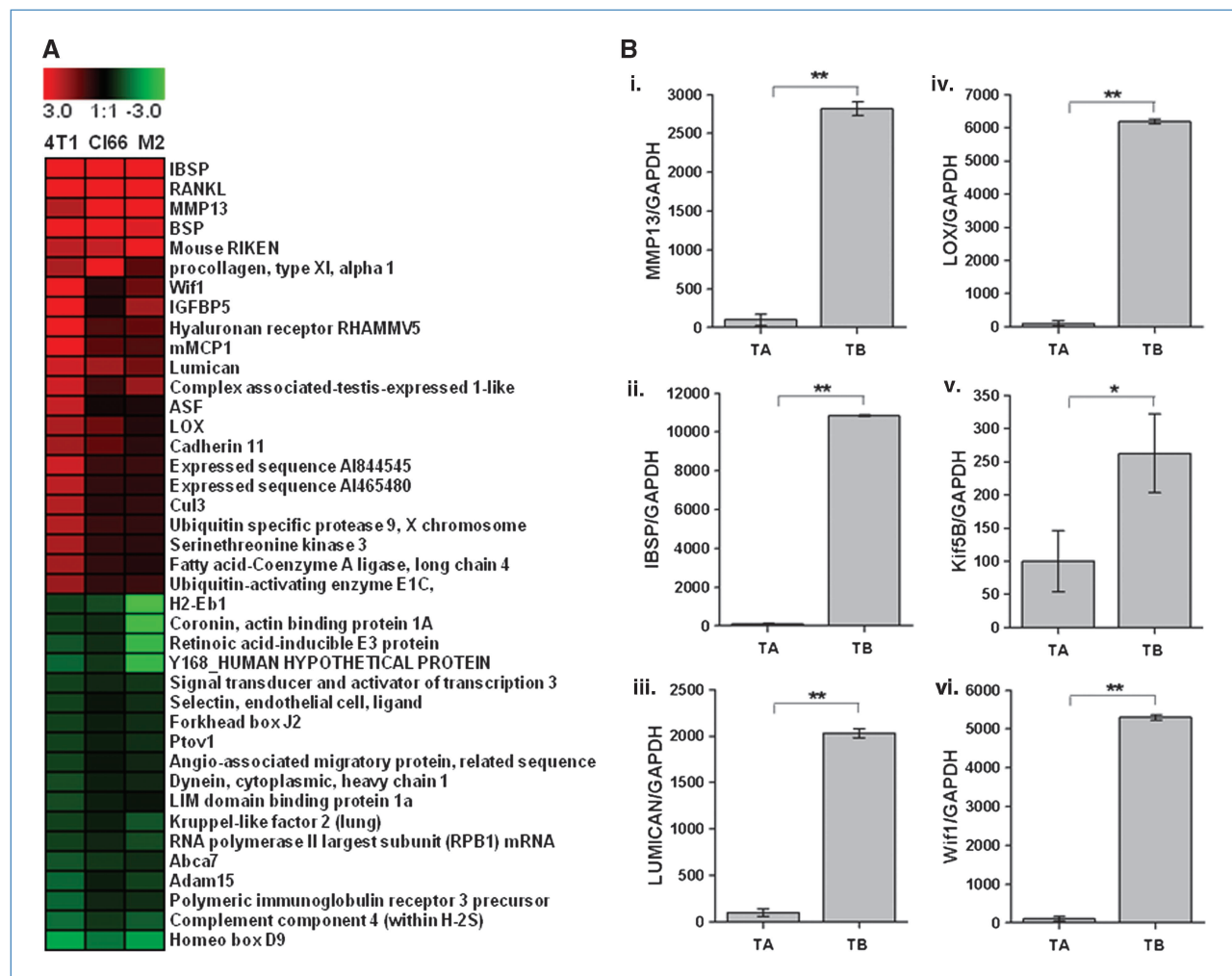


Figure 1. Gene expression profile at the TB interface. A, changes in the gene expression profile at the TB interface in comparison with the tumor alone area were determined using cDNA microanalysis using week 4 samples from 4T1, Cl66, and Cl66M2 tumors. B, i-vi, mRNA expression of *MMP13*, *IBSP*, *Lumican*, *LOX*, *Kif5b*, and *Wif1* was confirmed by real-time PCR analysis with gene-specific primers. Relative expression of these genes from tumor alone and TB interface samples were normalized to GAPDH expression. Real-time gene expression data presented are representative of all three cell lines done in triplicate. Bars, SEM. **, $P < 0.05$.

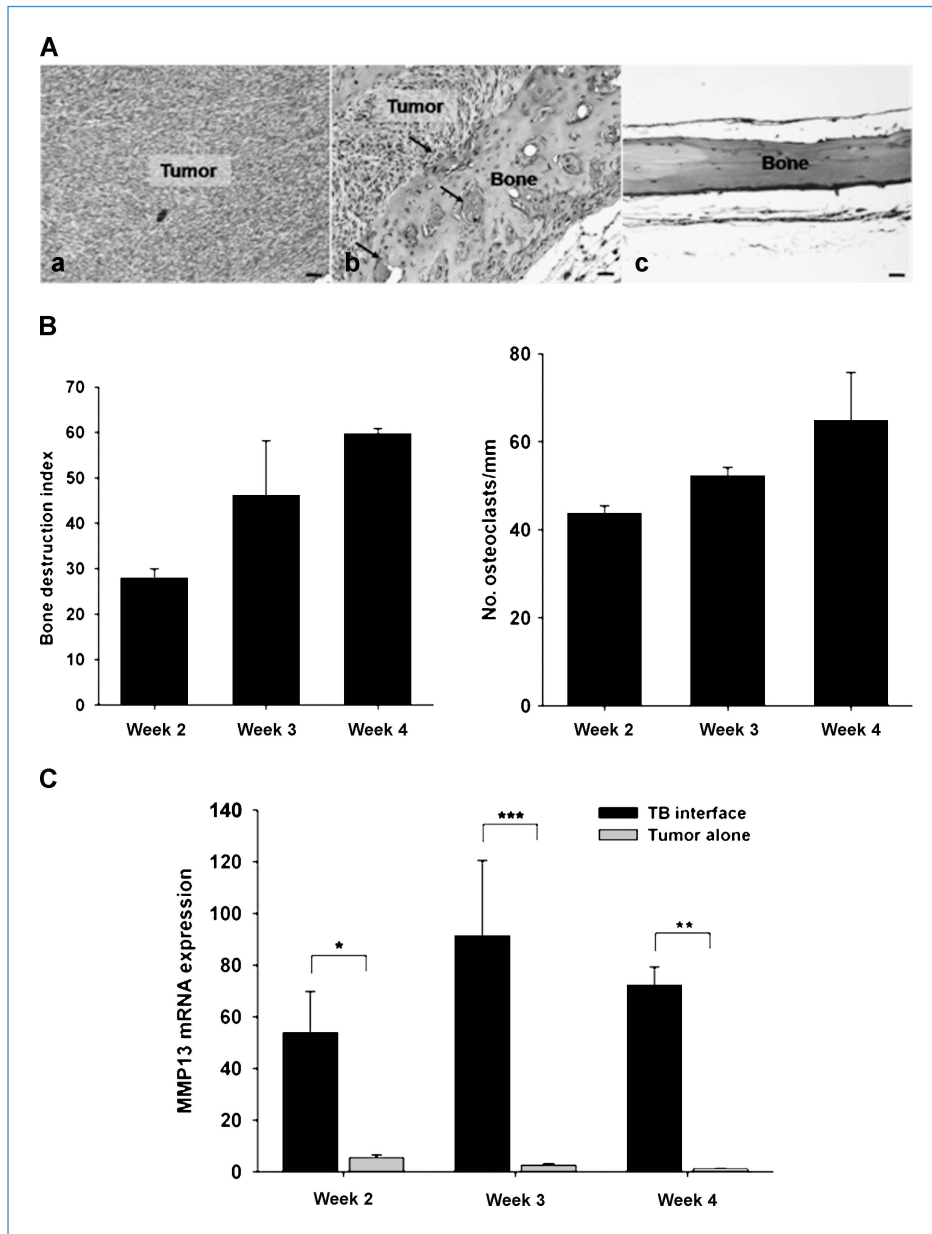


Figure 2. MMP13 expression at TB interface is associated with tumor-induced osteolysis. A, expression of MMP13 at the TB interface. Immunohistochemistry for MMP13 was done on sections from Cl66 tumor-bearing mice and non-tumor-bearing mice. b, tumor cells, osteoblasts, and stromal cells at the TB interface were stained positive for the MMP13 (arrows). a, tumor cells in the tumor alone area did not stain for MMP13. c, immunostaining of normal bone showing very low MMP13 expression. Bar, 0.01 mm. B, severity of tumor-induced osteolysis was computed by measuring the BDI on sections from Cl66 tumor-bearing mice at weeks 2, 3, and 4 after tumor implantation. We observed an increase in the BDI with time and an association with osteoclast homing at the TB interface. Bars, SD ($n = 5$). C, kinetics of *MMP13* expression at different time points after tumor implantation by RT-PCR. TB interface and tumor alone area samples from Cl66 tumor-bearing mice were analyzed for *MMP13* expression, and an increase in expression was observed at the TB interface at all time points. Relative *MMP13* expression was normalized to *GAPDH* expression. Bars, SD. *, $P < 0.05$; **, $P < 0.01$; ***, $P < 0.005$.

analysis reveals that *MMP13* is expressed by tumor cells, osteoblasts, and stromal cells at the TB interface, which are interacting with cells of bone microenvironment (Fig. 2A, b).

Kinetics of *MMP13* mRNA expression and tumor-induced osteolysis. In the next set of experiments, we examined the kinetics of *MMP13* expression and its association with tumor-induced osteolysis and the number of activated osteoclasts. Mice bearing Cl66 tumors were killed 2, 3, or 4 weeks after tumor implantation, and tumors were examined for bone destruction, osteoclast number, and *MMP13* expression at the TB interface and tumor alone areas. We quantified the severity of lesions by measuring bone destruction index (BDI), which is a ratio of the length of the bone that is destroyed by the tumor to the total length of the bone at the TB

interface. Results shown in Fig. 2B show an increase in bone destruction and osteoclast number over time. We observed higher levels of *MMP13* mRNA expression at the TB interface compared with tumor alone areas (Fig. 2C).

Inhibiting *MMP13* expression abrogates mammary tumor-induced osteolysis and number of activated osteoclasts at the TB interface. Next, we examined whether knocking down *MMP13* expression in Cl66 tumor-bearing mice using ASOs inhibited mammary tumor-induced osteolysis. We did not observe any weight loss or toxicity in any of the treatment groups (data not shown). We observed smaller tumors in *MMP13*-ASO-treated group compared with control-ASO-treated group; however, the decrease in tumor size was not significant (data not shown).

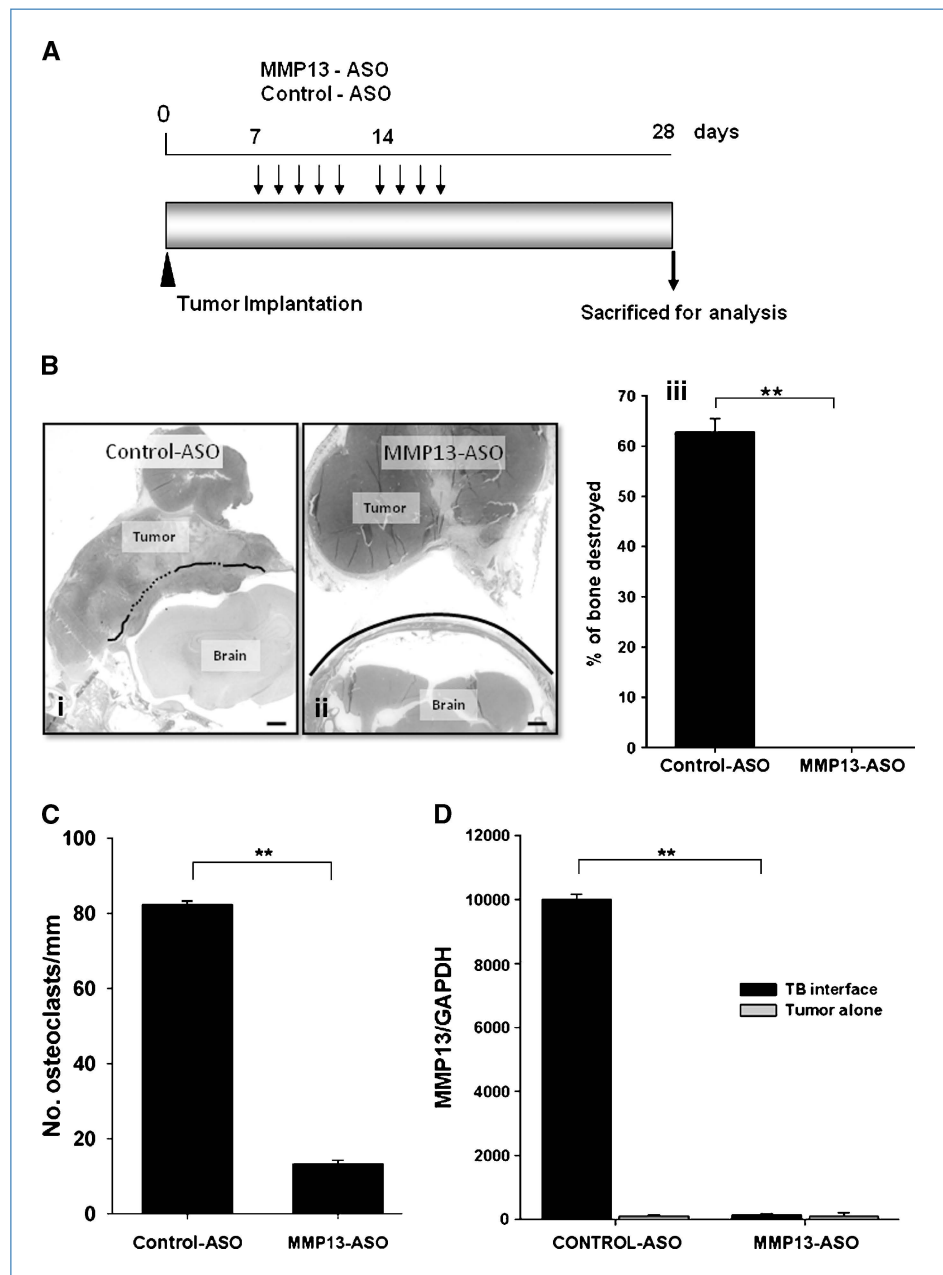
H&E staining of tumor sections showed severe bone destruction in control-ASO-treated tumors (Fig. 3B, i), whereas MMP13-ASO-treated tumors showed no osteolysis (Fig. 3B, ii). We observed a significant decrease in osteolysis in the MMP13-ASO-treated group compared with the control-ASO-treated group (Fig. 3B, iii). Similarly, we observed a significant decrease in the number of activated osteoclasts lining the TB interface in the MMP13-ASO-treated group (Supplementary Fig. S1; Fig. 3C).

We examined the expression of *MMP13* in tumors from MMP13-ASO-treated and control-ASO-treated mice using qRT-PCR. The expression of *MMP13* at the TB interface

was significantly lower in the MMP13-ASO-treated group compared with that in the control-ASO-treated group (Fig. 3D). We observed very low levels of *MMP13* expression in the tumor alone area, which was not altered by MMP13-ASO treatment (Fig. 3D).

Inhibition of *MMP13* decreases *RANKL* expression and regulates the *RANKL/OPG* ratio at the TB interface. Previous observations from our laboratory have shown the upregulation of *RANKL* at the TB interface in mammary tumor-induced osteolysis (28). *RANKL* interacts with its receptor *RANK* and activates osteoclasts. We evaluated *RANKL* mRNA levels in MMP13-ASO-treated and control-ASO-treated

Figure 3. Inhibition of *MMP13* *in vivo* reduces tumor-induced osteolysis. A, experimental strategy for treatment of Cl66 tumor-bearing mice with MMP13-ASO and control-ASO. B, H&E-stained sections (magnification, 20 \times) of tumors from control-ASO-treated (i) and MMP13-ASO-treated (ii) mice. Solid line, the intact bone; dotted line, the bone resorbed. iii, severity of the osteolytic lesion was measured by calculating the BDI; a significant reduction in the BDI was observed in MMP13-ASO-treated mice compared with control-ASO-treated mice. Bars, SD ($n = 5$ per group, and the study was repeated with same number of mice in each group). C, number of TRAP-positive osteoclasts in MMP13-ASO-treated and control-ASO-treated mice. D, expression of *MMP13* at the TB interface of MMP13-ASO-treated animal is significantly reduced compared with control-ASO-treated mice. *MMP13* expression was determined by RT-PCR and normalized to *GAPDH* expression. The values are mean \pm SEM. This is a representative of three experiments with similar results. Scale bar, 0.01 mm.



mice and observed a significant decrease in *RANKL* expression at the TB interface in the MMP13-ASO treatment group (Fig. 4A).

The RANKL/osteoprotegerin (OPG) axis has been shown to play a pivotal role in osteolytic bone metastasis (29). We examined how the RANKL/OPG ratio at the TB interface was altered due to MMP13-ASO treatment. RANKL levels were significantly reduced due to MMP13-ASO treatment (Fig. 4B), whereas we did not observe any significant difference in OPG levels between the two treatment groups (Fig. 4C). With the decrease in the RANKL levels, we observed a significant decrease in the RANKL/OPG at the TB interface in the MMP13-ASO treatment group (Fig. 4D). These observations suggest a functional role for MMP13 in tumor-induced osteolysis mediated by the regulation of the RANKL/OPG axis.

Targeting MMP13 inhibits MMP9 activation and TGF β signaling. Previously, we have shown that MMP9 is also upregulated at the TB interface in mammary tumor-implanted mice (22). We observed a decrease in *MMP9* mRNA expression at the TB interface in the MMP13-ASO-treated group

compared with the control-ASO-treated group (Fig. 5A). We evaluated the activity of MMP9 at the TB interface of Cl66 tumor-bearing mice treated with MMP13-ASO compared with control-ASO. We observed a significant decrease in gelatinolytic activity (at 92 kDa) in the MMP13-ASO-treated mice. We observed a significant decrease in active/pro-MMP9 enzyme levels in MMP13-ASO-treated mice (Fig. 5C). We did not observe significant difference in pro-MMP9 levels at the TB interface between control-ASO-treated and MMP13-ASO-treated group (Fig. 5B).

We have previously reported that upregulation of TGF β signaling during TB interaction promotes tumor-induced osteolysis (23). We observed a significant decrease in tumor-induced osteolysis with MMP13-ASO treatment. To examine whether MMP13 acts via TGF β signaling in mammary-induced osteolysis, we evaluated TGF β expression and activity at the TB interface of MMP13-ASO-treated and control-ASO-treated mice. We observed downregulation of *TGF β* mRNA expression in MMP13-ASO-treated mice (Fig. 6B). We evaluated TGF β signaling using immunohistochemistry for p-Smad-2 (30).

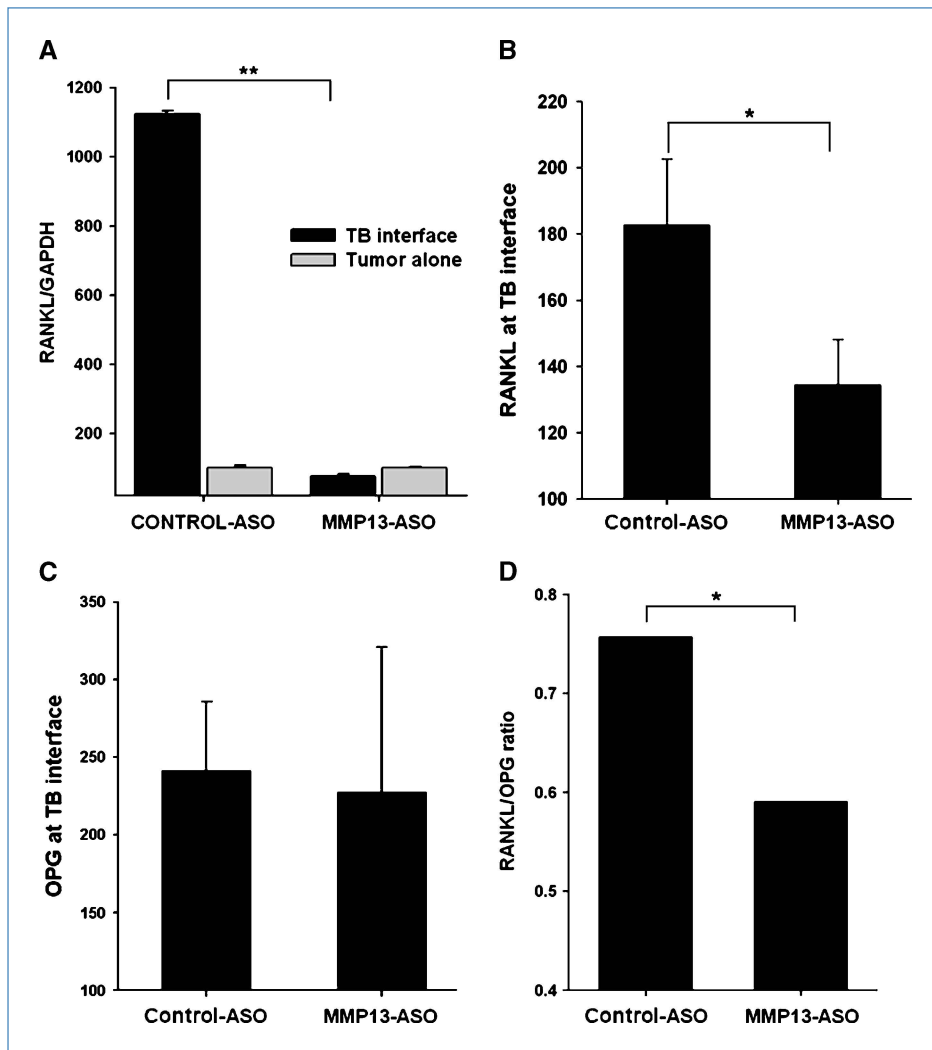
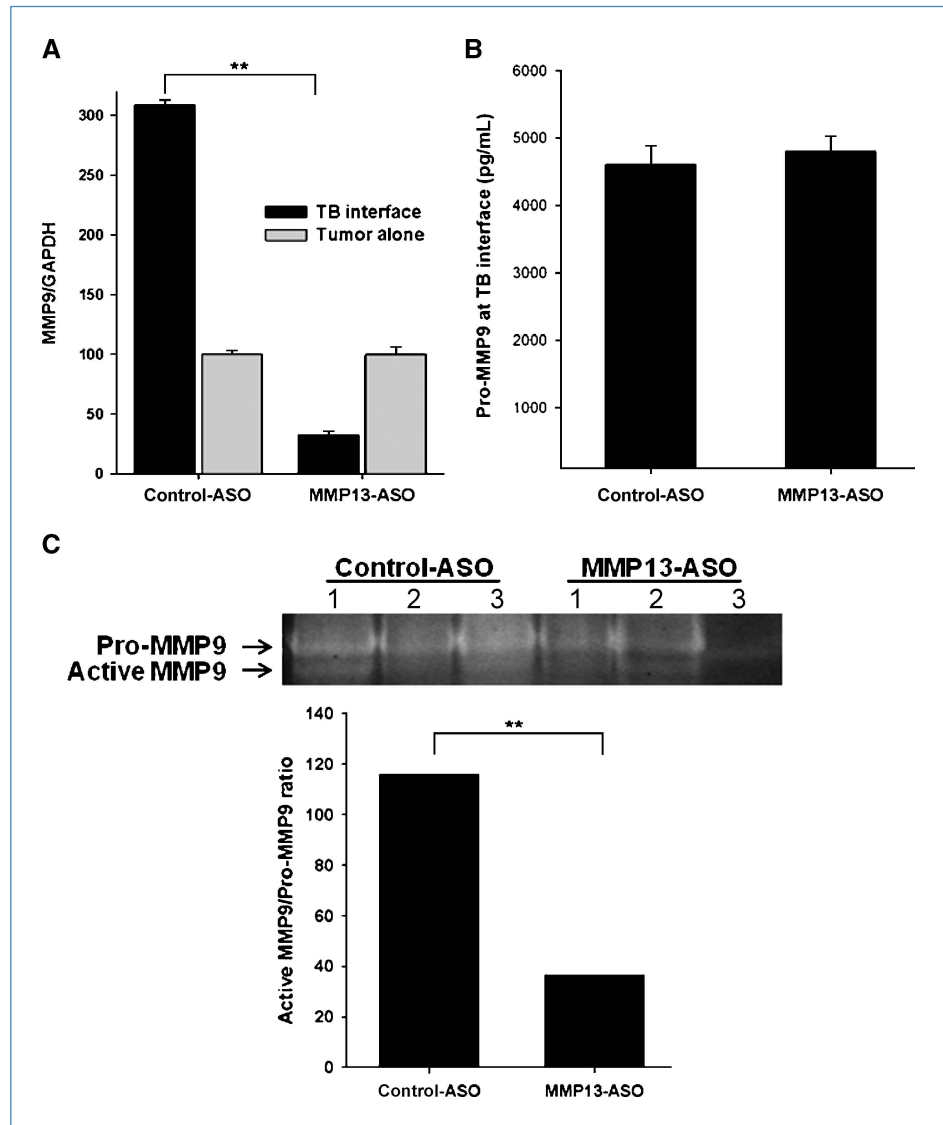


Figure 4. Inhibition of MMP13 *in vivo* regulates the RANKL/OPG ratio at the TB interface. RANKL mRNA (A) and protein (B) levels were significantly reduced in TB samples from MMP13-ASO-treated mice compared with control-ASO-treated mice. C, OPG levels at the TB interface did not differ between MMP13 and control-ASO groups as shown by ELISA. D, the RANKL/OPG is significantly decreased at the TB interface in MMP13-ASO-treated mice. The values are mean \pm SEM. This is a representative of three experiments with similar results.

Figure 5. MMP13-ASO treatment inhibited *MMP9* mRNA expression and activity at the TB interface. A, qRT-PCR showed that MMP13-ASO treatment significantly reduced mRNA expression of *MMP9* in TB samples. B, pro-MMP9 levels at TB interface determined by quantitative ELISA. The values are mean \pm SEM. This is representative of two experiments done in triplicate. C, a representative zymography showing pro-MMP9 and active MMP9 levels. MMP9 gelatinolytic activity (92 kDa) is significantly reduced in TB samples from MMP13-ASO-treated mice compared with control samples. The ratio of active MMP9 to pro-MMP9 is significantly reduced with MMP13 inhibition. **, $P < 0.01$.



We observed a significant decrease in the p-Smad-2 staining index and TGF β signaling at the TB interface of mice with MMP13-ASO treatment (Fig. 6A and C).

Discussion

In this study, we evaluated the gene expression signature at the TB interface and tumor alone areas in three different mammary adenocarcinoma cell lines differing in their metastatic potential. We identified *MMP13*, *RANKL*, *IBSP*, *Lumican*, *Kif5B*, *LOX*, and *Wif1* as potentially important genes involved in tumor-induced osteolysis, which are commonly upregulated at the TB interface in all three tumor types. Furthermore, overexpression of MMP13 at the TB interface promotes tumor-induced osteolysis and knockdown of MMP13 with ASO results in a significant inhibition of bone destruction. These data show that interaction of breast cancer cells with

bone stromal cells results in an altered gene expression pattern that is critical for tumor-induced osteolysis.

We identified genes that are potentially involved in the modulation of TB interaction during osteolytic bone metastasis using microarray analysis. We confirmed the microarray data by performing qRT-PCR analysis showing higher expression of *MMP13*, *RANKL*, *IBSP*, *Lox*, *Lumican*, *Wif1*, and *Kif5b* mRNA expression at the TB interface compared with the tumor alone area. Our previous studies have established the importance of RANKL upregulation during TB interaction in activating osteoclasts and promoting tumor-induced osteolysis (22, 23). IBSP is a secreted, noncollagenous glycoprotein of bone matrix and is expressed in breast, lung, thyroid, and prostate cancers that metastasize to bone (31). Expression of IBSP is associated with development of metastasis and poor prognosis (32, 33). Lumican is a small leucine-rich proteoglycon abundantly present in breast tissue, and it has

been shown that lumican expression parallels tumor progression in breast carcinoma with higher lumican expression associated with higher tumor grade and lower estrogen receptor levels in the tumor (34). However, their role in bone metastasis remains unclear. LOX is an ECM remodeling enzyme, and studies delineating the role of LOX in metastasis showed that it is essential for hypoxia-induced metastasis and inhibition of LOX proved to be promising in eliminating metastasis in mice with orthotopically grown tumors (35, 36). Silencing of WIF1 is associated with increased susceptibility to osteosarcoma (37). The role of the Kif5B gene in cancer progression is not well established. However, a recent report suggested a possible role for Kif5B as an oncofusion kinase

(38). These studies suggest possible roles for genes upregulated at the TB interface; however, little is known about their functional role in TB interaction during osteolytic metastasis.

MMPs have been implicated in tumor progression and metastasis in several tumor types (11, 39–41). Our present data showed the upregulation of MMP13 at the TB interface in three different mammary tumors. MMP13 expression was higher in both tumor cells and osteoblasts at the TB interface. Previous studies have shown expression of MMP13 in several cancers including breast (15), head and neck squamous carcinoma (18), melanoma, and chondrosarcoma (42). A previous report suggests involvement of MMP13 in the degradation of basement membrane during bone metastasis

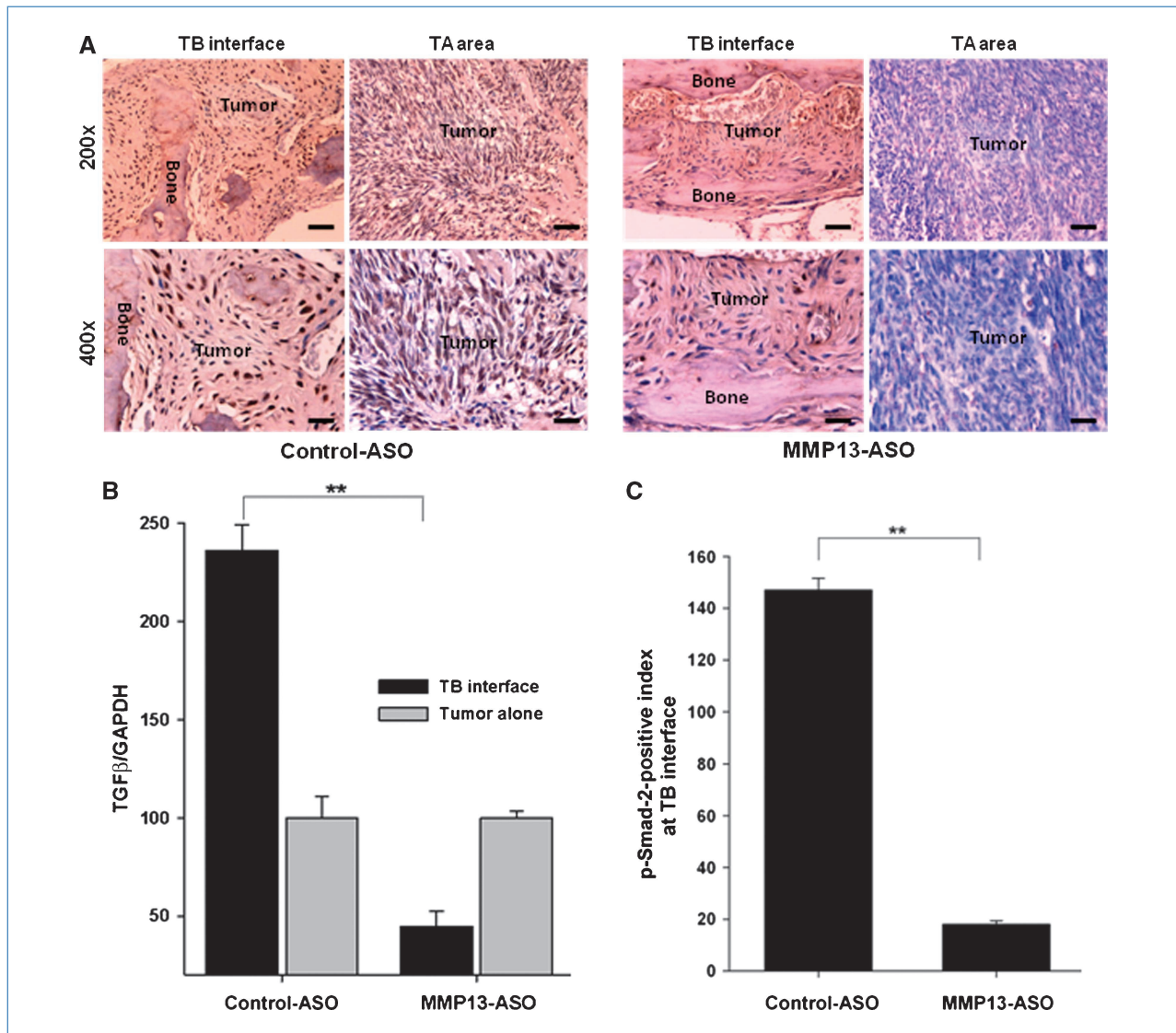


Figure 6. Inhibition of MMP13 blocks TGF β signaling at the TB interface. A and C, sections from MMP13-ASO–treated mice showed a significantly reduced p-Smad-2 staining index at the TB interface. Scale bars, 0.01 mm ($n = 5$). B, qRT-PCR showed a significant decrease in *TGF β* mRNA expression at the TB interface in MMP13-ASO–treated mice compared with control-ASO–treated mice. The values are mean \pm SEM. This is representative of three experiments with similar results. **, $P < 0.05$.

of breast cancer (41). We have observed an association between MMP13 expression, the number of osteoclasts, and tumor-induced osteolysis. Recent study has shown the upregulation of MMP13 in clinical bone metastatic samples from breast cancer patients (43). Our present data and the previous reports suggest an important role for the expression of MMP13 at the TB interface (11, 39–41, 44); hence, in this report, we focused on delineating the functional analysis of MMP13 in tumor-induced osteolysis.

To further strengthen our findings, we used MMP13-ASOs to target MMP13 expression *in vivo*. Treatment of mice with MMP13-ASOs significantly inhibited tumor-induced bone resorption as well as number of activated osteoclasts at the TB interface. The mechanism underlying MMP13-dependent osteoclast activation remains unclear. Previous reports have shown that RANKL/RANK/OPG signaling is important in osteoclast activation and subsequent bone destruction (45). It is possible that MMP13 inhibition might alter the expression of RANKL and OPG at the TB interface. We observed that targeting MMP13 decreased RANKL expression at TB interface without affecting OPG levels. As explained previously, the relative RANKL/OPG ratio is an important factor in driving osteolysis, and we observed a significant decrease in the RANKL/OPG ratio at the TB interface in MMP13-ASO-treated mice. These observations suggest the potential role of MMP13 in RANKL-dependent osteoclast activation and tumor-induced osteolysis. The actual mechanism through which MMP13 is involved in the regulation of the RANKL/OPG axis at the TB interface merits further investigation.

MMP13 has been shown to play a central position in the MMP activation cascade (46). MMP13 activates MMP9 by cleaving pro-MMP9 (47). In our previous studies, we have shown the upregulation of pro-MMP9 and active MMP9 during TB interaction (22). In this report, we observed a significant decrease in active MMP9 levels at the TB interface in MMP13-ASO-treated mice. MMP9 has been shown to recruit osteoclasts during development of long bones (48). These studies suggest that MMP13 might indirectly potentiate osteoclast recruitment and activation by regulating activation of MMP9 at the TB interface during TB interaction.

In a recent report, we showed the role of TGF β signaling during TB interaction in promoting mammary tumor growth and osteoclast activation (23). In this report, we analyzed the effect of MMP13 knockdown on TGF β signaling by p-Smad2 staining and observed a significant decrease in the p-Smad2 activity in the MMP13-ASO-treated group compared with control-treated group. The decrease in TGF β signaling could be due to lower levels of active MMP9 at the TB interface, which has been shown to be critical in TGF β activation

(49, 50). In our previous report, we did not observe an increase in TGF β mRNA expression at the TB interface (23). However, TGF β R1 expression and signaling was increased at the TB interface compared with the tumor alone area (23). Our data suggest that increased MMP13 levels at the TB interface potentiate TGF β signaling via activation of MMP9. In our previous study, we evaluated the functional role of cathepsin G in osteolytic bone metastasis of breast cancer and observed that cathepsin G was involved in activating MMP9 by cleaving pro-MMP9. Inhibition of cathepsin G resulted in increased latent TGF β levels. Thus, cathepsin G-mediated activation of MMP9 led to activation of TGF β and ultimately promotes tumor-induced osteolysis (50). Findings from our previous and present study allow us to speculate that MMP9 might be playing as a central molecule in tumor-induced osteolytic cascade, where it is activated by several factors including cathepsin G and MMP13 and leading to enhancement of TGF β signaling at the TB interface, ultimately contributing to the osteolytic bone metastasis.

In conclusion, our present study showed that TB interaction during osteolytic bone metastasis alters the gene expression signature at the TB interface, which further promotes bone resorption and establishment of osteolytic bone metastasis. These findings delineate the potential role of MMP13 as one of the key regulators, commonly upregulated at the TB interface, during TB interaction in osteolytic bone metastasis. MMP13 expression contributes to the osteolytic process by regulating RANKL/OPG levels, activating MMP9, and increasing TGF β signaling. Our study provides data for understanding the mechanistic role of MMP13 in osteolysis observed during bone metastasis. Additional studies are required to understand the regulation of MMP13 expression during osteolytic bone metastasis and the development of targeted therapeutics.

Disclosure of Potential Conflicts of Interest

No potential conflicts of interest were disclosed.

Grant Support

Susan G. Komen for the Cure grant KG090860, Cancer Glycobiology Program from Nebraska Research Initiative and grant CA72781 (R.K. Singh), Cancer Center Support grant P30CA036727 from National Cancer Institute, NIH, and Department of Defense Breast Cancer Research Program Predoctoral Traineeship Award BC083293 (K.C. Nannuru).

The costs of publication of this article were defrayed in part by the payment of page charges. This article must therefore be hereby marked *advertisement* in accordance with 18 U.S.C. Section 1734 solely to indicate this fact.

Received 08/31/2009; revised 02/15/2010; accepted 02/19/2010; published OnlineFirst 04/20/2010.

References

- Jemal A, Siegel R, Ward E, Hao Y, Xu J, Thun MJ. Cancer statistics. *CA Cancer J Clin* 2009, caac.
- Boyce BF, Yoneda T, Guise TA. Factors regulating the growth of metastatic cancer in bone. *Endocr Relat Cancer* 1999;6:333–47.
- Mundy GR. Metastasis to bone: causes, consequences and therapeutic opportunities. *Nat Rev Cancer* 2002;2:584–93.
- Mundy GR. Mechanisms of bone metastasis. *Cancer* 1997;80:1546–56.
- Coleman RE. Skeletal complications of malignancy. *Cancer* 1997;80:1588–94.
- Yoneda T, Hiraga T. Crosstalk between cancer cells and bone micro-environment in bone metastasis. *Biochem Biophys Res Commun* 2005;328:679–87.
- Powell GJ, Southby J, Danks JA, et al. Localization of parathyroid hormone-related protein in breast cancer metastases: increased

- incidence in bone compared with other sites. *Cancer Res* 1991;51:3059–61.
8. Guise TA, Yin JJ, Taylor SD, et al. Evidence for a causal role of parathyroid hormone-related protein in the pathogenesis of human breast cancer-mediated osteolysis. *J Clin Invest* 1996;98:1544–9.
 9. Roodman GD. Mechanisms of bone metastasis. *N Engl J Med* 2004;350:1655–64.
 10. Birkedal-Hansen H. Catabolism and turnover of collagens: collagenases. *Methods Enzymol* 1987;144:140–71.
 11. Lynch CC, Hikosaka A, Acuff HB, et al. MMP-7 promotes prostate cancer-induced osteolysis via the solubilization of RANKL. *Cancer Cell* 2005;7:485–96.
 12. Stetler-Stevenson WG. The role of matrix metalloproteinases in tumor invasion, metastasis, and angiogenesis. *Surg Oncol Clin N Am* 2001;10:383–92, x.
 13. Djonov V, Cresto N, Aebersold DM, et al. Tumor cell specific expression of MMP-2 correlates with tumor vascularisation in breast cancer. *Int J Oncol* 2002;21:25–30.
 14. Ruokolainen H, Paakko P, Turpeenniemi-Hujanen T. Expression of matrix metalloproteinase-9 in head and neck squamous cell carcinoma: a potential marker for prognosis. *Clin Cancer Res* 2004;10:3110–6.
 15. Freije JM, Diez-Itza I, Balbin M, et al. Molecular cloning and expression of collagenase-3, a novel human matrix metalloproteinase produced by breast carcinomas. *J Biol Chem* 1994;269:16766–73.
 16. Mauviel A. Cytokine regulation of metalloproteinase gene expression. *J Cell Biochem* 1993;53:288–95.
 17. Johansson N, Airola K, Grenman R, Kariniemi AL, Saarialho-Kere U, Kahari VM. Expression of collagenase-3 (matrix metalloproteinase-13) in squamous cell carcinomas of the head and neck. *Am J Pathol* 1997;151:499–508.
 18. Cazorla M, Hernandez L, Nadal A, et al. Collagenase-3 expression is associated with advanced local invasion in human squamous cell carcinomas of the larynx. *J Pathol* 1998;186:144–50.
 19. Johansson N, Vaalamo M, Grenman S, et al. Collagenase-3 (MMP-13) is expressed by tumor cells in invasive vulvar squamous cell carcinomas. *Am J Pathol* 1999;154:469–80.
 20. Hsu CP, Shen GH, Ko JL. Matrix metalloproteinase-13 expression is associated with bone marrow microinvolvement and prognosis in non-small cell lung cancer. *Lung Cancer* 2006;52:349–57.
 21. Aslakson CJ, Miller FR. Selective events in the metastatic process defined by analysis of the sequential dissemination of subpopulations of a mouse mammary tumor. *Cancer Res* 1992;52:1399–405.
 22. Wilson TJ, Nannuru KC, Futakuchi M, Sadanandam A, Singh RK. Cathepsin G enhances mammary tumor-induced osteolysis by generating soluble receptor activator of nuclear factor- κ B ligand. *Cancer Res* 2008;68:5803–11.
 23. Futakuchi M, Nannuru KC, Varney ML, et al. Transforming growth factor- β signaling at the tumor-bone interface promotes mammary tumor growth and osteoclast activation. *Cancer Sci* 2009;100:71–81.
 24. Massague J. TGF- β signal transduction. *Annu Rev Biochem* 1998;67:753–91.
 25. Miyazono K, Ten DP, Heldin CH. TGF- β signaling by Smad proteins. *Adv Immunol* 2000;75:115–57.
 26. Bennett CF, Cowsert LM. Antisense oligonucleotides as a tool for gene functionalization and target validation. *Biochim Biophys Acta* 1999;1489:19–30.
 27. Henry SP, Geary RS, Yu R, Levin AA. Drug properties of second-generation antisense oligonucleotides: how do they measure up to their predecessors? *Curr Opin Investig Drugs* 2001;2:1444–9.
 28. Nannuru KC, Futakuchi M, Sadanandam A, et al. Enhanced expression and shedding of receptor activator of NF- κ B ligand during tumor-bone interaction potentiates mammary tumor-induced osteolysis. *Clin Exp Metastasis* 2009;26:797–808.
 29. Dougall WC, Chaisson M. The RANK/RANKL/OPG triad in cancer-induced bone diseases. *Cancer Metastasis Rev* 2006;25:541–9.
 30. Nakao A, Imamura T, Souchelnytskyi S, et al. TGF- β receptor-mediated signalling through Smad2, Smad3 and Smad4. *EMBO J* 1997;16:5353–62.
 31. Bellahcene A, Merville MP, Castronovo V. Expression of bone sialoprotein, a bone matrix protein, in human breast cancer. *Cancer Res* 1994;54:2823–6.
 32. Bellahcene A, Kroll M, Liebens F, Castronovo V. Bone sialoprotein expression in primary human breast cancer is associated with bone metastases development. *J Bone Miner Res* 1996;11:665–70.
 33. Bellahcene A, Menard S, Bufalino R, Moreau L, Castronovo V. Expression of bone sialoprotein in primary human breast cancer is associated with poor survival. *Int J Cancer* 1996;69:350–3.
 34. Leygue E, Snell L, Dotzlaw H, et al. Expression of lumican in human breast carcinoma. *Cancer Res* 1998;58:1348–52.
 35. Erler JT, Bennewith KL, Nicolau M, et al. Lysyl oxidase is essential for hypoxia-induced metastasis. *Nature* 2006;440:1222–6.
 36. Bondareva A, Downey CM, Ayres F, et al. The lysyl oxidase inhibitor, β -aminopropionitrile, diminishes the metastatic colonization potential of circulating breast cancer cells. *PLoS One* 2009;4:e5620.
 37. Kansara M. Wnt inhibitory factor 1 is epigenetically silenced in human osteosarcoma, and targeted disruption accelerates osteosarcomagenesis in mice. *J Clin Invest* 2009;119:837–51.
 38. Takeuchi K, Choi YL, Togashi Y, et al. KIF5B-ALK, a novel fusion onco kinase identified by an immunohistochemistry-based diagnostic system for ALK-positive lung cancer. *Clin Cancer Res* 2009;15:3143–9.
 39. Lafleur MA, Drew AF, de Sousa EL, et al. Upregulation of matrix metalloproteinases (MMPs) in breast cancer xenografts: a major induction of stromal MMP-13. *Int J Cancer* 2005;114:544–54.
 40. Ellsworth RE, Seebach J, Field LA, et al. A gene expression signature that defines breast cancer metastases. *Clin Exp Metastasis* 2009;26:205–13.
 41. Ohshiba T, Miyaura C, Inada M, Ito A. Role of RANKL-induced osteoclast formation and MMP-dependent matrix degradation in bone destruction by breast cancer metastasis. *Br J Cancer* 2003;88:1318–26.
 42. Uria JA, Balbin M, Lopez JM, et al. Collagenase-3 (MMP-13) expression in chondrosarcoma cells and its regulation by basic fibroblast growth factor. *Am J Pathol* 1998;153:91–101.
 43. Klein A, Orendrowitz C, Schmutzler R, et al. Identification of brain- and bone-specific breast cancer metastasis genes. *Cancer Lett* 2009;276:212–20.
 44. Uria JA, Stahle-Backdahl M, Seiki M, Fueyo A, Lopez-Otin C. Regulation of collagenase-3 expression in human breast carcinomas is mediated by stromal-epithelial cell interactions. *Cancer Res* 1997;57:4882–8.
 45. Blair JM, Zhou H, Seibel MJ, Dunstan CR. Mechanisms of disease: roles of OPG, RANKL and RANK in the pathophysiology of skeletal metastasis. *Nat Clin Pract Oncol* 2006;3:41–9.
 46. Leeman MF, Curran S, Murray GI. The structure, regulation, and function of human matrix metalloproteinase-13. *Crit Rev Biochem Mol Biol* 2002;37:149.
 47. Knauper V, Smith B, Lopez-Otin C, Murphy G. Activation of progelatinase B (proMMP-9) by active collagenase-3 (MMP-13). *Eur J Biochem* 1997;248:369–73.
 48. Engsig MT, Chen QJ, Vu TH, et al. Matrix metalloproteinase 9 and vascular endothelial growth factor are essential for osteoclast recruitment into developing long bones. *J Cell Biol* 2000;151:879–90.
 49. Yu Q, Stamenkovic I. Cell surface-localized matrix metalloproteinase-9 proteolytically activates TGF- β and promotes tumor invasion and angiogenesis. *Genes Dev* 2000;14:163–76.
 50. Wilson TJ, Nannuru KC, Singh RK. Cathepsin G-mediated activation of pro-matrix metalloproteinase 9 at the tumor-bone interface promotes transforming growth factor- β signaling and bone destruction. *Mol Cancer Res* 2009;7:1224–33.